CHEMICAL REVIEWS

REVIEW

pubs.acs.org/CR

Fundamental Approaches to Nonadiabaticity: Toward a Chemical Theory beyond the Born−Oppenheimer Paradigm

Takehiro Yonehara, Kota Hanasaki, and Kazuo Takatsuka*

Department of Basic Sciences, Graduate School of Arts and Sciences, The University of Tokyo Komaba, 153-8902 Tokyo, Japan

CONTENTS

Special Issue: 2012 Quantum Chemistry

Received: March 29, 2011
Published: November 11, 2011

1. INTRODUCTION: MOTIVE AND BACKGROUND

Nonadiabatic transitions are one of the most important quantum mechanical phenomena in chemical reaction dynamics. This is because the most interesting chemical and even biological phenomena involve nonadiabatic transition events. Many theoretical methods for treating such nonadiabatic transitions have been proposed, and without a doubt their contribution to the progress of elementary dynamical processes of chemical reactions has been enormous. Yet, due to the rapid progress of experimental studies, we are often faced with complicated and difficult experimental situations that have not been studied before. For instance, due to advances in laser technology, an intense electromagnetic vector potential has become available, which now makes it possible to modify the molecular electronic states and thereby induce novel nonadiabatic coupling. This article reviews the recent theories of nonadiabatic transitions from a fundamental perspective. Particular attention will be paid to the recent notion of nonadiabaticity in electron dynamics. We will also discuss the interaction of molecular nonadiabatic states with intense laser fields. This review can also be read as a general review of mixed quantum-classical dynamics, in which quantum and classical subsystems kinematically contact each other, leaving the effects of quantum mechanical entanglement to survive in the classical subsystem.

The theory of nonadiabatic transitions was first proposed in 1932 by Landau,[1] Zener,[2] Stueckelberg,[3] and London,[4] to study phenomena including electron transfer between two atoms. Since then, nonadiabatic dynamics has been found in many other phenomena, mostly in chemical reactions. Among these, the dynamics across conical intersections is one of the most important subjects in current chemistry. These classic theories, however, suffer from severe limitations and/or drawbacks from their theoretical structures. For instance, the Landau−Zener formula assumes linearly crossed diabatic (one-dimensional) energy curves with a constant nonadiabatic transition coupling, thereby allowing a transition only at the crossing point. However, these assumptions are far from the reality in many systems. Another basic theory of nonadiabatic transitions is the semiclassical Ehrenfest theory (SET). Although it can cope with multidimensional nonadiabatic electronic-state mixing, it inevitably produces a nuclear path that runs on an averaged potential energy surface even after having passed across the nonadiabatic region, which is totally unphysical. Unfortunately, since SET seems intuitively correct, a naive and conventional derivation of this theory obscures how this critical difficulty arises. To overcome these difficulties, many theories have been proposed in the literature. For example, the Zhu−Nakamura theory[5] is regarded as an ultimate theory within the Landau−Zener type dynamics. The fewest switch surface hopping method[6] and the theory of natural decay of mixing[7−10] are among the most advanced methodologies so far proposed to practically resolve the critical difficulty of SET.

Yet, in spite of the availability of such advanced methodologies in modern molecular science, there are many situations that are not even considered by such state-of-the-art theories. For instance, experimentalists are often interested in systems of densely

degenerated electronic states, which are rather universal in very high excited states. Furthermore, recent advances in laser technology enable drastic modification in the molecular electronic states, which in turn can induce novel nonadiabatic coupling in addition to the native nonadiabatic transition. Such nonadiabatic chemistry in intense laser fields makes the current situation in science totally different from that of traditional theories of nonadiabatic transition.[11] It seems therefore obvious that we should reconsider the theory of nonadiabatic transitions from a deeper point of view rather than try to technically augment the classic theories that rest on sometimes naive assumptions. The present review has been written with a hope that the theory of nonadiabatic transition can be rebuilt from a more fundamental perspective.

There have been published many excellent review articles on the theory of nonadiabatic transitions, among which refs 12−17 are particularly recommended. Therefore, we should begin this article by discussing more explicitly why we should write another review. In doing this, we briefly overview on which basis the current theoretical chemistry stands and attempt to project to which direction we are proceeding.

1.1. Traditional Framework of Quantum Chemistry

Immediately after Heisenberg and Schrödinger established quantum mechanics, in 1927, Born and Oppenheimer developed a perturbation theory to help us comprehend how a molecule can exist in a stable state.[18] The notion of separation of the nuclear and electronic motions essentially emerged from this study along with the so-called Born−Oppenheimer fixed nuclear approximation (more simply referred to as the Born−Oppenheimer (BO) approximation). The BO approximation is so successful, actually even more successful than originally anticipated, it is quite often regarded as a robust paradigm of molecular science. Incidentally, in the same year, Heitler and London[19] proposed the quantum theory of valence, which was followed by Pauling with his powerful concepts of valence bond, resonance, electonegativity, and so on. In the theory of rate process in chemical reactions, Eyring[20] and Evans and Polanyi[21] established the transition-state theory in 1935, and the early theories of nonadiabatic transition of Landau,[1] Zener,[2] and Stueckelberg[3] date back to the year 1932. It is rather astonishing, therefore, that the theoretical foundations of present chemistry were established in such early days of quantum physics.

In order to discuss as accurately as possible these complex theories, we will now briefly review the traditional and canonical way of describing a molecular system. Within the nonrelativistic scheme, the quantum-mechanical molecular Hamiltonian is generally written as

$$\begin{aligned} H(\mathbf{r},\mathbf{R}) &= T_N + H^{\mathrm{el}}(\mathbf{r};\mathbf{R}) \\ &= \frac{1}{2}\sum_k \frac{\hat{P}_k^2}{M_k} + H^{\mathrm{el}}(\mathbf{r};\mathbf{R}) \end{aligned} \tag{1}$$

where a many-body electronic Hamiltonian is defined as

$$\begin{aligned} H^{\mathrm{el}}(\mathbf{r};\mathbf{R}) &= T_{\mathrm{e}} + V_{\mathrm{c}}(\mathbf{r};\mathbf{R}) \\ &= \frac{1}{2m}\sum_j \hat{p}_j^2 + V_{\mathrm{c}}(\mathbf{r};\mathbf{R}) \end{aligned} \tag{2}$$

Here and in what follows, $\mathbf{r}$ and $\mathbf{R}$ denote the electronic and nuclear coordinates, respectively, and $\hat{p}_j$ and $\hat{P}_k$ are the operators of their conjugate momenta of the jth and kth components of $\mathbf{r}$ (denoted as r_j) and $\mathbf{R}$ (R_k), respectively. $V_{\mathrm{c}}(\mathbf{r};\mathbf{R})$ represents collectively the Coulombic interactions among electrons and nuclei. Because nuclei move far more slowly than electrons due to their heavy masses, it is standard practice to expand the total wave function $\Psi(\mathbf{r},\mathbf{R},t)$ in stationary electronic basis functions $\{\Phi_I(\mathbf{r};\mathbf{R})\}$, which are determined at each nuclear position $\mathbf{R}$, in such a way that

$$\Psi(\mathbf{r},\mathbf{R},t) = \sum_I \chi_I(\mathbf{R},t)\,\Phi_I(\mathbf{r};\mathbf{R}) \tag{3}$$

This is often referred to as the Born−Huang expansion.[22] We assume that the electronic basis set $\{|\Phi_I\rangle\}$, either adiabatic or diabatic, is orthonormal at each nuclear configuration as

$$\langle\Phi_I(\mathbf{R})|\Phi_J(\mathbf{R})\rangle = \delta_{IJ} \tag{4}$$

In what follows, the bra-ket inner product represents integration over the electronic coordinates only.

Inserting this form of the total wave function into the time-dependent Schrödinger equation and using the above orthonormal property, one obtains the standard coupled equations of motion for nuclear wave functions

$$\begin{aligned} i\hbar\frac{\partial}{\partial t}\chi_I = \frac{1}{2}\sum_k \frac{\hat{P}_k^2}{M_k}\chi_I - i\hbar\sum_k\sum_J \frac{X_{IJ}^k\hat{P}_k}{M_k}\chi_J - \frac{\hbar^2}{2}\sum_k\sum_J \frac{Y_{IJ}^k}{M_k}\chi_J \\ + \sum_J H_{IJ}^{\mathrm{el}}\chi_J \end{aligned} \tag{5}$$

where

$$X_{IJ}^k = \left\langle \Phi_I \middle| \frac{\partial\Phi_J}{\partial R_k} \right\rangle, \quad Y_{IJ}^k = \left\langle \Phi_I \middle| \frac{\partial^2\Phi_J}{\partial {R_k}^2} \right\rangle \tag{6}$$

and

$$H_{IJ}^{\mathrm{el}}(\mathbf{R}) = \langle\Phi_I|H^{\mathrm{el}}|\Phi_J\rangle \tag{7}$$

These quantities are the main players in the theory of nonadiabaticity. In addition to these, H^{el} can contain spin−orbit couplings. We do not, however, discuss the relativistic effects any further, since it is beyond the scope of this review. Interested readers are referred to ref 23. This multistate coupled Schrödinger equation can be transformed into a compact matrix form as shown below

$$i\hbar\frac{\partial}{\partial t}\chi_I = \sum_J \left[\sum_k \frac{1}{2M_k}[(\mathbf{I}\hat{P}_k - i\hbar\mathbf{X}^k)^2]_{IJ} + H_{IJ}^{\mathrm{el}}\right]\chi_J \tag{8}$$

where $[\mathbf{I}]_{IJ} = \delta_{IJ}$ and $[\mathbf{X}^k]_{IJ} = X_{IJ}^k$.[14,16] The above reduction to eq 5 is mathematically complete, but these close coupling equations practically require much labor in solving even for small systems.[23−32]

It is generally accepted that one of the most successful fields in theoretical chemistry is so-called quantum chemistry. This is an electronic structure theory based on the fixed nuclei (Born−Oppenheimer) approximation, which is the eigenvalue problem with respect to the electronic Hamiltonian $H^{\mathrm{el}}(\mathbf{r};\mathbf{R})$ at each nuclear configuration, that is

$$H^{\mathrm{el}}(\mathbf{r};\mathbf{R})\,\Phi_I(\mathbf{r};\mathbf{R}) = V_I(\mathbf{R})\,\Phi_I(\mathbf{r};\mathbf{R}) \tag{9}$$

Quantum chemistry serves as quite a reliable tool for the interpretation and prediction of complex chemical phenomena and can aid in designing novel molecules prior to experimental synthesis. The result is a great contribution to chemistry and

dx.doi.org/10.1021/cr200096s |Chem. Rev. 2012, 112, 499–542

thereby human society. Techniques have been developed there that are highly sophisticated and are aimed at the study of larger molecular systems with faster and more accurate computation so as to make it possible to treat the more realistic molecules found in nature. The fixed nuclear approximation is extremely useful, not only for the bound states but also for the treatment of electronic scattering by molecules. For instance, stationary-state scattering theories within the fixed nuclear approximation have been extensively developed for molecular photoionization[33,34] and electron scattering from polyatomic molecules.[35,36] These scattering phenomena are quite important in several respects, since they are widely found in nature as elementary processes and even in industrial applications using plasma processes. These scatterings may be referred to as stationary-state *electron dynamics* in the fixed nuclei approximation.

Despite the undoubted success of quantum chemistry, it is important to recognize its theoretical limitations, since it is beyond such borders that the novel electronic states we do not yet know of may exist. These limitations may be summarized as follows. (1) Quantum electronic structure theory (alias quantum chemistry) does not contain time t. It assumes that molecules are basically long-lived. However, this is not necessarily the case in highly excited states or in the transient states encountered during the course of chemical reactions. Furthermore we should think about the energy-time uncertainty that imposes an unavoidable limitation on the accurate observation of the state energy. Moreover the energy distribution even in electronic wavepacket states cannot be neglected in an ultrashort time experiment. (2) The individual (adiabatic) electronic states are well-defined, only if their energies are sufficiently separated from each other. But in highly degenerate states, the notion of the individual adiabatic potential energy surfaces loses its sense. Rather, one should take explicit account of the kinematic coupling with nuclear motions, or nonadiabaticity.

On the other hand, nuclear dynamics on a given potential energy surface (PES) $V_I(\mathbf{R})$ within the BO separation scheme is reduced to solving the following equation

$$i\hbar \frac{\partial}{\partial t}\chi_I(\mathbf{R},t) = [T_N + V_I(\mathbf{R})]\chi_I(\mathbf{R},t) \tag{10}$$

The full quantum wavepacket dynamics, which is shown in eq 5, is based on the Born−Huang expansions and, if it were perfectly achieved, appears to be mathematically exact. However, since the wavelength of matter waves for heavy particles such as nuclei is much shorter in general than that of an electron, it is never easy to solve even eq 10 unless certain constraints are additionally imposed. Classical alternatives are therefore frequently adopted with the understanding that quantum effects are totally neglected. It is commonly believed that semiclassical mechanics compromises two conflicting factors: computability and the taking into account of quantum effects. However, to the best of our knowledge, semiclassical mechanics remains a tough challenge. (We will discuss this aspect briefly in section 4.1.) It should also be noted that these studies on nuclear dynamics, including the close coupling equations as shown in eq 5, are quite often performed without any deep concern about the change of electronic states. The electronic energies, together with the nonadiabatic coupling elements, are supposedly given independently by quantum chemistry. Indeed, this seems to be largely the case in the actual performance of chemical dynamics. Consequently, these two major fields have been separated from each other.

1.2. Entanglement of Nuclear and Electronic Motions as an Essential Feature in the Breakdown of the Born−Oppenheimer Approximation

There is no doubt that the Born−Oppenheimer approximation captures the essential feature of the molecular properties of stable molecules. (So many papers have been published on the mathematical and numerical analyses of the Born−Oppenheimer theory, but it is beyond the scope of the current review. See refs 37−39 for relevant recent literature.) The validity or the level of accuracy of the Born−Oppenheimer separation is roughly assessed as follows. Let m be the mass of an electron and let M_l be the mass of the lth nucleus. The perturbation parameter κ is taken as

$$\kappa = \sqrt[4]{\frac{m}{M}} \tag{11}$$

where M is a kind of average of the M_l values such that

$$M_l = M\frac{1}{\mu_l} = \frac{m}{\kappa^4\mu_l} \tag{12}$$

with μ_l being a dimensionless number of order $O(1)$. Born and Oppenheimer[18] studied the stationary Schrödinger equation

$$H(r,\mathbf{R})\,\psi(\mathbf{r},\mathbf{R}) = E\psi(\mathbf{r},\mathbf{R}) \tag{13}$$

using a perturbation theory with the total Hamiltonian represented by

$$H = H_0 + \kappa^4 H_1 \tag{14}$$

where the zeroth order Hamiltonian is the electronic Hamiltonian and the perturbation interaction $\kappa^4 H_1$ is the nuclear kinetic energy operator

$$T_N = \kappa^4 H_1 \tag{15}$$

They expanded the total energy according to the order of the perturbation interaction such that

$$W = W^0 + \kappa W^{(1)} + \kappa^2 W^{(2)} + \kappa^3 W^{(3)} + \kappa^4 W^{(4)} + \ldots \tag{16}$$

They showed that W^0 is the electronic energy, $\kappa^2 W^{(2)}$ corresponds to the harmonic nuclear vibrational energy, and $\kappa^4 W^{(4)}$ gives the anharmonic vibrational energy with molecular rotational energy. They also explicitly proved that

$$W^{(1)} = W^{(3)} = 0 \tag{17}$$

The energy terms up to $\kappa^4 W^{(4)}$ constitute the so-called Born−Oppenheimer energy of a molecule. The higher terms should represent the various couplings between electronic, vibrational, and rotational modes.

The critical question is how accurate (or inaccurate) the Born−Oppenheimer energy of a molecule defined as above is. Recently Takahashi and Takatsuka have addressed this question and reported a semiclassical analysis of this matter.[40] They explicitly showed that the fifth order term $W^{(5)}$ is also exactly zero, and therefore, the lowest-order correction to the Born−Oppenheimer energy must be of the order of

$$(m/M)^{6/4} \tag{18}$$

dx.doi.org/10.1021/cr200096s |Chem. Rev. 2012, 112, 499–542

This explicitly highlights that the Born−Oppenheimer approximation is far better than what would be expected from a simple mass ratio m/M. For example, if $m/M \sim 10^{-6}$, the error term is $(m/M)^{1.5} \sim 10^{-9}$.

In cases where the above perturbation theory is not valid, mainly as a result of the degenerate situation among the static electronic states, quantum mechanical mixing among them through the nuclear kinetic operator becomes significant. Consequently, a nonadiabatic transition takes place in the molecular configuration at which the nonadiabatic coupling elements, X_{IJ}^k in eq 6, are large enough and/or the potential energy surfaces "avoid-cross" each other. [See ref 24 for a latest review on the faithful approaches to solve the coupled equations.] In such a nonadiabatic situation, a nuclear wavepacket starting from an electronic state $\Phi_1(\mathbf{r};\mathbf{R})$ is bifurcated into two by a single passage across a nonadiabatic region, which is mathematically written as follows:

$$\chi_1(\mathbf{R}, t_b)\ \Phi_1(\mathbf{r};\mathbf{R}) \rightarrow \chi_1(\mathbf{R}, t_a)\ \Phi_1(\mathbf{r};\mathbf{R}) + \chi_2(\mathbf{R}, t_a)\ \Phi_2(\mathbf{r};\mathbf{R}) + \ldots \quad (19)$$

Here, t_b and t_a, respectively, indicate a time before and after passing through the nonadiabatic region. The right-hand side of this equation represents a typical situation of quantum entanglement, in which it is only after the relevant measurement that one can realize which one of $|\chi_1(\mathbf{R},t_a)\Phi_1(\mathbf{r};\mathbf{R})|^2$, $|\chi_2(\mathbf{R},t_a)\Phi_2(\mathbf{r};\mathbf{R})|^2$, and so on actually appears. This kind of quantum entanglement generated by the wavepacket bifurcation is one of the key features of nonadiabatic dynamics (see below for a more thorough argument about entanglement in the BO approximation).

To be a little more precise about the notion of quantum entanglement, it should be noted that even a single term in the Born−Huang expansion such as $\chi(\mathbf{R},t)\ \Phi(\mathbf{r};\mathbf{R})$ in eq 19 has already, at least to some extent, taken into account quantum entanglement through the functional form of the electronic wave function. This is made clearer if we formally expand it into an "independent" basis functions as

$$\chi(\mathbf{R}, t)\ \Phi(\mathbf{r};\mathbf{R}) = \sum_a \breve{\chi}_a(\mathbf{R}, t)\ \breve{\Phi}_a(\mathbf{r}) \quad (20)$$

where the electronic function is free from the nuclear coordinates and thereby does not track the nuclear motion. This is in contrast to the spirit of Born−Oppenheimer. The basis set $\{\breve{\Phi}_a(\mathbf{r})\}$ is sometimes referred to as a completely diabatic basis, and in fact it is physically poor and slowly converging. Moreover, it has been shown[14] that such a complete diabatic electronic basis does not globally "exist" (see also the Appendix in this review). Nevertheless, $\{\breve{\Phi}_a(\mathbf{r})\}$ is mathematically simple to handle. Hence, some of these basis functions might prove useful depending on how they are exploited. In fact, the simultaneous quantization of electronic and nuclear degrees of freedom is a somewhat classic problem in theoretical chemistry and consequently has a long history. A more recent development has been the direct determination of self-consistent nuclear orbitals along with electronic orbitals (molecular orbitals) in the functional form of eq 20.[41−46] These methods are expected to work for estimating the vibronic coupling energy, but only if a large amplitude displacement of nuclear positions does not take place. We will not consider these basis functions further in this review, not only because of the slow convergence expected in the expansion of eq 20, but more importantly because they obscure the essential characteristics of nonadiabaticity.

1.3. Experimental Reality of the Wavepacket Bifurcation

It is important to emphasize that the wavepacket bifurcation as represented in eq 19 is not simply a mathematical artifact but can be observed directly as a real time dynamics using spectroscopic techniques. [Quantum interference among these bifurcated wavepackets in their remerging area leading to an oscillation in the product distribution is known as the Stueckelberg oscillation.[3,47] This is an indirect observation of the wavepacket bifurcation.] Indeed, Arasaki et al. have shown explicitly that femtosecond pump−probe photoelectron spectroscopy can actually detect the instant of wavepacket bifurcation, in which the distribution functions of energy and angle of photoelectrons themselves bifurcate or suddenly change in a characteristic manner.[48] This is because as soon as a nuclear wavepacket undergoes a transition from one potential energy surface to another of different character, the nature of the photoelectrons can change drastically. This has been numerically shown to be the case in a study of the NaI system, in which the potential energy curves of NaI and Na^+I^- avoid-cross each other on the occasion of electron transfer.[48] Very recently, Suzuki et al. have developed a time-resolved photoelectron imaging technique and actually showed that such bifurcation dynamics can be experimentally observed.[49]

Similarly, Arasaki et al. explored the application of femtosecond time-resolved photoelectron spectroscopy for the real-time monitoring of wavepacket dynamics through the conical intersection between the first two $^2A'$ states of NO_2.[50] They employed global potential energy surfaces for the ground and first excited $^2A'$ states and for the ground singlet and first triplet ion states, to time-propagate the quantum vibrational wave function in full (three) dimensions using a short time propagator. They calculated the *ab initio* geometry- and energy-dependent photoionization amplitudes explicitly. These are incorporated to calculate the angle- and energy-resolved photoelectron spectra, thus reproducing the velocity map images. They have successfully shown that the bifurcation of a wavepacket across the conical intersection can also be directly observed in real time. Incidentally, they also proposed a modification of (shift the position of and change the nature of) the conical intersection in NO_2 by breaking the C_{2v} symmetry by shining a laser on it and thereby controlling the nonadiabatic transition probability.[51] In addition, they showed that the effect of such control of chemical reactions can be directly monitored in terms of pump−probe photoelectron spectroscopy in real time.[52] This is one of the exciting new aspects of the study of nonadiabatic transitions.

1.4. Necessity of Nonadiabatic Dynamical Electron Theory

As noted above, the foundations of theoretical chemistry were already established in the 1920s and 1930s, and even today the basic framework remains essentially the same. However, there are many reasons we need to lift the time-independent electronic state theory into the realm of dynamical electron theory by taking explicit account of time t in it. Below are listed some of the current attempts to achieve this goal.

1.4.1. Progress in Laser Chemistry. *1.4.1.1. Tracking Attosecond Electron Dynamics.* The most powerful driving force to demand for the advancement of the dynamical theory of electronic states comes from the progress being made in laser technology, of which there are two aspects. The first is in the rapid advances of ultrashort pulse lasers, whose width is shorter than 100 attoseconds. This is comparable with or shorter than the time scale of the valence electrons in a molecule.[53−63] For many years, nothing could be experimentally generated that was

dx.doi.org/10.1021/cr200096s |*Chem. Rev.* 2012, 112, 499–542

faster than the time scale of electrons. But that has changed and now the exploration of electron wavepacket dynamics in chemical reactions of polyatomic molecules becomes more and more realistic using such ultrafast laser pulse technology. To date, most of the full quantal numerical studies on electronic-nuclear entire dynamics are made for the hydrogen molecule or its cation. Those relevant works include refs 54 and 64−81.

However, to achieve further progress, more general *ab initio* methods need to be developed for the treatment of multielectronic and polyatomic molecules.

1.4.1.2. Modulating Electronic States and Control of Chemical Reactions. Intense lasers have brought about a revolutionary change in modern molecular spectroscopy. In the past, in the field of photochemistry, only a weak and/or almost resonant perturbation was applied to a molecule to observe its response. This meant that only the static states were characterized. On the other hand, a laser field which is more intense than 10^{16} W/cm^2 can apply as strong forces to nuclei and electrons, as their original interactions do. The result therefore is that it can readily modulate the electronic states directly by creating a new wavepacket state. It can also induce nonadiabatic interactions in addition to the original ones. For instance, an efficient way of inducing an electronic excitation can be possible through the use of vibrational excitation using IR lasers.[82] One of the ultimate aims in this context would be to create new electronic states, through which the control of chemical reactions could be achieved.

1.4.1.3. Dynamics of Internal and External Electrons. Similarly, intense lasers make it possible to study the early stages in the multiphoton ionization of molecules through multiply excited states. Above-threshold ionization gives rise to a quasi-free electronic wavepacket state, and the recombination (collision) of such an electronic wavepacket with the remaining cation species results in the high harmonic generation.[83−89] These issues give rise to an extremely interesting challenge on how to describe the electronic wavepacket states.

1.4.1.4. Secondary Effects of an Induced Electromagnetic Field by a Molecular Electron Current in External Laser Fields. The electron current within a molecule driven by an intense laser field should generate an induced electromagnetic field. This in turn will bring about the nontrivial secondary effects.[90−95] The more intense the external field is, the more prominent these secondary effects should be. However, they can be studied only by solving the coupled equations of the quantum electronic wavepacket and the Maxwell equations in a self-consistent manner.[96] To successfully achieve this project, a very good theory for nonadiabatic electron wavepacket theory must be constructed first.

1.4.2. Chemistry without Potential Energy Surfaces: Highly Degenerate Electronic States Far Beyond the Born−Oppenheimer Separation. The dynamics in densely degenerate electronic states such as those commonly found in highly excited states and metal-like states[97] are expected to undergo large fluctuations among the many electronic states involved. In addition, the energy−time uncertainty relation precludes dynamics that are confined to a single potential energy surface, and hence, the notion of a separated potential energy surface may lose any sense. This is what is called "chemistry without potential energy surfaces". Since it is a meaningless effort to single out an individual global adiabatic potential energy surface in such a situation, only the so-called "on-the-fly" method should be able to track such complicated nonadiabatic dynamics. (See section 3 for the definition of the on-the-fly method. A nice example of application of the on-the-fly method in a study of laser control of chemical reactions is seen in ref 98.)

1.4.3. Nonadiabatic Dynamical Electron Theory for Chemical Reactions. It turns out through our studies that the electron wavepacket description of chemical reactions offers an interesting and novel way of comprehending them when the shift of the nuclear configuration induces a qualitative change in the electronic states through nonadiabatic interactions. This situation is typically observed in chemical reactions which are nonconcerted reactions or Woodward−Hoffmann symmetry forbidden reactions, proton transfer dynamics associated with keto−enol tautomerization,[99] fast relaxation dynamics of excited states through conical intersections, and so on. Electron flow dynamics and their forces working on the nuclei will provide new insights into chemical reactivity.[100,101]

In addition, the influence of truly multidimensional nonadiabatic effects in the study of chemical reactions is quite important. So far most of the nonadiabatic theories have been limited to one-dimensional systems. They are applied to multidimensional systems by locally slicing the potential energy surface in a direction parallel to that of a classical trajectory under study. However, essentially multidimensional effects of nonadiabatic dynamics certainly exist. Conical intersection and the so-called geometric phase (for instance, the Longuet−Higgins phase,[102] the Berry phase,[103] as well as the phase in the molecular Aharonov−Bohm effect,[104,105] among others) are illuminating examples. Moreover, it is anticipated that other essentially multidimensional effects will be discovered in the future. In this review, in section 5.4, we will present a case study of electron wavepacket dynamics around a conical intersection, thereby showing some of its new features. Also, attention is drawn to a theoretical parallelism between the electromagnetic vector potential and the nonadiabatic interaction (see section 3.7), which should give a clue to finding a multidimensional effect of nonadiabatic interactions.

1.4.4. General Theory of Mixed Quantum and Classical Dynamics. Let us suppose it is possible to treat the nuclear subsystem in a molecule "classically" and the electronic subsystem quantum mechanically. This type of theoretical framework is called a mixed quantum-classical representation. Such a mixed representation can find many applications in science. For instance, a fast mode such as the proton dynamics in a protein should be considered as a quantum subsystem, while the rest of the skeletal structure can be treated as a "classical" subsystem.[106−108] It is quite important in this context to establish the correct equations of motion for each of the subsystems and to ask what are their rigorous solutions and how the quantum effects penetrate into the classical subsystems. By studying the quantum-electron and classical-nucleus nonadiabatic dynamics as deeply as possible, we will attain such rigorous solutions. This is one of the aims of the present review.

1.4.5. What Do We Mean by a "Fundamental Approach" to Nonadiabaticity? The title of this review, a "Fundamental Approaches to Nonadiabaticity" was suggested by the Guest Editors of this thematic issue. Therefore, before concluding this introductory section, we should summarize here what is meant by "fundamental approach". As stressed above, we need to set our starting point much deeper than the Born−Oppenheimer separation scheme to find the unknown molecular states, in order to cope with the advent of the latest advances in experimental studies. To be a little more precise, an accurate estimate of transition probability in one-dimensional nonadiabatic processes is not good enough; hence, we want to survey

(1) the notion of coherence and decoherence, (2) a description of electron−nuclear entanglement as one of the most quantum mechanical phenomena, (3) the identification of the quantum phases arising from electron and nuclear dynamics, (4) the establishment of practical equations of motion for the coupled dynamics between electrons and nuclei, and (5) the physics of interference between the nonadiabatic dynamics and external fields. With these final goals in mind, we will now address the issues involved.

The rest of this review is organized as follows. First, in section 2 we will briefly review the classic and recent studies of semiclassical methods for the evaluation of nonadiabatic transition amplitudes in coupled nuclear dynamics. These theories are useful for a quick estimate of the nonadiabatic transition probability. However, the dynamics of electrons is not considered explicitly at all. In section 3 we review nonadiabatic electron theories and simultaneous nuclear path dynamics. We begin the section with the Pechukas path integral theory, which is semiclassically reduced, by integrating the electronic motion first, to an equation of motion to determine a globally smooth "nuclear path" running through the nonadiabatic region connecting two end points located on two different PESs. This equation must be solved in a self-consistent manner (typically with an iteration method) if such a path indeed exists. Consequently, this brings to our attention the difficulty of quantum entanglement as manifested in nuclear path dynamics. We then turn to the electron-state mixing problem along a nuclear path in terms of the naive semiclassical Ehrenfest theory (SET). In contrast to the Pechukas theory, a classical path passing across a nonadiabatic region is given uniquely in SET. However, it is forced to run on an averaged potential energy surface, thus destroying the Born−Oppenheimer scheme after the passage. With respect to this, it is necessary to pay special attention to the issue of coherence and natural decoherence of electronic states to be realized along the corresponding nuclear paths. An important theory by Truhlar et al. will also be outlined. It uniquely (without iteration) gives a globally smooth "classical path" connecting two end points on two different PESs. This remarkable achievement, in marked contrast to the Pechukas theory, has been made possible by their introduced external (decoherence) field, which again highlights the difficulty of representing correctly the entanglement in non-Born−Oppenheimer paths. Finally, we will present the correct solution to this mixed quantum and classical dynamics, namely the branching paths generated in a nonadiabatic region along which to materialize the electronic state mixing. It will be shown that the entanglement is well represented up to the quantum phases of electron-nuclei dynamics in terms of the branching paths. Section 4 touches upon a representation of the total nonadiabatic wave function beyond the stage of the Born−Oppenheimer approximation. In section 5, we will present our recent case studies of nonadiabatic electron dynamics on (i) the migration dynamics of hydrated electrons, (ii) the laser response of selected molecules, and (ii) a precise analysis of conical intersection from the viewpoint of path branching. With these examples, albeit being limited to small systems, we intend to show how the electron dynamics can be exploited. One of the difficult problems that merits further study is the quantum chemical technique for the calculation of nonadiabatic matrix elements. Although it seems a rather technical issue, some deep-lying problems are hidden behind this matter. We cannot stress too much that practical studies on nonadiabatic electron dynamics are made possible by the progress in quantum chemistry. We consider this aspect in the Appendix. This review closes in section 6 with some concluding remarks.

2. SEMICLASSICAL THEORIES OF NONADIABATIC TRANSITION IN COUPLED NUCLEAR DYNAMICS

Although this review attempts to guide readers to the nonadiabatic electron wavepacket theory (in both the presence and absence of external laser fields), we should first review the basic ideas of traditional theories, addressing both their advantages and limitations in view of the aims mentioned in the Introduction. Only selected semiclassical theories of nonadiabatic transitions will be discussed, in which two potential energy surfaces (PESs), along with their nonadiabatic coupling elements, are assumed to be given externally. Those readers who are familiar with the traditional theory of nonadiabatic transitions may wish to skip to section 3, in which we discuss the nonadiabatic electron wavepacket theory.

2.1. Landau−Zener Theory of the Curve Crossing Model

Landau[1] and Zener[2] studied nonadiabatic transitions in atomic collisions and the dissociation of diatomic molecules. Although Landau also reached an equivalent conclusion independently, we will follow Zener's approach here. Zener reduced the original problem to a simplified two-state model, which is now called "the linear curve crossing model", in which a nonadiabatic dynamics is approximated as follows: (1) The relevant nuclear motion near the curve crossing point is one-dimensional, which is referred to as the "reaction coordinate" in this context. The reaction coordinate is denoted as X, which is the displacement from the curve crossing point. (2) Diabatic potentials near the crossing point, W_1 and W_2, are approximated as linear in X; $W_1 = -F_1X$ and $W_2 = -F_2X$ for states 1 and 2, respectively. (It was also assumed in the original formulation that F_1 and F_2 should be of the same sign, but this condition is not imposed on the modern curve-crossing theory.) (3) The off-diagonal term in the diabatic representation is approximated as the constant V throughout the region. (4) During the transition, the system is assumed to move with a constant velocity v, that is, $\dot{X} = v$.

Assumption 3 appears rather unphysical. However, it can be rationalized to some extent as follows. If the difference in the diagonal component is much larger than the off-diagonal component, that is, $|W_1(X) - W_2(X)| \gg V$, then the transition probability would be suppressed and moreover the spatial change of V should not qualitatively affect the final result, on the condition that $|W_1(X) - W_2(X)|$ grows fast. Assumption 4 is valid in cases where the incident energy is large enough compared to the change in the potential energy surface. In such cases, in the diabatic representation, the wave functions of the two electronic states can be represented by $\Phi_1(\mathbf{r};X)$ and $\Phi_2(\mathbf{r};X)$, respectively. The total wave function is then represented as

$$\Psi(\mathbf{r},X,t) = C_1(t)\,\Phi_1(\mathbf{r};X) + C_2(t)\,\Phi_2(\mathbf{r};X) \tag{21}$$

Using the assumption $X = vt$, the Schrödinger equation is thus reduced to a matrix equation

$$i\hbar\frac{\partial}{\partial t}\begin{pmatrix} C_1(t) \\ C_2(t) \end{pmatrix} = \begin{pmatrix} W_1(X) & V \\ V & W_2(X) \end{pmatrix}\begin{pmatrix} C_1(t) \\ C_2(t) \end{pmatrix} \tag{22}$$

This equation is to be solved as an initial value problem under the conditions $C_1(-\infty) = 0$ and $|C_2(-\infty)| = 1$. Then the probability of the system undergoing a nonadiabatic transition is given by $P = |C_2(+\infty)|^2$ per single crossing. The problem is reduced to a

second order differential equation, whose solution is given by the Weber functions. Zener obtained the transition probability in the asymptotic region as

$$P = \exp\left[-\frac{\pi}{2\hbar v}\frac{V^2}{|F_1 - F_2|}\right] \tag{23}$$

which is now well-known as the Landau−Zener formula. The dimensionless quantity appearing in the exponent, $[\pi/2\hbar v][V^2/|F_1 - F_2|]$, characterizes the strength of the nonadiabatic transition. Due to these somewhat crude approximations made in constructing the above linear curve crossing model, the resultant expression of the probability is often not accurate enough for realistic systems. But it is remarkable that the theory represents the essential nature of the nonadiabatic transition using such a simple analytic formula with a minimum number of parameters: nonperturbative exponential dependence on the off-diagonal coupling term V and the inverse dependence on velocity v, which is consistent with the adiabatic limit ($P \rightarrow 0$ as $v \rightarrow 0$). The Landau−Zener formula works as a rough but qualitatively useful estimate of nonadiabatic transition probabilities.[109]

The characteristic exponent in the Landau−Zener formula can actually be obtained without the explicit assumption of constant velocity or constant coupling. We consider the transition amplitude, say c_{21}, from the diabatic state 1 to the state 2 in the time interval t_1 to t_2, during which the system passes through the curve crossing point. Using the first order perturbation, it is evaluated as

$$c_{21} = -\frac{i}{\hbar}\int_{t_1}^{t_2} dt \exp\left[-\frac{i}{\hbar}\int_{t}^{t_2} dt'\, W_2(t')\right] V \times \exp\left[-\frac{i}{\hbar}\int_{t_1}^{t} dt''\, W_1(t'')\right] \tag{24}$$

Under semiclassical (small $\hbar$) assumptions, the integral is evaluated using the stationary phase approximation. The stationary phase condition becomes

$$W_2(t) - W_1(t) = 0 \tag{25}$$

which is satisfied at the crossing time t_c. The second order derivative of the exponent at the crossing time gives $v(t_c)(F_2(t_c) - F_1(t_c))$. Thus, we have

$$c_{21} \approx -i\sqrt{\frac{\pi V(t_c)^2}{\hbar v(t_c)|F_2(t_c) - F_1(t_c)|}} \exp\left[-\frac{i}{\hbar}\int_{t_c}^{t_2} dt'\, W_2(t')\right] \times \exp\left[-\frac{i}{\hbar}\int_{t_1}^{t_c} dt''\, W_1(t'')\right] \tag{26}$$

where the quantity in the square root is equivalent to the exponent in the Landau−Zener formula, apart from the constant factor. Thus, up to this approximation, the characteristic dimensionless strength of the nonadiabatic transition strength is $V(t_c)^2/[\hbar v(t_c)|F_2(t_c) - F_1(t_c)|]$, even if v or V are slowly varying functions of time. The above condition of the smooth connection of quantum phases is essential in the curve crossing problem. This was stressed in an application of phase-space quantum mechanics to nonadiabatic dynamics, with which the so-called Magnus approximation was obtained.[110]

It should be noted, however, that there are certain theoretical limitations in applying the Landau−Zener formula. For example, it does not work in cases where the two diabatic potential curves have mutually the opposite slopes, though this is a common situation in nonadiabatic processes related to chemical reactions. For more refined discussions on the validity of the Landau−Zener formula, readers are recommended to consult refs 12, 111, and 112. There is also a problem concerning the accuracy of the formula, in particular at a low collision energy. Since the Landau−Zener formula is aimed at estimating the transition probability within the "exponential accuracy", the claim that it lacks quantitative accuracy misses the point. Yet, *ab initio* calculations for actual molecular systems with the avoided crossing revealed that the Landau−Zener model is often far from the reality; in nature, the electronic-state mixing is more subtle and complicated than originally anticipated and is heavily dependent on the system chosen. All of which suggests that quantum chemical studies are inevitable for realistic research.

2.2. Quantum Phase Arising from Nonadiabatic Transitions

2.2.1. Phase in Nonadiabatic Interactions. We will now consider the Stueckelberg theory. Compared to the Landau−Zener theory, it is based on a more general assumption and gives a quantum phase associated with nonadiabatic reaction processes, which was missing in the Landau−Zener formula. The phase effect is obviously important, since, as suggested by Stueckelberg himself, it is experimentally observable. He reduced the two-state Schrödinger equation to a fourth order differential equation for a single state. With a semiclassical method, he derived an exponential factor that the wave function gains as it turns around the complex crossing point of two adiabatic surfaces in order to obtain the transition probability. The square of the transition amplitude per single passage over the crossing point becomes equivalent to the Landau−Zener formula under the assumptions adopted in the linear curve crossing model. A marked difference, however, comes from the use of the adiabatic representation. The wavenumber k_j of the heavy particle (nuclei) with the total energy E_{tot} explicitly reflects the electronic energy E_j (the energy of PES) in the form $(\hbar^2/2\mu)k_j^2 + E_j = E_{tot}$. This is in contrast to the Landau−Zener theory, where the heavy particle motion is assumed to be independent from or unaffected by the internal (electronic) state. As a consequence, Stueckelberg's formula selects (approximately) the phase factors from the nonadiabatic process. A wave function branching in the nonadiabatic region can proceed on two different adiabatic potential curves and, depending on the energy, can meet again in the same nonadiabatic region, where the phase interference takes place, leading to an oscillation of the population of the products. This effect is known as the Stueckelberg oscillation, and it is indeed experimentally observed in ultrafast spectroscopies.[47]

Child[12] developed a uniform diagrammatic approach for one-dimensional problems; classical turning points, barrier penetration, and curve crossings are represented in terms of individual diagrams. These are further connected with link matrices of the semiclassical wave function coefficients. Child showed that a wide range of spectroscopic phenomena such as predissociation and restricted rotation are described as a combination of these elementary diagrams. The wave function is written in a semiclassical form as

$$\psi(r) = \sqrt{\frac{\mu}{2\pi\hbar^2 k(r)}}\{C' \exp[i\int_{r_0}^{r} k(r)\, dr] + C'' \exp[-i\int_{r_0}^{r} k(r)\, dr]\} \tag{27}$$

dx.doi.org/10.1021/cr200096s |*Chem. Rev.* 2012, 112, 499–542

where μ is the reduced mass and $\hbar k(r) \equiv [2\mu(E - V(r))]^{1/2}$, with energy E and potential $V(r)$, and r_0 is the curve-crossing point. The link matrix M then connects the coefficient vector $\mathbf{C} = (C',C'')^T$ before and after the passage in the manner $\mathbf{C}^{(\text{after})} = M\mathbf{C}^{(\text{before})}$. Summarizing Stueckelberg's results in a compact manner, the curve crossing, in particular, takes the following form: The wave functions before and after the curve crossing are written as

$$\begin{aligned}\psi_j(r) \sim k_{\pm}^{-1/2}\{U_j' \exp[i\int_{r_0}^{r} k_{\pm}(r)\,\mathrm{d}r] \\ + U_j'' \exp[-i\int_{r_0}^{r} k_{\pm}(r)\,\mathrm{d}r]\} \quad \text{for} \quad r \ll R_0 \\ \psi_j(r) \sim k_{\mp}^{-1/2}\{V_j' \exp[i\int_{r_0}^{r} k_{\mp}(r)\,\mathrm{d}r] \\ + V_j'' \exp[-i\int_{r_0}^{r} k_{\mp}(r)\,\mathrm{d}r]\} \quad \text{for} \quad r \gg R_0 \end{aligned} \tag{28}$$

where the (diabatic) state indices j are either 1 or 2. $\pm$ ($\mp$) for $r \ll R_0$ ($r \gg R_0$) takes + (−) for j = 1 and − (+) for j = 2. $k_{\pm}$ are semiclassical wavenumbers on the adiabatic potential $V_{\pm} \equiv (W_1 + W_2)/2 \pm \{[(W_1 - W_2)/2]^2 + V^2\}^{1/2}$. Then the relation between the coefficients is given as

$$\begin{pmatrix} V_1' \\ V_2' \end{pmatrix} = \begin{pmatrix} \lambda & -(1-\lambda^2)^{1/2}\mathrm{e}^{-i\chi} \\ (1-\lambda^2)^{1/2}\mathrm{e}^{i\chi} & \lambda \end{pmatrix} \begin{pmatrix} U_1' \\ U_2' \end{pmatrix} \tag{29}$$

and

$$\begin{pmatrix} U_1'' \\ U_2'' \end{pmatrix} = \begin{pmatrix} \lambda & (1-\lambda^2)^{1/2}\mathrm{e}^{i\chi} \\ -(1-\lambda^2)^{1/2}\mathrm{e}^{-i\chi} & \lambda \end{pmatrix} \begin{pmatrix} V_1'' \\ V_2'' \end{pmatrix} \tag{30}$$

where $\lambda \equiv \mathrm{e}^{-\pi\nu}$ is the transition amplitude with $\nu = [1/(2\pi)]\mathrm{Im}[\int_{r_1}^{r_2}\mathrm{d}r\ [k_-(r) - k_+(r)]]$, with r_1 and r_2 being crossing points that exist on the analytically continued functions of the adiabatic potential surfaces, whereas the phase factor χ is given as $\chi = \arg\Gamma(i\nu) - \nu\ln\nu + \nu + \pi/4$. Thus, a unified semiclassical theory has been established for a chemical reaction in which plural elementary processes may be involved.

2.2.2. Curve Crossing in the Complex Plane. Miller and George[113] extended the Stueckelberg phase formalism to the complex plane of the internuclear distance. They started from the path integral expression of transition amplitude given by Pechukas.[114] For a given nuclear path $\mathbf{R}(t)$, and in the first order perturbative correction to the adiabatic limit, the transition amplitude along it is represented as

$$\begin{aligned}\mathscr{K}_{21}[\mathbf{R}(t)] = -\int_{t_1}^{t_2}\mathrm{d}t' \left\langle \phi_2 \left| \frac{\partial}{\partial t'}\phi_1 \right\rangle \right. \\ \times \exp\left[-\frac{i}{\hbar}\{ \int_{t'}^{t_2} E_2(\mathbf{R}(t''))\,\mathrm{d}t'' \right. \\ \left. \left. + \int_{t_1}^{t'} E_1(\mathbf{R}(t''))\,\mathrm{d}t''\} \right] \end{aligned} \tag{31}$$

where time t' is an instant of the transition and should be scanned over the possible time range. Evaluating the integral with the steepest descent method in the complex plane of $\mathbf{R}$, they obtained the expression

$$\mathscr{K}_{21}[\mathbf{R}(t)] = \exp\left[-\frac{i}{\hbar}\{ \int_{t_*}^{t_2} E_2(\mathbf{R}(t'))\,\mathrm{d}t' + \int_{t_1}^{t_*} E_1(\mathbf{R}(t'))\,\mathrm{d}t' \} \right] \tag{32}$$

where t_* is the complex crossing time, at which the complex path $\mathbf{R}(t)$ passes across a crossing seam. Since avoided crossing is being considered here, in the adiabatic representation, such a crossing seam is found only in the complex plane of $\mathbf{R}$, and by passing through the seam, a path can proceed from the original potential curve (Riemann surface) to the other counterpart. In running on the complex plane, the path acquires the complex action (the exponent on the right-hand side of eq 32), the magnitude of which depends on the location of the complex seam. Through the imaginary part of the action, $\mathscr{K}_{21}[\mathbf{R}(t)]$ can damp, thereby representing the nonadiabatic transition amplitude. Although this idea is quite interesting, its practical application may not be easy, depending on the analyticity of the adiabatic potentials. Besides, the general analyticity of complex continuation of the adiabatic potential energy surfaces in multidimensional systems is unknown yet.

2.3. Zhu−Nakamura Theory

Among the limitations of the Landau−Zener formula, the most serious is the fact that it does not work for cases where the incident energy is small in comparison to the off-diagonal coupling V, although such low energy collisions were excluded in the original derivation of the linear curve crossing model by Zener. It was only 60 years after the original Landau and Zener's works that Zhu and Nakamura achieved the complete solution of the linear curve crossing model and its generalization.[5] The linear curve crossing model is converted to a time-independent form where the coupled Schrödinger equations are

$$\begin{aligned}\left(-\frac{\hbar^2}{2m}\frac{\mathrm{d}^2}{\mathrm{d}x^2} - F_1 x \right)\psi_1 - V\psi_2 = E\psi_1 \\ \left(-\frac{\hbar^2}{2m}\frac{\mathrm{d}^2}{\mathrm{d}x^2} - F_2 x \right)\psi_2 - V\psi_1 = E\psi_2, \end{aligned} \tag{33}$$

These are then solved in the momentum representation. The solution is given in the form

$$\psi_j(x) = \int \frac{\mathrm{d}k}{2\pi}\mathrm{e}^{ikx}\frac{2}{|f_j|}A_j(k)\exp\left[\frac{i}{f_j}(\varepsilon k - k^3/3)\right] \tag{34}$$

where j is either 1 or 2, $f_j \equiv 2mF_j/\hbar^2$, and $\varepsilon \equiv 2mE/\hbar^2$ is the converted force and the energy, respectively (see ref 5 for more detail). From the argument of the asymptotic behavior in the $x \to \infty$ ($x \to -\infty$) for positive (negative) F_j solution,[111] the transition amplitude is obtained from the asymptotic behavior of $A_j(k)$ in the region $|k| \to \infty$, whose mutual relationship is given by the scattering matrix. The Zhu−Nakamura theory[5] is based on the analysis of the Stokes phenomena.[5,115] Since the Schrödinger equation (eq 33) in the momentum representation is reduced to the second order differential equation with quartic polynomials as coefficients, the asymptotic solution is affected by the Stokes phenomena from four transition points. In ref 5, they first analyzed the distribution of the four transition points in the whole range of two parameters, which represent the scale of the off-diagonal coupling and kinetic energy (a^2 and b^2 in ref 5). They next derived the reduced scattering matrix S^R as a function

dx.doi.org/10.1021/cr200096s |Chem. Rev. 2012, 112, 499–542

of six Stokes constants, which is then reduced to only one of them U_1 by making use of the symmetry properties of S^R. The Stokes constant U_1 is expressed formally as an infinite series of parameters, but for practical purposes, it is obtained using parameter-dependent approximate methods.

The Zhu−Nakamura theory is composed of many formulas which are dependent on the various physical situations under study. One example of wide interest is a formula for the case of $F_1F_2 < 0$, or what they call the nonadiabatic tunneling. Here we consider a single passage transition, and from the wide range of situations considered in the Zhu−Nakamura theory, we will quote only the simplest case in which the incident energy is higher than the adiabatic energy of the higher state at the crossing point ($b^2 \geq 1$). In such cases, the Stokes constant U_1 has a clear quasi-classical interpretation $U_1 = i(1 - P)^{1/2}e^{i\psi}$, where P is the Landau−Zener formula-like single transition probability and is given as (see eq 4.13 in ref 5)

$$P = \exp\left[-\frac{\pi}{4ab}\left(\frac{2}{1 + \sqrt{1 - b^{-4}(0.72 - 0.62a^{1.43})}}\right)^{1/2}\right] \quad (35)$$

Here a and b are again the scaled off-diagonal coupling and kinetic energy in ref 5.

The Zhu−Nakamura theory also covers other cases such as low-energy collision dynamics, where the incident energy is much lower than the barrier of the lower adiabatic potential (see ref 5 for the explicit form appropriate for this parameter range). That is, it can handle correctly and conveniently a system in which nonadiabatic dynamics couples with the relevant tunneling phenomenon.

One great advantage of the Zhu−Nakamura theory is that its transition amplitude can be represented in terms of the parameters related to the adiabatic potentials and incident energy alone. Although the derivation started from the diabatic representation of the system, transformation to the diabatic parameters from the adiabatic counterparts is in fact not needed, once the effective parameters as a and b in eq 35 are obtained. Thus, it is applicable solely within the adiabatic representation.[13]

2.4. Surface Hopping Scheme

Tully and Preston[116] proposed a drastically simplified computational scheme to treat nonadiabatic transitions, in which a multidimensional classical trajectory is allowed to suddenly hop at a selected place(s) on an adiabatic potential energy surface (PES) with a transition probability that has to be numerically provided by other methods, such as the Zhu−Nakamura theory. The first version of the surface hopping model is based on an assumption that nonadiabatic transitions take place only in a limited region of the potential energy surfaces, such as an avoided-crossing seam (or the crossing seam of the corresponding diabatic potential surfaces). On hopping, the velocity is readjusted with discontinuous change so as to satisfy the energy conservation. Concerning the idea on where and how to let a trajectory hop between two adiabatic PESs, Shenvi proposed the so-called "phase-space surface hopping".[117] Martínez et al. developed the method of an optimized way of hopping.[118] Statistical hopping is achieved through the Monte Carlo algorithm, and basically the phase information is destroyed in the hopping procedure. For technical issues, consult ref 116.

Using this approach, the nonadiabatic transition probability is estimated in terms of the number of classical trajectories reaching the goal areas of the individual PESs in asymptotic regions. Yet, another stochastic computation of the total transition probability is possible by using both daughter (one hops to another PES) and mother (the other remaining on the original PES) trajectories. The individual transition amplitudes can be estimated with, for instance, the Zhu−Nakamura formula. These pieces of transition-probability information carried by the individual trajectories can be summed up asymptotically. Besides, the transition-amplitude information containing the quantum phase, along with the phases coming from the action integral with each path, may be summed up asymptotically. An appropriate numerical method makes it possible to partly take into account the quantum interference among the paths in this way (see the comment in ref 119).

Thanks to the inherent simplicity and tractability, even in multidimensional systems, the surface hopping model and its modified versions have been applied to a wide range of phenomena.[120,121] Hence, they have made a large contribution to progress in chemistry. Meanwhile, the validity of this earlier version of the surface hopping method has also been tested intensively. In particular, Parlant et al.[122] tested the accuracy of the transition probability by a direct comparison with the exact quantum mechanical counterpart.

On the other hand, it is obvious that such a simplified treatment sacrifices some important features of nonadiabatic dynamics that are crucial in modern experimental studies. One such feature is the influence of interference effects arising from multiple transitions. In real systems, nonadiabatic coupling elements are not sharply localized on a single crossing seam, but rather can have a distribution of wide spatial range. In the first version of the surface hopping scheme, multiple transitions and their interference effects are missing. To overcome such severe limitations of the naive surface hopping scheme, many improved versions have been proposed. These include an important one by Tully himself,[6] which will be discussed in the next section.

2.5. Summary and Remaining Difficulties

Thus far we have reviewed the "classic" or "traditional" notion of nonadiabaticity . There have been so many theories developed in the spirit of this concept, many of which unfortunately lie outside the scope of this article. Presumably, one of the simplest yet more practical methods in this direction will result from a combination of the surface hopping model with the Zhu−Nakamura formula.[17]

Most of the theories reviewed in this section commonly assume that the nonadiabatic coupling is localized in a narrow space around the crossing point (crossing seam). However, this is often not the case. As seen in the example of the alkali halides, the nonadiabatic coupling spreads across a very broad range and the peak position of the coupling element lies far from the avoided crossing. In the latter case, the local transition view is no longer valid. Also, these theories are somewhat restricted in that they assume that the potential functions are always given by quantum chemistry. Consequently, they do not take into account the dynamical changes in the electronic states. However, it is indispensable, in the framework of modern theoretical and experimental chemistry, that a methodology capable of faithfully carrying out the electronic state mixing along nuclear paths be developed. This is the main subject in the next section.

3. COHERENT MIXING OF ELECTRONIC-STATES AND ITS DECOHERENCE ALONG NUCLEAR PATHS

Since nonadiabatic transitions are of highly quantum mechanical nature, it is natural to treat nuclear dynamics in a quantum mechanical or semiclassical manner. However, as a result of severe computational limitations, it is now common practice to use nuclear "classical" paths (not necessarily the Newtonian trajectory). This is where the nonadiabatic transitions are reduced to a problem of electronic state mixing caused by the nuclear kinematic interaction. The idea to use a "classical" nuclear path can be justified, since the wavelength of the nuclear matter wave is generally short enough anyway to be approximated in terms of a ray (trajectory-type) solution. The methods used to carry out electronic state calculations, either wavepackets or stationary states, along a nuclear path are collectively called the "on-the-fly method". More specifically, it is called *ab initio* molecular dynamics (ABMD) or the first principle dynamics if an *ab initio* eigenfunction of the electronic Hamiltonian is generated at each nuclear configuration and the nuclei are driven by the Newtonian force, which is calculated by using the energy gradient of the electronic bound state. ABMD has already attained much popularity in quantum chemistry (see refs 123 and 124 for examples of chemical use of ABMD). However, the method is valid only in the case where nonadiabatic interactions are negligible.

In the case of nonadiabatic electron wavepacket propagation along a nuclear path, an interesting problem arises; namely, the delicate and serious mismatching between the coherent electronic-state mixing and the decoherence of the nuclear classical dynamics. More explicitly put, how does the wavepacket bifurcation shown in eq 19 manifest itself in a classical path representation? What kind of quantum effects from electron dynamics will be expected to penetrate into classical nuclear subsystems? These questions are all common to the general systems composed of fast (quantum) and slow (classical) subsystems, which are kinematically coupled. Therefore, the coherence−decoherence problem in quantum systems surrounded by a classical moiety is one of the general issues to be considered in many fields of science.

3.1. Nuclear Paths Incorporating Electronic Motion in Pechukas Path Integrals

To clarify the central problem, we first outline the path-integral formulation[125,126] of nonadiabatic dynamics, since a classical approximation to quantum theory can be introduced into this framework in a systematic and natural manner using the stationary phase approximation.[126] It was Pechukas[114] who first established a path integral formalism for a vibrational excitation problem. This is theoretically equivalent to electron−nuclei coupled dynamics. The theory gives a clear description of electron−nucleus entangled dynamics. He first divided the dynamical variables into two groups: those of nuclear motion and those of electronic states. Here, the former are denoted as $\mathbf{R}$ and the latter are labeled by state indices α, β, ... (In his original formulation, Pechukas actually considered the atomic collision problem and set the former as the coordinate of the "heavy particle" and the latter as other "internal degrees of freedom".[114]) The total Hamiltonian is divided as $H = T + H^{\mathrm{el}}$, where T is the kinetic energy operator for the nuclei and H^{el} is the electronic Hamiltonian (treated as the internal degrees of freedom).

He then considered the transition amplitude of the system from a state $\{\mathbf{R}',\alpha\}$ at time t' to another $\{\mathbf{R}'',\beta\}$ at time t''. The kernel connecting the two end points is given by

$$\mathcal{K}_{\beta,\alpha}(\mathbf{R}'',t'';\mathbf{R}',t') = \int_{R'}^{R''} \mathcal{D}\mathbf{R}(t)\, \exp\left(\frac{i}{\hbar}S[\mathbf{R}(t)]\right) \mathcal{K}^{\mathrm{el}}_{\beta\alpha}[\mathbf{R}(t)] \tag{36}$$

where $S[\mathbf{R}(t)]$ is the action for the heavy particle and $\mathcal{K}^{\mathrm{el}}_{\beta\alpha}[\mathbf{R}(t)]$ is the transition amplitude of the electronic state for the nuclear position $\mathbf{R}(t)$, defined as

$$\mathcal{K}^{\mathrm{el}}_{\beta\alpha}[\mathbf{R}(t)] \equiv \lim_{N\to\infty} \langle\beta|\mathrm{e}^{-(i/\hbar)\varepsilon H^{\mathrm{el}}(\mathbf{R}(t_{N-1}))} \times \mathrm{e}^{-(i/\hbar)\varepsilon H^{\mathrm{el}}(\mathbf{R}(t_{N-2}))}\cdots\mathrm{e}^{-(i/\hbar)\varepsilon H^{\mathrm{el}}(\mathbf{R}(t_0))}|\alpha\rangle \tag{37}$$

where $\varepsilon \equiv (t''-t')/(N)$ is the time interval and $t_k \equiv t' + k\varepsilon$ is the kth time point with the time partition number being N. The path integration is performed step by step. The integration of the electronic degrees of freedom is performed at each given $\mathbf{R}(t)$, which is a function of time, and that over $\mathbf{R}$ is to be carried out using $S[\mathbf{R}(t)] + \hbar/i \ln K_{\beta\alpha}[\mathbf{R}(t)]$ as an effective action integral. Here we assume that the path-integration of the electronic part is performed in a quantum mechanical manner. Although Pechukas did not show how to perform the integrations, recent reports[127,128] have figured out the relevant method using the coherent-state path integrals and so on. We then apply the stationary phase approximation to the integral over $\mathbf{R}$. The stationary phase condition gives rise to

$$M\ddot{\mathbf{R}} = -\mathrm{Re}\frac{\langle\beta|\hat{U}(t'',t)\dfrac{\partial H^{\mathrm{el}}(\mathbf{R})}{\partial\mathbf{R}}\hat{U}(t,t')|\alpha\rangle}{\langle\beta|\hat{U}(t'',t')|\alpha\rangle} \tag{38}$$

where

$$\hat{U}(t'',t') \equiv \lim_{N\to\infty} \mathrm{e}^{-(i/\hbar)\varepsilon H^{\mathrm{el}}(\mathbf{R}(t_{N-1}))} \times \mathrm{e}^{-(i/\hbar)\varepsilon H^{\mathrm{el}}(\mathbf{R}(t_{N-2}))}\cdots\mathrm{e}^{-(i/\hbar)\varepsilon H^{\mathrm{el}}(\mathbf{R}(t_0))} \tag{39}$$

is the time evolution operator for the electronic degrees of freedom. The force in eq 38, which we refer to as the Pechukas force, is dependent on the initial and final states α and β as well as the path $\mathbf{R}(t)$, which is to be obtained as a solution of the dynamics equation (eq 38). Therefore, the nuclear equation of motion in eq 38 has to be solved in a self-consistent manner. There is no general proof, however, that can guarantee that eq 38 has a global path(s) solution connecting the two given end points. Even if it exists, it would not be easy to attain convergence in such a self-consistent classical dynamics. These difficulties reflect the quantum mechanical entanglement between the nuclear and electronic motions in the sense of eq 19.

One remarkable property of the Pechukas force is seen in the following conservation laws. Conservation of "energy" is assured by

$$\frac{\mathrm{d}}{\mathrm{d}t}\left(\frac{1}{2}M\dot{\mathbf{R}}^2 + \mathrm{Re}\frac{\langle\beta|\hat{U}(t'',t)H^{\mathrm{el}}\hat{U}(t,t')|\alpha\rangle}{\langle\beta|\hat{U}(t'',t')|\alpha\rangle}\right) = 0 \tag{40}$$

while the conservation of "angular momenta" for a system with central symmetry becomes

$$\frac{\mathrm{d}}{\mathrm{d}t}\left(M\mathbf{R}\times\dot{\mathbf{R}} + \mathrm{Re}\frac{\langle\beta|\hat{U}(t'',t)\mathcal{J}^{\mathrm{el}}\hat{U}(t,t')|\alpha\rangle}{\langle\beta|\hat{U}(t'',t')|\alpha\rangle}\right) = 0 \tag{41}$$

dx.doi.org/10.1021/cr200096s |Chem. Rev. 2012, 112, 499–542

where $\mathscr{J}^{el} \equiv \mathscr{J}^{tot} - M\mathbf{R} \times \dot{\mathbf{R}}$ is the angular momentum operator for the internal degrees of freedom. Although the conserved quantities in eqs 40 and 41 are not energy or angular momenta in the usual sense, they lead to the conservation of the corresponding quantities in the asymptotic region, where α and β label the eigenstates of the corresponding quantities. If the initial and final states are the energy eigenstates of $H^{el}(\mathbf{R}(t'))$ and $H^{el}(\mathbf{R}(t''))$ with eigenvalue $E_\alpha(\mathbf{R}(t'))$ and $E_\beta(\mathbf{R}(t''))$, respectively, then

$$E_\alpha(\mathbf{R}(t')) + \frac{M}{2}\dot{\mathbf{R}}(t')^2 = E_\beta(\mathbf{R}(t'')) + \frac{M}{2}\dot{\mathbf{R}}(t'')^2 \tag{42}$$

These conservation laws apply for each final state. In view of the fact that nonadiabatic interaction leads to multiple final states from a single initial state, the conservation laws as depicted in eq 42 apply in a per-branch manner. Although simple looking in many other approximation schemes, however, per-branch conservation does not hold automatically. Indeed, mean-field schemes such as the semiclassical Ehrenfest theory (SET) (see section 3.2 for details) only conserve state-averaged quantities and sometimes lead to severe violation of the conservation of per-branch energy. Surface hopping algorithms including the Tully fewest switching method can keep per-branch conservation only by imposing it on each hopping. In view of the theoretical clarity of its derivation and the favorable conserving natures, the Pechukas formalism, aside from its hard tractability, is certainly one of the best theories for extracting the essential nature of nonadiabatic dynamics in a mixed quantum and classical representation.

Recently, Krishna developed a path integral approach to electron−nucleus nonadiabatic dynamics where the electronic part of the path integral is formulated in an explicit manner using the coherent state representation.[127] The electronic path integral, in discretized form, is given as

$$\begin{aligned}\mathscr{K}^{el}_{\beta\alpha}[\mathbf{R}] = \int \prod_{n=0}^{N-1} \{ &d\mu[\xi_n(\mathbf{R}_n)]\, d\mu[\eta_n(\mathbf{R}_n)] \\ &\times \langle \xi_{n+1}(\mathbf{R}_{n+1})|\eta_n(\mathbf{R}_n)\rangle \\ &\times \langle \eta_n(\mathbf{R}_n)|e^{-(i/\hbar)\varepsilon H^{el}(\mathbf{R}_n)}|\xi_n(\mathbf{R}_n)\rangle\} \\ &\times \langle \xi_0(\mathbf{R}_0)|\alpha(\mathbf{R}_i)\rangle\end{aligned} \tag{43}$$

where $\mathbf{R}_n$ is the nuclear position at time t_n, while $d\mu\xi_n[(\mathbf{R}_n)]$ indicates an appropriate path integral measure, and ξ_N should be understood as being β. From eq 43, it turns out that the derivative coupling terms in the path-integral formalism arise from an overlap integral between electronic basis functions at different nuclear positions as

$$\begin{aligned}&\langle \xi_{n+1}(\mathbf{R}_{n+1})|\eta_n(\mathbf{R}_n)\rangle \\ &\quad = \sum_{I,J} \xi^{*I}_{n+1}(\delta_{IJ} - (\mathbf{R}_{n+1} - \mathbf{R}_n)\langle \Phi_I(\mathbf{R}_n)|\nabla\Phi_J(\mathbf{R}_n)\rangle)\eta^J_n\end{aligned} \tag{44}$$

where the electronic states are expanded as $|\xi\rangle = \Sigma_I \xi^I |\Phi_I(\mathbf{R})\rangle$ with an appropriate basis set $\{|\Phi_I(\mathbf{R})\rangle\}$. Krishna then applied the stationary phase approximation to the nuclear path integral to obtain a classical nuclear equation of motion. In his paper, Krishna attempted to set a theoretical foundation for the surface hopping model of Tully.[6,116] Thus, the resulting equation, eq 40 of ref 127, is different from eq 38 but rather close in nature to eq 50 in that the force working on the nuclei is given in an explicit and path-independent manner as the expectation value of electronic operators.

Another contribution to the path-integral formulation has been made by Hanasaki and Takatsuka,[128] in which nonadiabatic nuclear path dynamics manifestly represents the quantum wavepacket bifurcation (recall section 1.3) in a path-branching manner rather than the electron−nucleus self-consistent dynamics within a single path. This aspect highlights the fundamental aspects of nonadiabaticity and will be discussed in greater detail in section 3.7.

3.2. Semiclassical Ehrenfest Theory as a Starting Model

In clear contrast to the Pechukas path integral formalism, the semiclassical Ehrenfest theory (SET) rests on the rather intuitive idea that electronic state mixing to propagate electronic wavepackets should be explicitly taken into account along a nuclear path, which is in turn driven by the Newtonian force (actually the Hellmann−Feynman force) averaged over thus to-be-obtained electronic wavepackets. This idea seems quite natural and has attained much popularity. To describe SET more explicitly, we first expand the electronic wave function $|\Psi(\mathbf{R}(t))\rangle$ at a nuclear position $\mathbf{R}(t)$ in basis functions $\{\Phi_J(\mathbf{R}(t))\}$ as

$$|\Psi(\mathbf{R}(t))\rangle = \sum_J C_J(t)|\Phi_J(\mathbf{R}(t))\rangle \tag{45}$$

The most naive expression for the equation of electronic motion is

$$i\hbar \frac{\partial}{\partial t} C_J = \sum_K [H^{el}_{JK} - i\hbar\dot{\mathbf{R}}(t)\cdot\mathbf{X}_{JK}]C_K \tag{46}$$

where

$$X^k_{JK} \equiv \left\langle \Phi_J(\mathbf{R}(t)) \middle| \frac{\partial}{\partial R_k} \middle| \Phi_K(\mathbf{R}(t)) \right\rangle \tag{47}$$

The propagation of $|\Psi(\mathbf{R}(t))\rangle$ is coupled with that of a nuclear path $\mathbf{R}(t)$, with the force working on it being given as

$$M_k\ddot{\mathbf{R}}_k = -\sum_J \sum_K C^*_J C_K \left\langle \Phi_J(\mathbf{R}(t)) \middle| \frac{\partial H^{el}}{\partial R_k} \middle| \Phi_K(\mathbf{R}(t)) \right\rangle \tag{48}$$

where M_k is the nuclear mass in the k-direction.

Since one can readily derive these equations in an analogous way to that of the Ehrenfest theory, they seem to be correct. However, in reality they are not quite right and indeed need some correction terms, as we will discuss later. Also, when our electronic basis set at hand $\{\Phi_J(\mathbf{R}(t))\}$ is incomplete, which is overwhelmingly the case, the force of eq 48 should be replaced with the expression[129]

$$M_k\ddot{\mathbf{R}}_k = -\sum_{I,J,K} C^*_I(X^k_{IK}H^{el}_{KJ} - H^{el}_{IK}X^k_{KJ})C_J - \sum_{IJ} C^*_I \frac{\partial H^{el}_{IJ}}{\partial R_k} C_J \tag{49}$$

This is a practical working equation, since the Hellmann−Feynman force is of low quality, in general, for a finite basis set.

SET gives quite a vivid view of electron wavepacket dynamics in a very compact manner. It works quite well for a system with a broad distribution of nonadiabatic coupling elements, and there is no need to assume an explicit functional form of it. Besides, SET has no particular difficulty in handling multidimensional nonadiabatic systems. All these technical advantages are made available by progress in *ab initio* quantum chemistry (see Appendix A for this aspect).

The most undesired characteristic of SET, on the other hand, arises from eq 48. It is widely known that a nuclear classical path propagated by the mean force as shown in eq 48 keeps running on the resultant mean field without converging to one of adiabatic potentials even in the asymptotic region far beyond the nonadiabatic coupling region. This indicates that the Born−Oppenheimer view, that a path should run on an adiabatic potential energy surface, will be lost, once a path passes across any one of the nonadiabatic region. This erratic behavior is often ascribed to the persistence of electronic quantum-coherence without decoupling ever.[14] Exploring this aspect of coherence and decoherence in mixed quantum and classical dynamics is one of the main topics in the remaining part of this section.

Let us compare the mean-field force formulated in SET with the Pechukas force of eq 48. This confirms that the former is not quite right, which again gives us an opportunity to consider the nature of the "classical force" working on nuclei in nonadiabatic systems. For clarity, here we define what we call the mean-field force as a force that is expressed as the expectation value of an electronic matrix, which is essentially $-\partial H^{\mathrm{el}}(\mathbf{R})/\partial \mathbf{R}$, although details may depend on methods. Thus, the Newtonian equation of motion for nuclei should look like

$$M\ddot{\mathbf{R}} = -\frac{\langle \alpha|\hat{U}(t',t)\,\dfrac{\partial H^{\mathrm{el}}(\mathbf{R})}{\partial \mathbf{R}}\,\hat{U}(t,t')|\alpha\rangle}{\langle \alpha|\hat{U}(t',t)\,\hat{U}(t,t')|\alpha\rangle} \tag{50}$$

The difference between eq 50 and a more accurate one, eq 38, should be clearly appreciated. As can be readily seen, the SET dynamics can be integrated explicitly without iteration; this is in contrast to eq 38. We also note that the conserved quantities are also different. For example, that for energy-related quantity becomes

$$\frac{\mathrm{d}}{\mathrm{d}t}\left(\frac{1}{2}M\dot{\mathbf{R}}^2 + \frac{\langle \alpha|\hat{U}(t',t)H^{\mathrm{el}}\hat{U}(t,t')|\alpha\rangle}{\langle \alpha|\hat{U}(t',t')|\alpha\rangle}\right) = 0 \tag{51}$$

which only states the conservation of the state-averaged energy.

3.3. Quantum Variables Mapped to Classical Ones: The Meyer−Miller Method

We next proceed to an interesting variant of the SET. Imagine a chemical reaction on a single PES, whose initial and final vibrational quantum numbers are denoted as n_i and n_f, respectively. In semiclassical theory, these quantized states are specified in terms of the action integral satisfying the quantization condition such as

$$\oint_{C_\alpha} \sum_j p_j\,\mathrm{d}q_j = \left(n_\alpha + \frac{\lambda_\alpha}{2}\right)\hbar \tag{52}$$

where $\{q_j,p_j\}$ are the positions and the associated momenta, respectively, in the initial or final states and λ_α is the Maslov index along the circuit path C_α. The computation of the reaction S-matrix from n_i to n_f in the classical S-matrix theory[130−132] is reduced to the problem of finding a classical trajectory connecting those having the relevant action variables. This is an example of mapping of a quantum degree of freedom to a (set of) classical degree(s) of freedom. In this way, the quantum numbers are replaced with the classical action integral. Meyer and Miller[133] showed that an analogous mapping is also possible in the case of nonadiabatic chemical reactions.

We start with an expansion of the expectation value of the electronic Hamiltonian in a *diabatic* basis

$$\langle \Psi(t)|H^{\mathrm{el}}(\mathbf{R}(t))|\Psi(t)\rangle = \sum_{J,K} C_J^* C_K H_{JK}^{\mathrm{el}} \tag{53}$$

Meyer and Miller map the quantum-mechanical degree of freedom C_K to a pair of classical degrees n_K and q_K, which are analogues of "action" and "angle" variables, respectively, in the manner

$$C_K = \sqrt{n_K}\mathrm{e}^{-iq_K} \tag{54}$$

Equation 53 now becomes

$$\sum_{J,K} \sqrt{n_J(t)\,n_K(t)}\,\mathrm{e}^{i(q_J(t)\,-\,q_K(t))}H_{JK}^{\mathrm{el}} \equiv H^{\mathrm{el}}(\mathbf{n},\mathbf{q};\mathbf{R}(t)) \tag{55}$$

which is combined with the nuclear kinetic term as

$$H(\mathbf{n},\mathbf{q};\mathbf{R}(t)) = \sum_k \frac{\mathbf{P}_k^2}{2M_k} + H^{\mathrm{el}}(\mathbf{n},\mathbf{q};\mathbf{R}(t)) \tag{56}$$

to give the total effective Hamiltonian. The variational principle shows that the new variables now satisfy the Hamilton canonical equations of motion such that

$$\dot{n}_K = -\frac{\partial H(\mathbf{n},\mathbf{q};\mathbf{R}(t))}{\partial q_K} \quad \text{and} \quad \dot{q}_K = \frac{\partial H(\mathbf{n},\mathbf{q};\mathbf{R}(t))}{\partial n_K} \tag{57}$$

which makes it possible to analyze the electronic dynamics with the semiclassical propagator.

In practical applications of the above "classical" dynamics of electrons to the classical S-matrix theory, the choice of the initial phase degrees of freedom, $\{q_K\}$, is crucial for a path initiated in this manner to be able to reach the desired final condition on $\{n_K\}$. In order to realize the special condition $n_K(t_i) = \delta_{K,\alpha}$ and $n_K(t_f) = \delta_{K,\beta}$, the electronic Hamiltonian of eq 55 has to be further converted to a Langer-modified form,

$$H^{\mathrm{el}}(\mathbf{n},\mathbf{q};\mathbf{R}(t)) = \sum_{J,K} \sqrt{\left(n_J(t) + \frac{1}{2}\right)\left(n_K(t) + \frac{1}{2}\right)} \times \mathrm{e}^{i(q_J(t)\,-\,q_K(t))}H_{JK}^{\mathrm{el}} - \frac{1}{2}\sum_K H_{KK}^{\mathrm{el}} \tag{58}$$

If one can find such a path, the transition probability is then obtained by

$$P_{\beta\alpha} = \left[(2\pi)^{N_s}\left|\frac{\partial \mathbf{n}(t_f)}{\partial \mathbf{q}(t_i)}\right|^{-1}\right] \tag{59}$$

where N_s is the number of states that are taken into account. On the basis of the above reformulation, Sun and Miller[134] demonstrated the success of this nonadiabatic theory in three typical models proposed by Tully by using their algorithm combined with the initial value representation in path integration. Following this work, Sun, Wang, and Miller[135] also showed that a linear approximation of the time correlation function can capture the nature of nonadiabatic transition dynamics qualitatively quite well.

A similar type of semiclassical approach was developed by Stock and Thoss.[136,137] Here again electronic states and operators are "mapped" into c-number variables and treated classically:

dx.doi.org/10.1021/cr200096s |Chem. Rev. 2012, 112, 499–542

Quantum mechanical states $\{|\Phi_I\rangle\}$ and the associated operators are mapped into the Fock states $\{|n_1, ..., n_N\rangle\}$ and to the associated creation/annihilation operators $\{a_I^\dagger, a_I\}$ in the following manner,

$$|\Phi_I\rangle \rightarrow |0_1, ..., 1_I, ..., 0_N\rangle$$

$$|\Phi_I\rangle\langle\Phi_J| \rightarrow a_I^\dagger a_J \tag{60}$$

Then the creation/annihilation operators are transformed into pairs of operators $q_I \equiv (a_I + a_I^\dagger)/(2)^{1/2}$ and $p_I \equiv i(a_I^\dagger - a_I)/(2)^{1/2}$, which satisfy $[q_I p_J] = i\hbar\delta_{IJ}$. The total Hamiltonian (again in a diabatic representation) becomes

$$H = \sum_k \frac{\mathbf{P}_k^2}{2M_k} + \frac{1}{2}\sum_{I,J} H_{IJ}^{el}(q_I q_J + p_I p_J) - \frac{1}{2}\sum_I H_{II}^{el} \tag{61}$$

From the transformed Hamiltonian in eq 61, a classical approximation is derived by the standard procedure of replacing the operators q_I, p_I by classical variables and commutators to Poisson brackets. The time evolution of these variables, together with the nuclear degrees of freedom **R** and **P**, are calculated using the semiclassical initial value representation (IVR) propagator.[134,135] In construction, the method closely resembles the mean-field method. The electronic part of the Hamiltonian equation (eq 61) is actually equivalent to the expectation value of eq 53 apart from the last term in eq 61. However, there is one interesting aspect to this mapping technique. Stock and Thoss[136] claim that it can reproduce the correct density of states in a double well model whereas the mean-field approach cannot.

3.4. Tully's Fewest Switch Surface Hopping Method and Its Variants

As explained already in this review, the naive surface hopping model allows a classical trajectory on an adiabatic potential surface to jump from one to another at a specific point with a transition probability borrowed from other theories. Although this artificial procedure sometimes provides a good description of population dynamics, depending on the geometrical condition of nonadiabatic dynamics under study, the electronic coherence is totally neglected. In other words, the dynamical self-consistency between electrons and nuclei is totally violated. To overcome this drawback, Tully proposed an algorithm which takes into account the electronic coherence along a path, and the hopping points are modified by the electronic transitions.[6]

The basic idea of the algorithm is to allow a path to jump with the probability that is estimated internally (in a self-contained manner) with the electronic-state mixing, as happens in the semiclassical Ehrenfest theory, but the number of hops should be minimized. If we have an electronic wavepacket $|\Phi(t)\rangle = \Sigma_I C_I(t)|\Phi_I\rangle$ as in the SET, the dynamics of the corresponding density matrix, $\rho_{IJ}(t) \equiv C_I^*(t)\, C_J(t)$, is written as

$$\dot{\rho}_{IJ} = \frac{1}{i\hbar}\sum_K (H_{IK} - i\hbar\dot{\mathbf{R}}\cdot\mathbf{X}_{IK})\rho_{KJ} - \frac{1}{i\hbar}\sum_K (H_{JK}^* + i\hbar\dot{\mathbf{R}}\cdot\mathbf{X}_{JK})\rho_{KI}^* \tag{62}$$

Our main interest is in its diagonal part, which is compactly expressed as

$$\dot{\rho}_{II} = \sum_K B_{IK} \tag{63}$$

where

$$B_{IK} \equiv \frac{2}{\hbar}\mathrm{Im}\{H_{IK}\rho_{KI}\} - 2\mathrm{Re}\{\dot{\mathbf{R}}\cdot\mathbf{X}_{IK}\rho_{KI}\} \tag{64}$$

Using this, one can estimate the transition probability going from the state K to the state I during a short time step, $\tau \rightarrow \tau + d\tau$, as

$$G_{IK} \equiv \begin{cases} 0 & (B_{IK} \le 0) \\ \dfrac{B_{IK}(\tau + d\tau)\, d\tau}{\rho_{KK}(\tau + d\tau)} & (B_{IK} > 0) \end{cases} \tag{65}$$

This in turn can be used to determine stochastically the points of trajectory hopping in the dynamics without any external parameter. One exception is that of nonclassical cases due to the uncertainty principle.[138] It should also be noted that momentum scaling for energy conservation of a hopping trajectory cannot be free of ambiguity with respect to its direction in a multidimensional case. This may be partly augmented by using a semiclassical analysis.[139,140] One can, however, make a compromise in determining the number of hops and the quality of the transition probability obtained. The "fewest switch surface hopping method" has been recently extended to a study of laser control of electron−nuclear coupled dynamics. Here the time-dependent electric field, rather than nonadiabatic coupling, causes a state transition.[98]

Recently, Shenvi[117] proposed using the scheme of the fewest switching surface hopping algorithm combined with the so-called phase-space adiabatic basis, which is defined as follows. Consider that the Hamiltonian for nuclei is as follows

$$H_{JK}(\mathbf{R}, \mathbf{P}) = \frac{1}{2M}(\delta_{JK}\mathbf{P} - i\hbar\mathbf{X}_{JK}(\mathbf{R}))^2 + H_{JJ}^{el}(\mathbf{R})\delta_{JK} \tag{66}$$

where the nonadiabatic coupling is explicitly included. (See ref 16 for an extensive discussion and algebra arising from this gauge-field type Hamiltonian.) It follows that one can now diagonalize this matrix defined at each nuclear phase-space point, attaining $E_n(\mathbf{R},\mathbf{P})$ as its eigenvalues. Furthermore, if one regards $E_n(\mathbf{R},\mathbf{P})$ as a classical Hamiltonian, one can now generate classical paths. In turn, these are used in the fewest switch surface hopping method. Shenvi illustrated that this method, known as the phase-space surface hopping method, gives an excellent nonadiabatic transition probability even in a low energy case.

Another rather obvious aspect that needs to be improved is that of classically forbidden transitions. Truhlar et al. proposed a time-energy uncertainty approach as a remedy for jumping positions.[10]

Furthermore, there are some theoretical problems remaining which need to be discussed with a view to attaining the ultimately ideal nonadiabatic-transition theory: Although a multihopping trajectory converges to run on an adiabatic potential surface asymptotically, the off-diagonal density matrix element $\rho_{IJ}(t)$ does not actually vanish. This is ascribed to an incomplete treatment of the nuclear-electronic entanglement. This issue, often referred to as "the problem of decoherence", has its origins in the nuclear wavepacket bifurcation due to different slopes of potential surfaces. This will be discussed more precisely below.

3.5. Notion of Decoherence in Quantum Subsystems and Decoherence Time

Decoherence is an essential issue that appears in a system in which a quantum subsystem is in contact with a classical subsystem in one way or another. As is widely recognized, the SET cannot

describe such dynamics, since there is no mechanism in it to switch off the electronic coherence along the nuclear path. The decoherence problem is critically important, not only in our nonadiabatic dynamics but also in other contemporary science such as spin-Boson dynamics in quantum computation theory and, more extensively, in quantum theory in open (dissipative) systems.[141] The decoherence problem is also critical to chaos induced by nonadiabatic dynamics.[142−146] Therefore, in the rest of this section, we will pay deeper attention to the aspect of the effect of electronic state decoherence strongly coupled with the relevant nuclear motion. A review regarding the notion of decoherence related to quantum mechanical measurement theory is found in papers by Rossky et al.[147]

Neria and Nitzan[148] proposed an idea for "artificially" removing the electronic coherence by damping the off-diagonal terms of the electronic density matrix. To do so, they defined a damping time, or decoherent time, in terms of the characteristic time for a wavepacket $\chi(t)$ running on a reference potential energy surface to lose its overlap with its bifurcating counterpart into the Kth surface $\chi_K(t)$. They assume such an overlap integral and approximate it in a Gaussian process as

$$|\langle\chi_K(t)|\chi(t)\rangle| \approx \exp\left(- \sum_n \frac{\left(F^n(0) - F_K^n(0)\right)^2}{4a_n\hbar^2} t^2 \right) \tag{67}$$

Here a_n is a Gaussian width for the nuclear nth degree of freedom. $F^n(0)$ and $F_K^n(0)$ are the nth component of mean-force and Kth adiabatic force vectors, respectively. This suggests that the decoherence time τ_K is

$$\tau_K = \left(\sum_n \frac{\left(F^n(0) - F_K^n(0)\right)^2}{4a_n\hbar^2} \right)^{-1/2} \tag{68}$$

This property is expected to reflect the basic feature of "damping of coherence". Subtonik et al.[149,150] proposed even more sophisticated formulas to remove the artificial parameter a_n.

3.6. Decay of Mixing with Coherence Switching

In their studies of nonadiabatic dynamics in condensed phases, Rossky and his co-workers emphasized the role of stochastic perturbations that actually decohere the quantum system that are surrounded by an outer classical system (solute state). This is one of the most significant phenomena in the dynamics of open systems. On the other hand, where nonadiabatic dynamics within a single molecule or isolated molecular reaction system is concerned, it is Hack, Jasper, and Truhlar[7−10] who first devised how to implement the decay of electronic state coherence, or decay of mixing, into the nuclear dynamics of an individual path. Hence, they brought about the notion of a non-Born−Oppenheimer path in an explicit manner.

As in the work of Neria and Nitzan,[148] Truhlar et al. also studied how the off-diagonal elements of the electronic density matrix can vanish after the nonadiabatic coupling is switched off. Then they introduced an external force into the semiclassical Ehrenfest nuclear dynamics such that it can cancel the persisting coherence. The construction of this force is rather artificial, but it is quite well designed in such a way as to fulfill the conservation laws of energy and linear momentum. It is summarized as follows. Let us consider the semiclassical Ehrenfest dynamics of the off-diagonal electronic density matrix ρ_{IJ}^{SE}, to which an additional term $\dot{\rho}_{IJ}^{\mathrm{D}}$ is added in the form of $\dot{\rho}_{IJ} = \dot{\rho}_{IJ}^{\mathrm{SE}} + \dot{\rho}_{IJ}^{\mathrm{D}}$. Here, ρ_{IJ}^{D} is responsible for canceling the coherence remaining in ρ_{IJ}^{SE}, thus making the off-diagonal elements of ρ_{IJ} vanish. To realize such dynamics, the Hamilton canonical equations of motion (in the SET dynamics) are modified by adding external velocity and force in such a way that $\dot{\mathbf{R}} = \dot{\mathbf{R}}^{\mathrm{SE}} + \dot{\mathbf{R}}^{\mathrm{D}}$ and $\dot{\mathbf{P}} = \dot{\mathbf{P}}^{\mathrm{SE}} + \dot{\mathbf{P}}^{\mathrm{D}}$, respectively, to decohere in the electronic state mixing. These additional terms $(\dot{\mathbf{R}}^{\mathrm{D}},\dot{\mathbf{P}}^{\mathrm{D}})$ are designed such that they are switched off after a decoherence time and asymptotically, and as a result, the path should run on one of the desired adiabatic potentials. Various ways of determining the key quantities, the decoherence time and $(\dot{\mathbf{R}}^{\mathrm{D}},\dot{\mathbf{P}}^{\mathrm{D}})$, have been proposed by the original authors.[7−10] With this intelligent but artificial treatment, a nonadiabatic path is continuously evolved in time without surface hopping and with the correct momentum and energy conserved. The electronic-state mixing is carried out consistently along every non-Born−Oppenheimer path. Thus, the transition probability may be determined in terms of the ratio of the number of asymptotic paths accumulated on the individual potential surfaces. On the other hand, the electronic-state mixing, due to the semiclassical Ehrenfest dynamics on each path, should give a nonadiabatic transition-amplitude along with an associated phase. It is not clear though whether these two pieces of information about transition probability are always consistent with each other.

It is interesting to compare the Truhlar non-Born−Oppenheimer path with those expected to emerge from the treatment according Pechukas as in eq 38. In the latter, a non-Born−Oppenheimer path, if it indeed exists, starts from one adiabatic potential energy surface and it continues to another continuously without hopping, yet it is being driven by the nonadiabatic coupling. It should be remembered, however, that it can be determined only through a self-consistent manner. This, of course, requires essentially an iterative computation. This is the way of decoherence according to the Pechukas theory. On the other hand, Truhlar's theory produces a smooth path connecting two different potential energy surfaces without any self-consistent procedure. It is therefore an interesting issue to comprehend how these two paths are theoretically related. For instance, one may be led to the conjecture that if the Truhlar paths are geometrically akin to the Pechukas paths, then Pechukas' self-consistent procedure can be avoided only by introducing an external force. This can further lead to the conclusion that a global solution in the mechanics of eq 38 does not always exist. This is not an absurd notion, if we recall that the essential feature of nonadiabatic dynamics is, in fact wavepacket branching, which is hard to represent directly in terms of a set of continuous nonbranching global paths.

3.7. Spontaneous Entanglement and Decoherence between Electrons and Nuclei along Smoothly Branching Non-Born−Oppenheimer Paths

In order to overcome the difficulty associated with the SET regarding the decoherence mechanism, some interesting and theoretically exciting ideas and inputs have been proposed, as we saw above. However, it seems to the present authors that most of these studies simply accepted the SET as it stands. In other words, to the best of our knowledge, there has been no clear derivation of the semiclassical Ehrenfest theory in a way that identifies and isolates the actual origin of the difficulty. This is essential if progress is to be made.

Another aspect we have to take account to go beyond the SET is the coupling of native nonadiabatic dynamics with the induced one by intense pulse and continuous lasers. Almost all the classic theories presented in the preceding section, from the Landau−Zener to the primitive surface hopping method, are not designed

dx.doi.org/10.1021/cr200096s |Chem. Rev. 2012, 112, 499–542

to cope with this very important aspect of modern chemical dynamics. Likewise, it is not easy to imagine that the methods reviewed in this section, such as the fewest switch surface hopping method and the method of natural decay of mixing, can handle this problem without tremendous additional efforts in reformulation. On the other hand, interestingly and ironically, it is easy to incorporate the classical electromagnetic vector potential into the SET. Hence, rather than abandoning this convenient theory, we should really restart from the very basic point of quantum-classical correspondence to identify the origin of the in-built difficulties of the problem.

3.7.1. Mixed Quantum-Classical Hamiltonian in an Optical Field. We now resume the study of nonadiabaticity by representing the total Hamiltonian in a specific way, rather than the standard one as shown in eq 1. In addition, an explicit account of the classical vector potential **A** of an electromagnetic field, according to our general scenario of electron dynamics in laser fields, will be considered. First we will write the standard form of the Hamiltonian as

$$\mathscr{H}(\mathbf{r},\mathbf{R}|\mathbf{A}) = \frac{1}{2}\sum_{k=1}^{3N_n}\left(\hat{P}_k - \frac{Z_k e}{c}A_k(\mathbf{R})\right)^2 + \mathscr{H}^{\mathrm{el}}(\mathbf{r};\mathbf{R}|\mathbf{A}) \tag{69}$$

with $\mathscr{H}^{\mathrm{el}}(\mathbf{r};\mathbf{R}|\mathbf{A})$ being the electronic Hamiltonian under the electromagnetic field

$$\mathscr{H}^{\mathrm{el}}(\mathbf{r};\mathbf{R}|\mathbf{A}) = \frac{1}{2}\sum_{j=1}^{3N_e}\left(\hat{p}_j + \frac{e}{c}A_j(\mathbf{r})\right)^2 + V_c(\mathbf{r};\mathbf{R}) \tag{70}$$

where V_c collectively denotes the electron−electron, electron−nuclei, and nuclei−nuclei Coulombic interactions. **R** is the collective vector of all the nuclear positions with $\hat{\mathbf{P}} = \{\hat{P}_k | k = 1, ..., 3N_n\}$ being the vector of associated momenta. N_e and N_n are the number of electrons and nuclei in a molecule, respectively. Throughout this section, we use the mass-weighted coordinates, in which all the masses are scaled to unity. $Z_k e$ and c are the nuclear charge and the light velocity, respectively, with $-e$ being the electron charge. The hats, as in $\hat{P}$, denote the quantum operators. $A_k(\mathbf{R})$ and $A_j(\mathbf{r})$ are the vector potentials of the classical electromagnetic field, with the vector components x, y, and z, and the particle positions of each nucleus and electron are denoted collectively by the suffices k and j, respectively, in the standard manner.

We next reexpress the Hamiltonian in eq 69, which is represented in configuration space $\{\mathbf{r},\mathbf{R}\}$, in the electronic Hilbert space, and in nuclear configuration space, whose basis is $\{|\Phi_I(\mathbf{R})\rangle|\mathbf{R}\rangle\}$, such that[82,151]

$$\mathscr{H}(\mathbf{R},\mathrm{elec},\mathbf{A}) \equiv \frac{1}{2}\sum_k\left\{\hat{P}_k - \frac{Z_k e}{c}A_k - i\hbar\sum_{IJ}|\Phi_I\rangle X_{IJ}^k\langle\Phi_J|\right\}^2 + \sum_{IJ}|\Phi_I\rangle\mathscr{H}_{IJ}^{\mathrm{el}}\langle\Phi_J| \tag{71}$$

where $X_{IJ}^k \equiv \langle\Phi_I|(\partial/\partial R_k)\Phi_J\rangle$ and $\mathscr{H}_{IJ}^{\mathrm{el}} \equiv \langle\Phi_I|\mathscr{H}^{\mathrm{el}}(\mathbf{r};\mathbf{R}|\mathbf{A})|\Phi_J\rangle$. By comparison of eq 71 with eqs 8, 56, and 66, Σ_{IJ} in eq 71 may include an integral over the continuum states. Although this is a slight extension of the gauge-type Hamiltonian in nuclear configuration space, such as in eq 8, the difference in outcome is quite significant. This Hamiltonian manifests a parallelism between the electromagnetic effects and nonadiabatic coupling. It is well-known that the Longuet−Higgins[102] (or Berry[103]) phase arising from nonadiabatic interactions induces an effect similar to the Aharonov−Bohm effect.[152] Also, a Lorentz-force-like term arising from the nonadiabatic coupling is worth discussing.[82]

To attain a mixed quantum-classical representation, we classicalize the above Hamiltonian (eq 71) so as to make it more easily accessible to its (approximate) solutions. This is done by simply changing the nuclear momentum operator $\hat{P}_k$ in $\mathscr{H}(\mathbf{R},\mathrm{elec},\mathbf{A})$ to its classical counterpart P_k such that

$$\tilde{\mathscr{H}}(\mathbf{R},\mathbf{P},\mathrm{elec},\mathbf{A}) \equiv \frac{1}{2}\sum_k\left(P_k - \frac{Z_k e}{c}A_k - i\hbar\sum_{IJ}|\Phi_I\rangle X_{IJ}^k\langle\Phi_J|\right)^2 + \sum_{IJ}|\Phi_I\rangle\mathscr{H}_{IJ}^{\mathrm{el}}\langle\Phi_J| \tag{72}$$

The tilde over $\mathscr{H}$ indicates this type of mixed quantum-classical representation.

The dynamical equations of motion for the electron wavepacket are derived in terms of the time-dependent variational principle, subject to

$$\delta\int \mathrm{d}t\,\langle\Phi(\mathbf{R},t)|\left(i\hbar\frac{\partial}{\partial t} - \tilde{\mathscr{H}}(\mathbf{R},\mathbf{P},\mathrm{elec},\mathbf{A})\right)|\Phi(\mathbf{R},t)\rangle = 0 \tag{73}$$

where $\tilde{H}(\mathbf{R},\mathbf{P},\mathrm{elec},\mathbf{A})$ are the total Hamiltonian as defined in eq 72. As usual, we expand the electronic wavepacket as

$$\Phi(\mathbf{r},t;\mathbf{R}(t)) = \sum_I C_I(t)\,\Phi_I(\mathbf{r};\mathbf{R})|_{\mathbf{R}=\mathbf{R}(t)} \tag{74}$$

where $\{\Phi_I(\mathbf{r};\mathbf{R})\}$ are basis functions such as the Slater determinants generated at each nuclear position **R**. Hence, the electronic dynamics is cast into the associated coefficients $\{C_I(t)\}$. Taking into account the right as well as the left variation in eq 73, we obtain the coupled equations for the electron dynamics as

$$i\hbar\frac{\partial}{\partial t}C_I = \sum_J\left[\mathscr{H}_{IJ}^{\mathrm{el}} - i\hbar\sum_k\left(P_k - \frac{Z_k e}{c}A_k\right)X_{IJ}^k - \frac{\hbar^2}{4}\sum_k(Y_{IJ}^k + Y_{JI}^{k*})\right]C_J \tag{75}$$

Equation 75 represents the generalization of the electron wavepacket theory to the dynamics in the optical field.[151] Note that the second derivative coupling elements, $Y_{IJ}^k \equiv \langle\Phi_I|(\partial^2/\partial R_k^2)|\Phi_J\rangle$, in this expression have no direct interaction with the external vector potential **A**, while the first derivative coupling elements X_{IJ}^k do.

We next establish the nuclear equations of motion. The classical analogue of the Hamilton canonical equations of motion gives the following set of equations.[151,153−155]

$$\frac{\mathrm{d}^2}{\mathrm{d}t^2}\mathscr{R}^k = -\sum_{IJ}\frac{\partial}{\partial R_k}(|\Phi_I\rangle\mathscr{H}_{IJ}^{\mathrm{el}}\langle\Phi_J|) - \frac{Z_k e}{c}\frac{\partial}{\partial t}A_k(\mathbf{R},t) + i\hbar\sum_{IJ}\sum_l\dot{R}_l\left[\frac{\partial}{\partial R_k}(|\Phi_I\rangle X_{IJ}^l\langle\Phi_J|) - \frac{\partial}{\partial R_l}(|\Phi_I\rangle X_{IJ}^k\langle\Phi_J|)\right] + \frac{e}{c}\sum_l\dot{R}_l\left(\frac{\partial}{\partial R_k}Z_l A_l - \frac{\partial}{\partial R_l}Z_k A_k\right) \tag{76}$$

This is defined in the joint nuclear $(\mathbf{R},\mathbf{P})$-space and the electronic Hilbert space. Therefore, to use this operator in practice, we

dx.doi.org/10.1021/cr200096s |Chem. Rev. 2012, 112, 499–542

should project it into a matrix form by sandwiching two electronic states. For example, $\langle\Phi_I|$ and $|\Phi_J\rangle$ give

$$\mathscr{T}^{i_a}_{IJ} \equiv \langle\Phi_I|\ddot{\mathscr{R}}^{i_a}|\Phi_J\rangle = -\sum_K [X^{i_a}_{IK}\mathscr{H}^{\mathrm{el}}_{KJ} - \mathscr{H}^{\mathrm{el}}_{IK}X^{i_a}_{KJ}] - \frac{\partial\mathscr{H}^{\mathrm{el}}_{IJ}}{\partial R_{i_a}} + i\hbar\sum_b^{\mathrm{nuc}}\sum_{i_b}^{x,y,z}\dot{R}_{i_b}\left[\frac{\partial X^{i_b}_{IJ}}{\partial R_{i_a}} - \frac{\partial X^{i_a}_{IJ}}{\partial R_{i_b}}\right] + Z_a e(\mathbf{E}_a + \dot{\mathbf{R}}_a \times \mathbf{B}_a)_{i_a}\delta_{IJ} \quad (77)$$

Here we have rewritten the suffixes such that a and b specify the nuclei and i_b, for instance, specifies one of the (x, y, z) coordinates in the Euclidean space for the nuclei. Equation 77 is a natural generalization of the classical force and is called the force matrix. Equations 75 and 77 highlight the present mixed quantum-classical dynamics beyond the Born−Oppenheimer framework, and solving them simultaneously is our ultimate goal. We will describe the relevant procedure to do so in section 3.7.3.

If a complete electronic basis were available, then the first three terms in the rightmost hand of eq 77 can be combined into a single term called the Hellmann−Feynman force

$$-\sum_K [X^{i_a}_{IK}\mathscr{H}^{\mathrm{el}}_{KJ} - \mathscr{H}^{\mathrm{el}}_{IK}X^{i_a}_{KJ}] - \frac{\partial\mathscr{H}^{\mathrm{el}}_{IJ}}{\partial R_{i_a}} = -\left(\frac{\partial\mathscr{H}^{\mathrm{el}}}{\partial R_{i_a}}\right)_{IJ} \quad (78)$$

Furthermore, it holds that

$$\left(\frac{\partial\mathscr{H}^{\mathrm{el}}}{\partial R_{i_a}}\right)_{IJ} = \left(\frac{\partial H^{\mathrm{el}}}{\partial R_{i_a}}\right)_{IJ} \quad (79)$$

Thus, the effect of the laser field on the force matrix through the reorganization of the electronic state should be quite limited (actually zero for a complete basis set). Only the classical Lorentz forces working on the nuclei are the dominant contribution to the force matrix.

3.7.2. The Semiclassical Ehrenfest Theory Revisited with Correction Terms. On the above theoretical basis, we can now revisit the semiclassical Ehrenfest theory (SET). Going back to the force (acceleration) operator in eq 76, let us take a simple average of it over an electron wavepacket as represented in eq 74. The result becomes

$$\langle\Phi|\ddot{\mathscr{R}}^{i_a}|\Phi\rangle = -\sum_{I,J,K} C^*_I(X^{i_a}_{IK}\mathscr{H}^{\mathrm{el}}_{KJ} - \mathscr{H}^{\mathrm{el}}_{IK}X^{i_a}_{KJ})C_J - \sum_{IJ} C^*_I\frac{\partial\mathscr{H}^{\mathrm{el}}_{IJ}}{\partial R_{i_a}}C_J + q_a e(\mathbf{E}_a + \dot{\mathbf{R}}_a \times \mathbf{B}_a)_{i_a} \quad (80)$$

This expression is theoretically valid even for finite bases. But, if a complete basis set were available, this expression would be reduced to the form using the Hellmann−Feynman force as

$$\langle\Phi|\ddot{\mathscr{R}}^{i_a}|\Phi\rangle = -\sum_{I,J} C^*_I\left(\frac{\partial\mathscr{H}^{\mathrm{el}}}{\partial R_{i_a}}\right)_{IJ}C_J + q_a e(\mathbf{E}_a + \dot{\mathbf{R}}_a \times \mathbf{B}_a)_{i_a} \quad (81)$$

Furthermore, if the optical interaction for electrons is independent of the nuclear coordinates, then the Hellmann−Feynman force in eq 81 turns out to be free of the optical term such that

$$\langle\Phi|\ddot{\mathscr{R}}^{i_a}|\Phi\rangle = -\sum_{I,J} C^*_I\left(\frac{\partial H^{el}}{\partial R_{i_a}}\right)_{IJ}C_J + q_a e(\mathbf{E}_a + \dot{\mathbf{R}}_a \times \mathbf{B}_a)_{i_a} \quad (82)$$

These nuclear dynamical equations should be solved simultaneously with the electronic dynamics of eq 75. The second order terms $-(\hbar^2/4)\Sigma_k(Y^k_{IJ} + Y^{k*}_{JI})$ in eq 75 are not found in the conventional (intuitively derived) semiclassical Ehrenfest theory.

Thus, the field-free semiclassical Ehrenfest theory has been extended to the case of electron dynamics in a laser field within the confines of the present theoretical scheme. In SET, the total electronic and nuclear wave function with an initial electronic wavepacket launched on a path $\mathbf{R}_{Ii}$ (the ith path on an electronic state I) should be represented as

$$\Phi_I(\mathbf{r};\mathbf{R}(t_{\mathrm{before}}))\,\delta(\mathbf{R} - \mathbf{R}_{Ii}(t_{\mathrm{before}})) \rightarrow \delta(\mathbf{R} - \langle\mathbf{R}\rangle(t_{\mathrm{after}}))\sum_K^{\mathrm{adiabatic\ PES}} C_K(t_{\mathrm{after}})\,\Phi_K(\mathbf{r};\langle\mathbf{R}\rangle(t_{\mathrm{after}})) \quad (83)$$

Here the left-hand side denotes the initial wave function, while the right-hand one represents a linear combination of the mixed components due to the nonadiabatic interaction and/or laser shining, and $\langle\mathbf{R}\rangle$ denotes a path running on the average potential energy surface.

Some observations regarding the property of the SET are in order at this point. As repeatedly emphasized, a path generated in the mean-field in the sense of eq 82 is totally unphysical after the passage of a nonadiabatic region in that it runs on an averaged potential energy surface. This is simply because *we* (not nature) keep taking an average of the force matrix as in eq 80 even after the nonadiabatic interaction is finished. To be more precise, the averaged potential in SET is simply a consequence of our wrong use of the force matrix, eq 77. Therefore, we really should stop averaging after the nonadiabatic interaction is switched off.

Nevertheless, where only a single passage is under consideration, SET using a single path gives quite an accurate transition probability (see ref 154 for numerical examples). This is because the coherent electronic state mixing, represented by eq 75, is taken into account all the way through the nonadiabatic interaction region. In fact, the SET equations in intense laser fields, using eqs 75 and 80 and neglecting $-(\hbar^2/4)\Sigma_k(Y^k_{IJ} + Y^{k*}_{JI})$, have been applied extensively to chemical dynamics by the present authors.[82,151,156] In particular, the role of the nonadiabatic coupling elements in electronic excitation with infrared lasers has been highlighted;[82] a calculation without the X^k_{IJ} term significantly underestimates the electronic transition.

3.7.3. Path Branching. We shall now seek out the correct solutions for the coupled equations shown in eqs 75 and 77. The electronic wavepacket propagates along nuclear paths that are driven by the force matrix. Suppose we have an electronic wavepacket $\Phi(\mathbf{r};\mathbf{R}(t))$ at a nuclear phase-space point $(\mathbf{R},\mathbf{P})$. To materialize an electronic-state mixing among given basis functions $\{\Phi_I(\mathbf{r};\mathbf{R})\}$ (either adiabatic or any diabatic basis), we must first integrate eq 75 for a short time, say, Δt, to give a new set of $\{C_I(t)\}$. Next we want to run a path using the force matrix $\mathscr{T}(\mathbf{R})$ of eq 77, again for a short time Δt. To avoid the additional

dx.doi.org/10.1021/cr200096s |Chem. Rev. 2012, 112, 499–542

mixing due to the off-diagonal elements of the force matrix, we diagonalize it at $\mathbf{R}$ such that

$$U(\mathbf{R})\ \mathscr{T}(\mathbf{R})\ U(\mathbf{R})^{-1} = \begin{pmatrix} f_1(\mathbf{R}) & 0 & \cdots \\ 0 & f_2(\mathbf{R}) & \\ \vdots & & \ddots \end{pmatrix} \tag{84}$$

with the associated electronic basis-set transformation

$$U(R)\begin{pmatrix} \Phi_1(\mathbf{r};\mathbf{R}) \\ \Phi_2(\mathbf{r};\mathbf{R}) \\ \vdots \end{pmatrix} = \begin{pmatrix} \lambda_1(\mathbf{r};\mathbf{R}) \\ \lambda_2(\mathbf{r};\mathbf{R}) \\ \vdots \end{pmatrix} \tag{85}$$

The electronic wavepacket obtained, as shown above, can be re-expanded in the eigenfunctions $\{\lambda_K(\mathbf{r};\mathbf{R})\}$ such that

$$\Phi(\mathbf{r};\mathbf{R}(t)) = \sum_K D_K(t)\ \lambda_K(\mathbf{r};\mathbf{R})|_{\mathbf{R}=\mathbf{R}(t)} \tag{86}$$

so that each electronic component $D_K(t)\ \lambda_K(\mathbf{r};\mathbf{R})$ can be carried by its own path, being driven by the eigenforce f_K to reach a new point after Δt. However, different eigenforces make different paths, even if they start from a single phase-space point $(\mathbf{R},\mathbf{P})$ as

$$(\mathbf{R},\mathbf{P}) \rightarrow (\mathrm{R}_K,\mathbf{P}_K) \tag{87}$$

Therefore, a path at $\mathbf{R}$ should be branched into as many components as the number of electronic states involved in the nonadiabatic coupling. The electronic-state mixing must be considered again at the individual points $(\mathbf{R}_K,\mathbf{P}_K)$, thus making the corresponding component $D_K(t)\ \lambda_K(\mathbf{r};\mathbf{R})$ in eq 86 renew, such that the integration of eq 75 can be resumed. Hence, the smooth cascade of path-branching should continue as long as the nonadiabatic coupling cannot be effectively ignored. This path-branching is a general feature of the dynamics of coupled quantum and classical subsystems, which is a quantum-classical representation of the quantum wavepacket bifurcation discussed in section 1.3. It should be noted that this dynamically natural branching requires no artificial hoppings, no extra force, no decoherence timing, and no self-consistent procedure.

After both the nonadiabatic coupling and the laser are switched off,

$$X^k_{\alpha\beta} = 0 \quad \text{and} \quad \mathbf{A} = 0 \tag{88}$$

and the force matrix becomes diagonal

$$\mathscr{T}^k_{\alpha\beta} = -\delta_{\alpha\beta}\frac{\partial E^{\mathrm{ad}}_\beta}{\partial R_k} \tag{89}$$

It is of course most convenient to adopt the adiabatic wave functions $\{\psi_\alpha\}$, satisfying

$$H^{\mathrm{el}}\psi_\alpha = E^{\mathrm{ad}}_\alpha\psi_\alpha \tag{90}$$

where H^{el} is the field-free electronic Hamiltonian of eq 70. Thus, each of the branched pieces of the path is supposed to run on one of the adiabatic potential energy surfaces carrying the information of electronic-state mixing ($C_{Kk}(t_{\mathrm{after}})$, as shown below in eq 91, and thereby, the Born−Oppenheimer view is revived individually.

To emphasize how different the branching paths are from the SET paths, it is pertinent to revisit eq 83. As a result of the fact that an electronic wavepacket, launched initially on a path $\mathbf{R}_{Ii}$ (the ith path on an electronic state I), undergoes bifurcation and mixing, the propagation of the total wave function (before quantization of nuclear paths) should be represented as

$$\begin{aligned}&\Phi_I(\mathbf{r};\mathbf{R}(t_{\mathrm{before}}))\ \delta(\mathbf{R}-\mathbf{R}_{Ii}(t_{\mathrm{before}})) \\ &\rightarrow \sum_K^{\text{adiabatic PES}}\ \sum_k^{\text{on K}} C_{Kk}(t_{\mathrm{after}})\ \Phi_K(\mathbf{r};\mathbf{R}_{Kk}(t_{\mathrm{after}}))\ \delta(\mathbf{R}-\mathbf{R}_{Kk}(t_{\mathrm{after}}))\end{aligned} \tag{91}$$

which indicates that the final paths labeled with k are supposed to run on the Kth potential surfaces.

3.7.4. Averaging over the Branching Paths To Extract a (Few) Representative Path(s): A Tractable Approximation. The exact and faithful treatment of the above branching procedure leads to a cascade of infinitely many paths. However, one can find several approximations to reduce the number of paths to a finite level, thereby making the nonadiabatic calculation tractable. As an example, we now take the following "phase-space averaging" of the to-be-branched paths. It is generally anticipated that the fine branching paths should not geometrically deviate much from each other in phase space for a short time propagation. In other words, they should localize along a representative path, forming a tubelike structure. Therefore, we extract such a representative path by taking an average of phase-space points in the following manner:

(i) Suppose we have a path ending at $(\langle\mathbf{R}(t)\rangle,\langle\mathbf{P}(t)\rangle)$ in phase space. At this point, the force matrix is diagonalized as follows:

$$\mathscr{T}(\langle\mathbf{R}\rangle)|\lambda_K(\langle\mathbf{R}\rangle)\rangle = |\lambda_K(\langle\mathbf{R}\rangle)\rangle f_K(\langle\mathbf{R}\rangle) \tag{92}$$

to obtain the eigenforces $\{f_K\}$ and its eigenstates $\{|\lambda_K\rangle\}$. The wavepacket $\Phi(\mathbf{r};\langle\mathbf{R}(t)\rangle)$ is expanded in terms of these eigenstates, as was shown in eq 86.

(ii) The K-th eigenforce drives a path starting from $(\langle\mathbf{R}(t)\rangle,\langle\mathbf{P}(t)\rangle)$ for a short time Δt in terms of the Hamilton canonical equations of motion as

$$\mathbf{R}_K(t+\Delta t) = \langle\mathbf{R}(t)\rangle + \Delta\mathbf{R}_K \tag{93}$$

$$\mathbf{P}_K(t+\Delta t) = \langle\mathbf{P}(t)\rangle + \Delta\mathbf{P}_K \tag{94}$$

(iii) When they are averaged into the form

$$\langle\mathbf{R}(t+\Delta t)\rangle = \langle\mathbf{R}(t)\rangle + \sum_K |D_K(t)|^2\Delta\mathbf{R}_K \tag{95}$$

$$\langle\mathbf{P}(t+\Delta t)\rangle = \langle\mathbf{P}(t)\rangle + \sum_K |D_K(t)|^2\Delta\mathbf{P}_K \tag{96}$$

this makes the next point $(\langle\mathbf{R}(t+\Delta t)\rangle,\langle\mathbf{P}(t+\Delta t)\rangle)$ of the representative path.

(iv) With this averaged point, we calculate

$$\begin{aligned}&\mathscr{T}(\langle\mathbf{R}(t+\Delta t)\rangle)|\lambda_K(\langle\mathbf{R}(t+\Delta t)\rangle)\rangle \\ &\quad = |\lambda_K(\langle\mathbf{R}(t+\Delta t)\rangle)\rangle f_K(\langle\mathbf{R}(t+\Delta t)\rangle)\end{aligned} \tag{97}$$

and return anew to step (ii). The successive applications of the procedure (i)−(iii) give a single finite path.

Path generation using the above averaging procedure should be performed simultaneously with the coherent electronic wavepacket mixing through eq 75. Also, the force matrix in eq 92 and the weighting factors $|D_K(t)|^2$ are renewed in their repeated use as the path and electronic wavepackets are evolved in time. Therefore, as in SET (see subsection 3.7.2), coherence among

dx.doi.org/10.1021/cr200096s |Chem. Rev. 2012, 112, 499–542

the electronic transition amplitudes is retained during the above process.

3.7.4.1. Branching of the Averaged Path. Let us now stop the averaging procedure at a point, which can be an exit point of the interaction region or even an inner position in the coupling region. Let us suppose that we are tracking one of the averaged paths, say, the Kth path, $(\mathbf{R}_K(t),\mathbf{P}_K(t))$. To emphasize that every force is generated along this path, we rewrite eq 84 explicitly as

$$\mathbf{U}(\mathbf{R}_K)\,\mathscr{F}(\mathbf{R}_K)\,\mathbf{U}(\mathbf{R}_K)^{-1} = \begin{pmatrix} f_1(\mathbf{R}_K) & 0 & \cdots \\ 0 & f_2(\mathbf{R}_K) & \\ \vdots & & \ddots \end{pmatrix} \tag{98}$$

where the dependence of the force matrix on $\mathbf{R}_K$ has been stressed. The right-hand side of this representation reminds us that other eigenforces, say f_L, are also calculated along $\mathbf{R}_K(t)$. Therefore, at a point on the path $(\mathbf{R}_K(t),\mathbf{P}_K(t))$, one can switch the force from f_K to f_L to emanate *another* path, such that $(\mathbf{R}_K(t),\mathbf{P}_K(t)) \rightarrow (\mathbf{R}_L(t+\Delta t),\mathbf{P}_L(t+\Delta t))$ is driven by f_L. If one uses f_K at the same point, it follows that $(\mathbf{R}_K(t),\mathbf{P}_K(t)) \rightarrow (\mathbf{R}_K(t+\Delta t),\mathbf{P}_K(t+\Delta t))$. Thus, by applying this procedure, one obtains a path that can naturally branch as soon as the averaging is terminated. These are the first generation of path branching. Along these branching paths, the momentum of the trajectory point varies continuously with time. Meanwhile its time derivative obviously does not, since the time derivative of the momentum is proportional to the force. There are many possibilities when establishing the criteria for branching.[154,155,157] Further study in order to find the best criteria is currently under way.

The individually branching paths of the first generation can resume the averaging to the next branching points. This gives rise to the second generation of branching and once again can undergo further branching, if these are embedded in a strong interaction region. On the other hand, if the path comes to an exit point of the nonadiabatic and/or optical interactions, beyond which the coupling effectively vanishes, the mixing of electronic states is switched off and we no longer take the average as in eqs 95 and 96. Instead, each individual component

$$D_K(t)\,\lambda_K(\mathbf{r};\mathbf{R}_K(t)) \tag{99}$$

is driven by its own force, which comes from the gradient of each potential energy surface. As a result, the coefficients $D_K(t)$ coherently carry the information of the transition amplitudes. After the final branching at the exit point, electronic-state mixing no longer occurs. The method presented in this section is referred to as phase space averaging and natural branching (PSANB).[154,155]

PSANB is similar to the semiclassical Ehrenfest theory in that the coherent electronic-state mixing is performed along each branching path. It is definitely different in that the averaging which gives rise to such a non-Born−Oppenheimer path (or nonclassical trajectory) is made over the force (SET) or performed over the phase-space positions of the future-branching-paths (PSANB). A path can bifurcate as many times as one designates, and eventually, it converges to classical trajectories, once all the nonadiabatic and optical couplings are nullified (PSANB). Numerical examples of PSANB paths can be found in ref 154, 155, and 157 and in Figure 13 in the present review.

3.7.5. Path Integral Analysis of Path Branching. The above path branching dynamics, based on the force matrix, has been reexamined using the path integral formalism,[128] in which all the electronic and nuclear coordinates are treated as c-number from the outset. This procedure avoids classicalization of the nuclear momentum operators, as was performed in eq 72. The dynamics of path branching has been successfully reproduced, and the authors analyzed the nature of paths from several perspectives, including the conservation law of energy and momentum. For instance, since the approximation of PSANB takes an average of future-branching-paths in *phase space*, the exact energy conservation along a path is generally no longer guaranteed. The magnitude of its deviation depends on the number of times of averaging. The path integral analysis thus offers a guiding principle for the improvement of the averaging procedure in the current procedure of PSANB.

3.7.6. What, in Fact, Is the Decoherence? The main results of the studies described above concerning the kinematically coupled mixed quantum-classical dynamics can be summarized as follows. A quantum subsystem undergoes a pure quantum mixing among the electronic states with a slow change of the classical subsystem (electronic-state coherence is involved). On the other hand, the dynamics of the classical subsystem results in an infinite number of cascades of path branching as a manifestation of the bifurcation of the nuclear wavepackets. Such path branching never arises in the well-posed initial value problem such as the Newtonian equation. This can happen because the "classical" dynamics couples with the quantum subsystem. This is known as "coherence", and it penetrates into the classical subsystem. Electronic-state coherence should always be accompanied by path branching. Meanwhile, as the nonadiabatic couplings diminish, the branching terminates automatically (or, in other words, decoheres) and converges so that each path eventually runs on one of the adiabatic potential energy surfaces. This is a picture of spontaneous decoherence we have obtained in the theory of path branching.

4. REPRESENTATION OF THE TOTAL NUCLEAR AND ELECTRONIC WAVE FUNCTIONS IN AN ON-THE-FLY SCHEME

4.1. Semiclassical Quantization of non-Born−Oppenheimer Nuclear Paths

At this point it is desirable to construct the total wave function to proceed further beyond the mixed quantum and classical representation. To do so, we should first prepare an initial quantum wave function including both electronic and nuclear components. Since the nuclear motion has been "classicalized" in terms of path solutions, the initial nuclear wavepacket is transformed into a phase-space distribution as an ensemble of initial conditions of the paths. It is these non-Born−Oppenheimer paths that should be quantized during their time evolution. For purely classical paths (Born−Oppenheimer Newtonian paths running on an individual potential energy surface), it is standard practice to apply the Wentzel−Kramers−Brillouin (WKB) theory in order to quantize them. However, the non-Born−Oppenheimer paths such as those of PSANB are not this kind. In particular, it should be remembered that the paths in the PSANB scheme are continuously branching due to nonadiabatic interactions and an external electromagnetic field. Therefore, it is one of the most crucial parts in the theory of nonadiabatic transition to establish a method to quantize such nonclassical paths. Below are described some general attempts.

dx.doi.org/10.1021/cr200096s |*Chem. Rev.* 2012, 112, 499–542

4.1.1. Frozen Gaussians: Spawning Method of Martínez. Let us imagine a surface hopping model, in which a mother path gives birth to a daughter path on a single hopping, leaving two paths behind. The daughter path is also a classical one. It was proposed by Martnez et al.[139,158−161] that each nuclear path can be partly quantized by placing a frozen Gaussian function (Gaussian functions with a fixed exponent totally irrespective of the underlying dynamics[162]) individually. In fact, their entire method is rather sophisticated in that they use electronic-state mixing to identify the hopping points. Since these paths run on the adiabatic PESs, the action integrals can be readily evaluated. In addition, within this context, the Heller thawed Gaussian approximation or the WKB theory can be applied. Many extensive applications of the so-called spawning method have been made to the analyses of nonadiabatic dynamics.[118,139,158−161]

The greatest advantage of the frozen Gaussian is its simplicity, with the result that it can be applied to many generalizations of the naive surface hopping method and so on. For instance, it is not difficult to imagine that the spawning method can be applied to the fewest switch surface hopping method.[6] It can also be applied to the natural decay of mixing method of Truhlar et al.[7−10] as well as to the branching paths in the PSANB method.

On the other hand, the obvious concern regarding this method is the inaccuracy arising from freezing the Gaussian exponents (see below in section 4.5 though). It is desirable, therefore, to seek a more satisfactory theory for quantizing the *nonclassical* path as efficiently or more so than that of the WKB theory.

4.1.2. Action Decomposed Function in Laser Fields for PSANB. The action decomposed function (ADF) is a candidate for quantizing non-Born−Oppenheimer paths much more accurately.[157,163] It is outlined below. Let us consider the following nonrelativistic Schrödinger equation in an electromagnetic vector potential

$$i\hbar\frac{\partial}{\partial t}\chi(\mathbf{R},t) = \left[\frac{1}{2}\sum_k \frac{1}{M_k}\left(\hat{P}_k - \frac{Z_k e}{c}A_k(\mathbf{R})\right)^2 + V(\mathbf{R})\right]\chi(\mathbf{R},t) \tag{100}$$

where $\hat{P}_k$ is the quantum momentum operator

$$\hat{P}_k = \frac{\hbar}{i}\frac{\partial}{\partial R_k} \tag{101}$$

and it should be distinguished from its classical canonical momentum P_k. Here again, we resort to the mass weighted coordinates, rescaling all the masses to

$$M_k = 1 \tag{102}$$

The velocity of a particle is correlated with its momentum in such a way that

$$v_k = P_k - \frac{Z_k e}{c}A_k \tag{103}$$

The classical counterpart of this dynamics is represented in the following Hamilton−Jacobi equation

$$\frac{\partial}{\partial t}S(\mathbf{R},t) + \frac{1}{2}\sum_k\left(\frac{\partial S(\mathbf{R},t)}{\partial R_k} - \frac{Z_k e}{c}A_k\right)^2 + V(\mathbf{R}) = 0 \tag{104}$$

where the momentum is generated through the action integral as

$$P_k = \frac{\partial S(\mathbf{R},t)}{\partial R_k} \tag{105}$$

Here we set the total wave function as shown in the following equation

$$\chi(\mathbf{R},t) = \exp\left(\frac{i}{\hbar}S(\mathbf{R},t)\right)F(\mathbf{R},t) \tag{106}$$

After some manipulation, we have an equation of motion which can be used to determine $F(\mathbf{R},t)$ as follows

$$\frac{\partial F(\mathbf{R},t)}{\partial t} = \left[-v\cdot\nabla - \frac{1}{2}(\nabla\cdot v) + \frac{i}{2}\hbar\nabla^2\right]F \tag{107}$$

It should be noted that this ADF equation is in exactly the same form as that for the field-free case.[157,163] This is not surprising, since the ADF equation represents the kinematics only.

One of the most important features of the ADF lies in the fact that its determining equation (eq 107) is composed of the velocity field only. The function $F(\mathbf{R},t)$ can be integrated along a path if it is uniquely specified in phase space $(\mathbf{R}(t),\mathbf{v}(t))$. Technically, we do not have to care about how the information of $(\mathbf{R}(t),\mathbf{v}(t))$ has been given. Even the presence of a well-defined potential function is not required, as is the case in our branching path case. Likewise, the action integral $S(\mathbf{R},t)$ can be integrated along a path under the same conditions. Thus, the ADF can be effectively applied to the quantization of nonclassical paths, provided only $(\mathbf{R}(t),\mathbf{v}(t))$ is available.

Among many possibilities in an application of ADF, we particularly choose the normalized variable Gaussian (NVG), a semiclassical Gaussian approximation to ADF. The ADF equation, eq 107, can be transformed into an integral form such that

$$F(\mathbf{R}-\mathbf{R}(t+\Delta t),t+\Delta t) = \exp\left[\Delta t\left(-\frac{1}{2}\vec{\nabla}\cdot\vec{v} + \frac{i\hbar}{2}\vec{\nabla}^2\right)\right]F(\mathbf{R}-\mathbf{R}(t),t) \tag{108}$$

to which one can then apply the so-called Trotter decomposition. $F(\mathbf{R}-\mathbf{R}(t),t)$ is approximated in terms of the Gaussian function

$$F(\mathbf{R}-\mathbf{R}(t),t) = \pi^{-N/4}[\det(\Gamma+\Gamma^*)]^{1/4} \times \exp[-(\mathbf{R}-\mathbf{R}(t))^T\Gamma(t)(\mathbf{R}-\mathbf{R}(t))] \tag{109}$$

It was found that the Gaussian of the inverse exponent

$$\Gamma(t) = \frac{1}{\mathbf{C}(t) + i\mathbf{D}(t)} \tag{110}$$

is particularly useful.[164] The exponent $\mathbf{C}(t)$ is responsible for describing the velocity gradient only, $-(1/2)\vec{\nabla}\cdot\vec{v}$ in eq 108, while $\mathbf{D}(t)$ reflects the dynamics not only for the velocity gradient but that arising from the quantum diffusion term, $(i\hbar/2)\vec{\nabla}^2$ of eq 108. The Planck constant appears only in the quantum diffusion term. Therefore, only $\mathbf{D}(t)$ needs to be scaled to the magnitude of $\hbar$. See refs 154, 155, 157, and 164 for the practical implementation and applications of PSANB paths.

4.2. Branching-Path Representation of the Total Wave Function

Accumulating all the dynamical components as constructed above, we can now build total electronic and nuclear wavepackets

dx.doi.org/10.1021/cr200096s |Chem. Rev. 2012, 112, 499–542

along the non-Born−Oppenheimer paths as follows

$$\Psi^{\mathrm{tot}}_{\mathrm{OTF}}(\mathbf{r},\mathbf{R},t) = \sum_{K}^{\mathrm{state}} \sum_{k}^{\mathrm{path}} \Phi_K(\mathbf{r},t;\mathbf{R}_{Kk}(t))\, C_{Kk}(t) \times F(\mathbf{R}-\mathbf{R}_{Kk}(t),t)\, \exp\left[\frac{i}{\hbar}S(\mathbf{R}-\mathbf{R}_{Kk}(t))\right] \quad (111)$$

Here the suffix OTF stands for on-the-fly and $F(\mathbf{R} - \mathbf{R}_{Kk}(t),t)$ may be an ADF. This representation of the total wave function is a little different from the standard Born−Huang expansion, which, for comparison, is

$$\Psi^{\mathrm{tot}}_{\mathrm{QM}}(\mathbf{r},\mathbf{R},t) = \sum_{K}^{\mathrm{state}} \Phi_K(\mathbf{r};\mathbf{R})\, \chi^{\mathrm{QM}}_K(\mathbf{R},t) \quad (112)$$

Then it is clear that rigorous comparison between these wave functions is required to be made in the $(\mathbf{r},\mathbf{R})$ space, even if the common electronic basis functions are used. Or, formally, we carry out an integration

$$\chi^{\mathrm{OTF}}_K(\mathbf{R},t) = \int \mathrm{d}r\, \Phi^*_K(\mathbf{r};\mathbf{R})\, \Psi^{\mathrm{tot}}_{\mathrm{OTF}}(\mathbf{r},\mathbf{R},t) \quad (113)$$

to attain the Born−Huang expansion from $\Psi^{\mathrm{tot}}_{\mathrm{OTF}}(\mathbf{r},\mathbf{R},t)$. To avoid such a tedious task, we rewrite the wave function given in eq 111 by assuming that $F(\mathbf{R} - \mathbf{R}_{Kk}(t),t)$ is well localized spatially. As an extreme approximation, we can set $F(\mathbf{R} - \mathbf{R}_{Kk}(t),t) = \delta(\mathbf{R} - \mathbf{R}_{Kk}(t))$, which leads to the approximation $\Psi^{\mathrm{tot}}_{\mathrm{OTF}}(\mathbf{r},\mathbf{R},t)$ as

$$\Psi^{\mathrm{tot}}_{\mathrm{OTF}}(\mathbf{r},\mathbf{R},t) \cong \sum_{K}^{\mathrm{state}} \Phi_K(\mathbf{r},t;\mathbf{R}) \sum_{k}^{\mathrm{path}} C_{Kk}(t) \times F(\mathbf{R}-\mathbf{R}_{Kk}(t),t)\, \exp\left[\frac{i}{\hbar}S(\mathbf{R}-\mathbf{R}_{Kk}(t))\right] = \sum_{K}^{\mathrm{state}} \Phi_K(\mathbf{r},t;\mathbf{R})\, \chi^{\mathrm{OTF}}_K(\mathbf{R},t) \quad (114)$$

which has the obvious definition

$$\chi^{\mathrm{OTF}}_K(\mathbf{R},t) = \sum_{k}^{\mathrm{path}} C_{Kk}(t)\, F(\mathbf{R}-\mathbf{R}_{Kk}(t),t)\, \exp\left[\frac{i}{\hbar}S(\mathbf{R}-\mathbf{R}_{Kk}(t))\right] \quad (115)$$

As a result this makes it possible to compare it with its quantum mechanical counterpart, $\chi^{\mathrm{QM}}_K(\mathbf{R},t)$. It should be remembered that the $C_{Kk}(t)$ terms included in the nuclear wavepacket $\chi^{\mathrm{OTF}}_K(\mathbf{R},t)$ of eq 115 originally emerged from the electronic wavepacket bifurcation along the branching paths.

The quantization effects of the nuclear paths on the actual mixing of the electronic states, as described above, remain a further challenge[165] (see also the discussion of section 4.5). However, our numerical calculations have clearly demonstrated that the nonadiabatic transition probabilities given so far are excellent without any consideration of such secondary effects.[154,155,157,164]

4.3. Numerical Examples of the Branching-Path Representation

Before proceeding to the further development of theory, we would like to graphically illustrate what the geometry of branching paths emerging from the PSANB scheme and the associated quantities looks like. Two examples will be shown: one without a laser field and the other representing a path-branching due to nonadiabatic coupling and a vector potential. To clarify the geometrical view, both systems are chosen to be one-dimensional. For the same reason, we here allow the paths to branch only once at each interaction: nonadiabatic or optical. Therefore, this is the lowest and simplest level approximation in the PSANB scheme (see sections 3.7.3 and 3.7.4). In reality, infinitely many path-branchings should be allowed to achieve exactness in the mixed quantum-classical dynamics. Such numerical examples for multiple-branching can be seen in refs 154, 155, 157, and 164. The technical details, such as a threshold condition under which a path branches, have been described in ref 155.

4.3.1. A System of Nonadiabatic Coupling with Reflection. The first system is the so-called one-dimensional model of extended coupling with reflection, which was proposed by Tully as one of the model systems for a stringent test in his study of the fewest switching surface hopping algorithm.[6] We have slightly modified this model so as to raise the barrier height a little. First, the following diabatic representation is given analytically as

$$\begin{aligned} V_{11}(R) &= A \\ V_{22}(R) &= -A \\ V_{12}(R) &= V_{21}(R) = B\exp(CR) \quad \text{for} \quad R \le 0 \\ V_{12}(R) &= V_{21}(R) = B(2-\exp(-CR)) \quad \text{for} \quad R \ge 0 \end{aligned} \quad (116)$$

with $A = 6 \times 10^{-4}$, $B = 0.15$, and $C = 0.9$. The mass is set to 1000 au. (The atomic units are used in this subsection.) The adiabatic potential curves along with the nonadiabatic coupling element, all being generated by diagonalizing the above diabatic potentials, are graphically represented in Figure 1 panel A. Panel B, the left box shows the history of branching of a path starting at $R = -10.0$ on the lower potential curve (in red in panel A) with $k = 20.0$ (the classical momentum is given by $\hbar k$. The path is first propagated in time and driven by the force matrix, but those to-be-branched-paths are averaged in phase space to form only a single path until a point marked with the first green square, which is located close to an exit of the inidividual coupling region, and hence, the nonadiabatic coupling element is sufficiently small. The path is branched there to two pieces, one running down on the lower slope and the other making a transition to the upper curve. The latter eventually undergoes reflection by the potential barrier and returns into the nonadiabatic region. After the similar averaging process of to-be-branched-paths, it further bifurcates into two pieces, running on the ground state (in red) and the excited state (in blue). (Note that the last two branching paths are not geometrically distinguished in this scale.) Thus, three paths have been smoothly generated after all.

In the central box of panel B is displayed the similar history of the densities $|\chi_1(R,t)|^2$ and $|\chi_2(R,t)|^2$ for the nuclear wavepacket $\chi(R,t) = (\chi_1(R,t), \chi_2(R,t))$ in the adiabatic representation. $\chi_1(R,0)$ was chosen to be the so-called minimum uncertainty coherent-state Gaussian centered at $R = -10.0$ with $k = 20.0$ on the ground state, while $\chi_2(R,0) = 0$. Only the components of $|\chi_1(R,t)|^2$ and $|\chi_2(R,t)|^2$ that are higher than a threshold value are graphically exhibited. The inspection shows very clearly that both the geometrical and branching behaviors of the PSANB paths are quite similar to those of the full quantum mechanical counterparts. The third box from the left of panel B indicates that not only the geometrical behavior but also the transition probability is in excellent agreement, in which the total population found on the excited state at time t is represented as a green dotted curve

dx.doi.org/10.1021/cr200096s |Chem. Rev. 2012, 112, 499–542

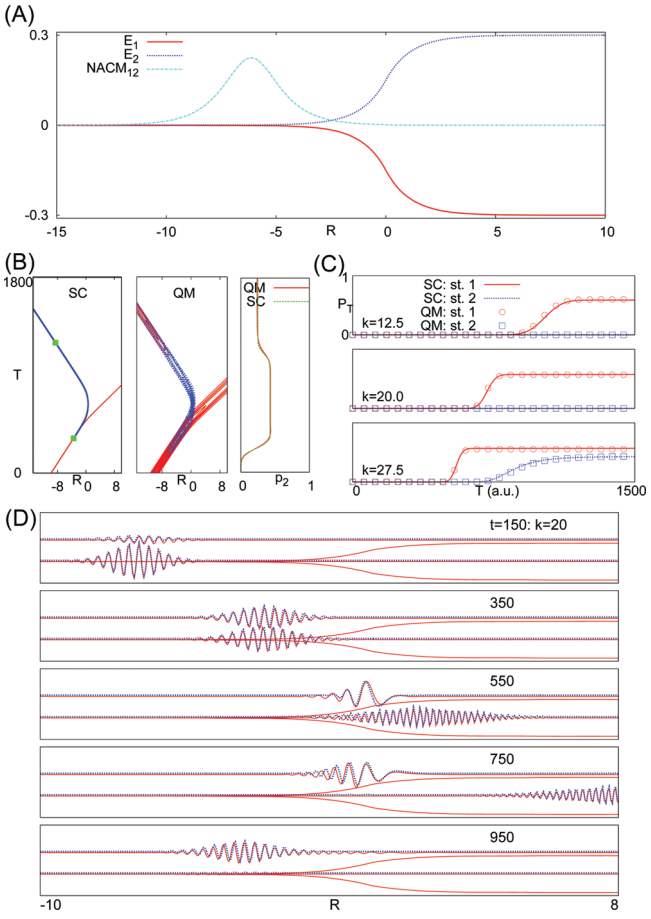

Figure 1. Branching path representation and its comparison with the full quantum counterparts in the extended coupling with the reflection model system (all quantities in atomic units). (A) Adiabatic potential curves and nonadiabatic coupling element as functions of the coordinate R. (B) [Left labeled with SC] Branching paths in $R - t$ space. The initial condition is $R = -10$ and $k = 20$ on the ground electronic state. Red (blue) curves represent paths "belonging" to the ground (excited) state. [Middle with QM] Tracks of the corresponding quantum wavepackets. [Right] Population in the excited state. Red solid and blue dotted curves represent the PSANB-NVG and full quantum values, respectively. (C) Time integral of the flux of the probability current in the positive direction at $R = 7$. The initial wavenumbers of the wavepackets are $k = 12.5$, 20.0, and 27.5. The results by the branching path representation for the upper and lower electronic states are depicted, respectively, by blue dotted and red solid lines. Full quantum mechanical results are correspondingly presented by red solid circles and blue squares. (D) Snapshots of the real part of the PSANB-NVG and full quantum wave functions at selected times. Blue dotted and red solid curves denote the wave functions for PSANB-NVG and full quantum mechanics, respectively.

and the red solid one is estimated with full quantum mechanics and PSANB, respectively.

We next survey the energy dependence of the dynamics. To see this, we have calculated a time integral of the flux of the probability current (P_T) that passes through the point $R = 7$, which is far from the interaction region. (Quantum mechanical flux will be discussed in a detail in section 5.1.) P_T is the accumulated population passing across the point by time t. We examined three cases, each having the initial wavenumber k = 12.5, 20.0, and 27.5, respectively. Only the initial condition of k = 27.5 can give birth to a path that can mount the barrier of the excited state, and those paths of k = 12.5 and 20.0 should be reflected by it. Panel C shows the P_T values that are estimated in terms of PSANB-NVG and the full quantum mechanics for these three cases. P_T values on the ground state are denoted by a red solid curve (PSANB) and red circles (full quantum mechanics), while those on the excited state are represented by a blue dotted curve (PSANB) and blue squares (full quantum mechanics). Only in the case of k = 27.5 are nonzero values of P_T for the excited state observed. As seen in the graphs, the PSANB-NVG reproduces the full quantum values excellently.

Finally, we examine the nuclear wavepackets approximately extracted from the PSANB-NVG function in the manner of eq 115. Panel D presents five snapshots of the real part of the PSANB-NVG function (in blue dotted curves) at k = 20 and the corresponding full quantum values (in red curves) at times 150, 350, 550, 750, and 950. Each box contains the ground and excited potential curves (the copy of panel A). The wave functions on the ground (excited) state are drawn in a lower (higher) level in each box. At time as early as t = 150, the wavepacket begins to bifurcate, and at t = 750, we see the ground-state wavepacket running out of the place. At t = 950, only the reflected wave in the excited state remains, which is about to bifurcate again. As seen in this panel, the agreement of the two wave functions, both starting from a single coherent Gaussian, is very good up to the phase.

4.3.2. Multiple Path-Branching Due to Nonadiabatic Coupling and Laser Field. We next study the path branching and the associated wave functions in a system where both a vector potential and nonadiabatic interaction coexist. The system we adopt here is the same as that taken in ref 157. The adiabatic potentials and nonadiabatic coupling element are depicted in panel A of Figure 2. The field parameters for pulses are as follows; the strength of the electronic field Es_1 = 0.03, the central peak time t_{c1} = 215, the width duration time t_{w1} = 50, the central frequency ω_1 = 0.290, and the carrier envelope phase $\delta_1 = \pi/2$.

The wavepacket begins to run from R = 4.0 toward the left with $k = -30.0$ on the ground state. It first bifurcates due to the nonadiabatic coupling, and then the laser is applied, which is turned on as in the rightmost box (denoted as Field) in panel B of Figure 2. The two wavepackets already bifurcated to the ground and excited states individually undergo the next bifurcation by this vector field, giving birth to four components. Further, each hits a turning point on one of the left slopes and returns to the nonadiabatic region, and each further bifurcates at an individual timing. Such a history of the quantum wavepacket, actually the square modulus of it, is shown as in the above example in $R - t$ space in the second box (denote as QM) of panel B in Figure 2. The red and blue codes are used to represent the ground and excited state components, respectively. (Since transparent painting is not used here, the figure does not faithfully represent their overlapping.)

The first box (marked with SC) in panel B of Figure 2 shows a history of the corresponding PSANB paths. The color assignment to the paths is the same as that in the quantum counterparts. The small green squares indicate points where the averaging process in PSANB is finished and branching is allowed, which are located at an exit area of the nonadiabatic and/or optical interactions. It is immediately recognized that the geometry and history of the path-branching are quite similar to those of the full quantum wavepackets. Thus, even the simplest application of the PSANB successfully represents the smooth branching geometry of the quantum wavepackets.

Finally, we track the history of the transition probability of this process, by examining the population on the excited state

dx.doi.org/10.1021/cr200096s |Chem. Rev. 2012, 112, 499–542

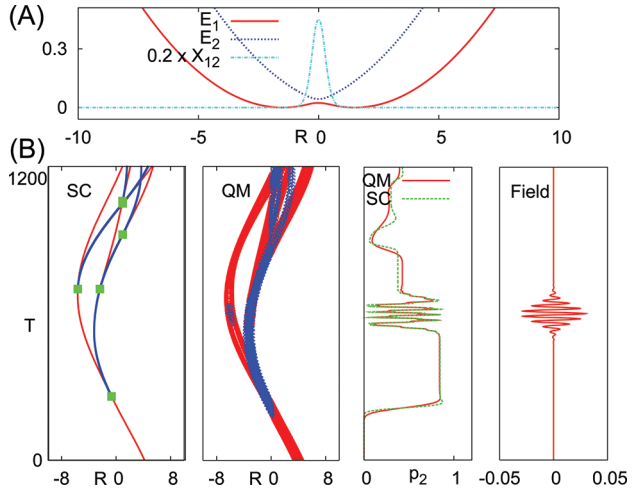

Figure 2. Path branching due to nonadiabatic and optical interactions (in atomic units). (A) Adiabatic potentials and nonadiabatic coupling element. Field parameters for the pulse laser; the strength of the electronic field $Es_1 = 0.03$, the central peak time $t_{c1} = 215$, the width duration time $t_{w1} = 50$, the central frequency $\omega_1 = 0.290$, and the carrier envelope phase $\delta_1 = \pi/2$. The wavepacket begins to run from $R = 4.0$ toward the left with $k = -30.0$ on the ground state. (B) [Left] Path branching in the PSANB scheme. Red (blue) curves represent paths "belonging" to the ground (excited) state. [Second from left] History of the full quantum wavepacket bifurcation. [Third from left] Time variation of the population on the excited state. Green dotted and red solid curves represent the PSANB and full quantum values, respectively. [Right] Optical field applied.

(denoted as p_2). The third box from the left displays p_2 given by the full quantum mechanics (red solid curve denoted as QM) and the PSANB-NVG (green dotted curve marked with SC). Although we notice a minor deviation between the two, it is surprising that the PSANB starting from a single path marks such a good achievement after three times of branchings. Again, we note that we have established a general method to run more paths in the initial state.[157]

4.4. Electronic Wavepackets Extracted from the Total Wave Function

In eq 115 we have shown how it is possible to make an approximate extraction of the nuclear wavepacket in the Born−Huang expansion from the on-the-fly total wave function. Conversely, de Vivie-Riedle and co-workers[166] proposed an interesting method for the extraction of an electronic wavepacket from a total wave function in the form of a Born−Huang expansion as in eq 112. In a study of time-dependent problems such as molecular propagation under an intense laser field, it is often interesting to visualize the electron dynamics around a slow nuclear motion. First let us assume that the close coupling equation under a dipole field for the nuclear part shown below is solved

$$i\hbar \frac{\partial}{\partial t}\begin{pmatrix}\chi_g\\ \chi_u\end{pmatrix} = \begin{pmatrix}T_{\mathrm{nuc}} + V_g & -\mu(R)\,\varepsilon(t)\\ -\mu(R)\,\varepsilon(t) & T_{\mathrm{nuc}} + V_u\end{pmatrix}\begin{pmatrix}\chi_g\\ \chi_u\end{pmatrix} \tag{117}$$

Here the dipole interaction $\mu(R)\ \varepsilon(t)$ by a laser field is considered to lie between gerade (g) and ungerade (u) electronic states. As a result, one can build a total wave function in the Born−Huang expansion approximately, which is denoted as $\tilde{\Psi}_{\mathrm{mol}}(\mathbf{R},\mathbf{r},t)$. So far, nonadiabatic coupling has not been taken into account, but such an extension is formally straightforward. The above total wave function is then rewritten as

$$\tilde{\Psi}_{\mathrm{mol}}(\mathbf{R},\mathbf{r},t) \rightarrow \sum_I \chi_I(\mathbf{R},t)\ \Phi_I(r;\mathbf{R}_I(t)) \tag{118}$$

Here $\mathbf{R}_I(t) \equiv \int d\mathbf{R}\chi_I^*(\mathbf{R},t)\hat{R}\chi_I(\mathbf{R},t)$ was used to pick up the propagated electron wavepacket at a representative nuclear position $\mathbf{R}_I(t)$ at a time t, and Φ_I is the electronic wave function. χ_I is either χ_g or χ_u as obtained above. These electronic packets are defined by the following projection as

$$\begin{pmatrix}\tilde{\phi}_1(\mathbf{r},t;\mathbf{R}(t))\\ \tilde{\phi}_2(\mathbf{r},t;B(t))\end{pmatrix} \equiv \begin{pmatrix}\langle\chi_g|\tilde{\Psi}_{\mathrm{mol}}(\mathbf{R},\mathbf{r},t)\rangle_R\\ \langle\chi_u|\tilde{\Psi}_{\mathrm{mol}}(\mathbf{R},\mathbf{r},t)\rangle_R\end{pmatrix} \tag{119}$$

where the last integrals in eq 119 should be carried out over the $\mathbf{R}$-coordinates. Some numerical techniques and assumptions are required in this procedure.[166] It should be noted that $\tilde{\phi}(\mathbf{r},t;\mathbf{R},t)$ attains a proper phase. This method is applied to the system in an attempt to design and control the electronic states induced by lasers as well as the dynamics of the nearby conical intersections.[167]

4.5. Remixing of Electronic States To Incorporate the Quantum Nature of Nuclear Dynamics and the Interference among the Paths

What we have surveyed for the mixed quantum-classical dynamics thus far in this section is to consider (i) how the electronic state mixing is performed along non-Born−Oppenheimer paths or the locally classical paths in the hopping scheme and then (ii) how these resultant nuclear paths are quantized. Consequently, the subsequent effect of the quantization of nuclear paths on the electronic state mixing has not yet been considered. Also, it should be remembered that, in most of the theories discussed above, the electronic-state mixing is performed independently along each path.[139] However, after hopping or branching, paths coresiding in a strong nonadiabatic region can still interfere, as in the final state interaction. (This procedure reminds us of the self-consistent procedure of Pechukas as discussed in section 3.1.) These effects are also missing, at least theoretically, in these. The seminal step to resolving this issue was once again made by Martnez and co-workers.

Consider the total Hamiltonian, $\hat{H} = -(\hbar^2/2)\Sigma_k^{\mathrm{nuc}}(1/M_k)\partial^2/\partial R_k^2 + \hat{H}^{\mathrm{el}}$, where k denotes a nuclear degree of freedom and M_k presents its corresponding mass. A total electronic and nuclear wave function given by the on-the-fly scheme is generally written as

$$\Psi(\mathbf{r},\mathbf{R},t) = \sum_I^{\text{el state}} \sum_i^{N_I(t)} C_I^i(t)\ \chi_I^i(\mathbf{R};\mathbf{R}_I^i(t),\mathbf{P}_I^i(t),\gamma_I^i(t)) \times \Phi_I(\mathbf{r};\mathbf{R}_I^i(t),\mathbf{P}_I^i(t)) \tag{120}$$

The function in eq 111 represents an example. In the multiple spawning method developed by Martnez et al., the time-dependent Gaussian nuclear wavepacket basis functions $\chi_I^i(t)$ are supposed to be parametrized with their guiding centers in phase space, $\{R_I^i(t),P_I^i(t)\}$, and width matrix, $\gamma_I^i(t)$. The classical phase is implicitly included in the nuclear basis. I denotes an electronic state and i labels a guiding center (path) running on it. The electronic basis function, $\Phi_I(\mathbf{r};\mathbf{R}_I^i(t),\mathbf{P}_I^i(t))$, is carried along

dx.doi.org/10.1021/cr200096s |Chem. Rev. 2012, 112, 499–542

$(\mathbf{R}_I^i(t),\mathbf{P}_I^i(t))$, satisfying $\langle\Phi_I|\Phi_J\rangle = \delta_{IJ}$ at each given nuclear position. The idea itself is rather straightforward: Substituting the wave function from eq 120 into the total Schrödinger equation, $i\hbar|\dot{\Psi}\rangle = \hat{H}|\Psi\rangle$, makes it possible to determine the electronic mixing coefficients $C_I^i(t)$. The functions $\chi_I^i(\mathbf{R};\mathbf{R}_I^i(t),\mathbf{P}_I^i(t),\gamma_I^i(t))$ $\Phi_I(\mathbf{r};\mathbf{R}_I^i(t),\mathbf{P}_I^i(t))$ are therefore regarded as basis functions to expand $\Psi(\mathbf{r},\mathbf{R},t)$. The determining coupled equations obtained after some appropriate approximations are not simple but can be derived in a seemingly compact form as

$$i\hbar \sum_i [S_{JJ}^{ji}\dot{c}_J^i + \dot{\vec{S}}_{JJ}^{ji} c_J^i] = \sum_{\alpha i} T_{\alpha JJ}^{ji} c_J^i + \sum_{Ii} \bar{H}_{JI}^{ji} S_{JI}^{ji} c_I^i - \hbar^2 \sum_{\alpha Ii} \frac{1}{M_\alpha} \mathbf{F}_{\alpha JI}^{ji} \bar{\mathbf{f}}_{\alpha JI}^{ji} c_I^i \quad (121)$$

Here a generalized nuclear kinetic operator supermatrix is $T_{\alpha JI}^{ji} \equiv -(\hbar^2/2M_\alpha)\langle\chi_J^j|\nabla_\alpha^2|\chi_I^i\rangle$. α denotes atoms. The terms $S_{JI}^{ji} \equiv \langle\chi_J^j|\chi_I^i\rangle$ and $\dot{\vec{S}}_{JI}^{ji} \equiv \langle\dot{\chi}_J^j|\chi_I^i\rangle$ which appeared in this equation of motion are nuclear wavepacket transition coupling matrix elements induced from the zeroth- and first-order time derivative, respectively. The nuclear derivative terms consist of $\mathbf{F}_{\alpha JI}^{ji} \equiv \langle\chi_J^j|\nabla_\alpha|\chi_I^i\rangle$, $\bar{\mathbf{f}}_{\alpha JI}^{ji} \equiv \langle\Phi_J^j|\nabla_\alpha|\Phi_I^i\rangle$. The electronic potential matrix elements are described in the form $H_{JI}^{ji} \equiv \langle\Phi_J^j|\hat{H}^{\mathrm{el}}|\Phi_I^i\rangle$. Practically, the two center electronic integrals, $\bar{f}_{\alpha JI}^{ji}$ and $\bar{H}_{JI}^{ji}$, often demand much computational effort and ultimately require practical approximations. An overbar in the equation denotes an approximation of one center electron integral, the details of which, along with other technical matters, can be found in refs 168 and 169.

Clearly, the essence of Martínez's work as described above both inspired and proves useful for the wave function of PSANB in eq 111 to improve the electronic mixing coefficients $C_{Kk}(t)$ in order to incorporate the quantum nature of nuclei into the electronic-state mixing. However, it has been shown numerically[154,155,157] that the wave function in eq 111 is already very accurate before such remixing.

5. NONADIABATIC DYNAMICAL ELECTRON THEORY FOR CHEMICAL REACTIONS: CASE STUDIES

This section is devoted to the presentation of three case studies of nonadiabatic electron wavepacket dynamics as carried out by the present authors. These examples are used to stress the fact that the theory of electron dynamics thus far developed is indeed worth studying more extensively.

5.1. Characteristic Quantities Emerging from Dynamical Electron Wave Functions

Before presenting the numerical studies, we first select two quantities that are particularly useful for tracking electron dynamics induced by chemical reactions and/or laser applications.

Current of Probability Density. Let

$$i\hbar\frac{\partial}{\partial t}\psi(\mathbf{r},t) = \left[-\frac{\hbar^2}{2m}\nabla^2 + V(\mathbf{r},t)\right]\psi(\mathbf{r},t) \quad (122)$$

be a one-body Schrödinger equation and consider that the flux vector naturally arises as[170]

$$\vec{j}(\mathbf{r},t) = \frac{\hbar}{2im}[\psi^*(\mathbf{r},t)\nabla\psi(\mathbf{r},t) - \psi(\mathbf{r},t)\nabla\psi^*(\mathbf{r},t)] \quad (123)$$

This is automatically followed by the N-particle extension

$$\vec{j}_N(\mathbf{r}_1,\mathbf{r}_2,\ldots,\mathbf{r}_N) = \frac{\hbar}{2im}(\psi^*(t)\tilde{\nabla}_N\psi(t) - \psi(t)\tilde{\nabla}_N\psi^*(t)) \quad (124)$$

with

$$\tilde{\nabla}_N = \sum_{j=1}^N \left(\frac{\partial}{\partial x_j}\ \frac{\partial}{\partial y_j}\ \frac{\partial}{\partial z_j}\right) \quad (125)$$

This N-body flux is readily reduced to the one-particle flux

$$\vec{j}(\mathbf{r}) = N\int \vec{j}_N(\mathbf{r},\mathbf{r}_2,\ldots,\mathbf{r}_N)\,d\mathbf{r}_2\ldots d\mathbf{r}_N \quad (126)$$

For a complex-valued wave function such as those given by SET and PSANB, this flux vector gives a nonzero value, which represents an electron current induced by configuration mixing caused by the nonadiabatic coupling and/or other external perturbations. If, on the other hand, a wave function is real-valued as in stationary-state quantum chemistry, $\vec{j}(\mathbf{r})$ is identically zero, simply because such a stationary-state wave function does not know to which time-direction it is proceeding. Flux analyses have been made extensively for electron flow associated with proton transfer dynamics, laser application, chemical reactions, and so on,[99,100,156] and those arising from nuclear-electronic wave functions have been thoroughly investigated by Manz and co-workers.[90,101,171,172]

Complex-Valued Natural Orbitals in Electron Wavepacket Dynamics. The natural orbitals, which are eigenfunctions of the first order density matrix, are among the well-known quantities in standard quantum chemistry. However, the way of time-evolution of the natural orbitals resulting from a time-dependent electronic wave function such as SET and PSANB is quite interesting. In general, they are complex-valued, and through this the state-mixing is well realized, as actually shown later in this subsection. The first-order spin-free density matrix for an (instantaneous) electronic wave function $\Phi(t)$ is defined as

$$\rho(\mathbf{r},\mathbf{r}',t) \equiv N\int d\omega_1 dq_2\ldots dq_N\ \Phi^*(\mathbf{r}',\omega_1,\mathbf{r}_2,\omega_2,\ldots,\mathbf{r}_N,\omega_N) \times \Phi(\mathbf{r},\omega_1,\mathbf{r}_2,\omega_2,\ldots,\mathbf{r}_N,\omega_N) = \sum_{\mu,\nu}\rho_{\mu\nu}(t)\,\chi_\mu(\mathbf{r}')\,\chi_\nu(\mathbf{r}) \quad (127)$$

where $\mathbf{r}_i$ and ω_i are the spatial and spin coordinates, respectively, of the ith electron. Here, $\int dq_i$ is a short-hand notation for spatial integration and spin summation. χ_μ are basis functions such as atomic orbitals, which are chosen to be real functions. The natural orbitals in electron dynamics can become complex and are given as eigenfunctions of the matrix $\rho_{\mu\nu}$ such that

$$\sum_\nu \rho_{\mu\nu}\xi_\nu^{(\lambda)} = n^{(\lambda)}\xi_\nu^{(\lambda)} \quad (128)$$

where $\xi_\mu^{(\lambda)}$ is the λth eigenvector of $\rho_{\mu\nu}$ with a real eigenvalue (occupation number) $n^{(\lambda)}$, giving rise to a natural orbital

$$\phi_\lambda(\mathbf{r}) = \sum_\nu \xi_\nu^{(\lambda)}\chi_\nu(\mathbf{r}) \quad (129)$$

dx.doi.org/10.1021/cr200096s |Chem. Rev. 2012, 112, 499–542

Equation 128 does not determine the phase of the natural orbital. Therefore we simply to fix the phase factor so that the real part of ξ has the largest norm.

5.2. Nonadiabatic Electron Migration in a Model Water Cluster Anion System

In the first instance let us consider the dynamics of hydrated electrons in water clusters in the context of the approximation level of the semiclassical Ehrenfest theory (SET). The purpose of this subsection is to show how useful nonadiabatic electron wavepacket dynamics can be. Electron hydration is quite an interesting and important issue, and many experimental and theoretical studies have already been devoted to the issue.[173−182] It is a prototype of solution-phase chemistry in a polar solvent. Also, the dynamics are expected to provide an important insight into charge-transfer chemistry.

Static structural calculations for the water cluster anion have revealed the quantum mechanical origin of the binding force for the excess electron and various equilibrium structures.[183−187] It is now established that the excess electron is bound principally by the dipole field formed by the water molecules. In their elaborate studies on the potential landscape of anion water clusters, Choi and Jordan[187] explored a large number of local minima as well as the transition states on the potential energy surface of $(H_2O)_6^-$. They identified the minimal energy pathway from the neutral isomer to low-energy anion isomers.

With respect to the dynamical properties of the hydrated electron in cluster systems, the first principle dynamics using *ab initio* molecular dynamics and so on have been extensively applied.[188−192] They revealed information about the structure and relative stabilities of the isomer clusters. Nonadiabatic dynamics of a solvated electron in various photochemical processes has also been studied experimentally.[182,193−195] Rossky and co-workers[196,197] also studied the relaxation dynamics of excess electrons using quantum molecular dynamics simulation techniques. Here the nonadiabatic interactions were taken into account basically within the scheme of the surface hopping technique.[116]

On the other hand, there are very few studies available on nonadiabatic dynamics in cluster deformation dynamics. We expect that, in the course of cluster deformation and the accompanying change in electronic orbitals, the nonadiabatic transition may in fact play a critical role. The dynamics of the hydrated electron in a water cluster anion consist of two or three molecules. The electronic structure of such a small cluster, however, is known to have a very small energy scale (the vertical detachment energy (VDE) is of order 10^1 to 10^2 meV[184,198]). Furthermore, it is known that the accuracy of the theoretically calculated energy levels sensitively depends on the choice of the size and quality of the basis functions. On the other hand, the SET calculations that will be shown in this section are so much limited by the computational capacity available to us that the results are not necessarily accurate enough to be predictive at a quantitative level. In addition, the present SET does not quantize the nuclear vibrational and rotational modes, which may be delicately coupled with the densely degenerated electronic states. In spite of these limitations, SET calculations are performed because it is expected that they can give a qualitative view of the nonadiabatic migration of the excess electrons within the model water clusters.

5.2.1. Computational Details in the Nonadiabatic Dynamics of a Hydrated Electron. *5.2.1.1. Electronic States.*

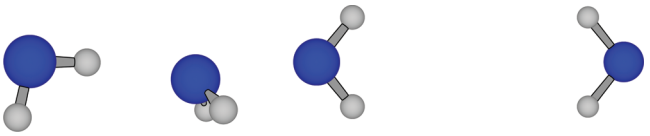

Figure 3. Equilibrium structures of water−anion dimers. Here and throughout this section, small gray circles indicate hydrogen atoms while large blue circles indicate oxygen atoms. Left dimer: nonplanar configuration. Atoms in the left monomer and the oxygen atom in the right monomer are on a single plane while the two hydrogen atoms in the right monomer are out of the plane. Right: planar configuration. All the atoms reside in a single plane.

Our dynamical simulation with SET is implemented into the GAMESS package.[199] The basis functions used were those of the TZV basis set,[200] to which an s-type diffusion base and two sets of p-type polarization functions were added on hydrogen atoms while s- and p-type diffusion functions were augmented on oxygen atoms. (The exponent is 0.03600 for the s-type diffusion base, 0.08450 for the s- and p-type diffusion bases, respectively, and 2.00 and 0.50 for the p-type polarization bases.) The total number of (contracted) basis functions is 38 for each water molecule. We admit that the size of the basis set is considerably smaller than that adopted in previous studies on static electronic structure calculations,[184] and therefore, the computational results will not necessarily be accurate at the quantitative level.

The electronic states and the relevant matrix elements have been determined using the restricted open-shell Hartree−Fock (ROHF) method,[201] followed by a configuration interaction (CI) calculation with double excitations. The active space is limited to 10 molecular orbitals (MO), consisting of 2 occupied, 1 singly occupied, and 7 unoccupied MOs. Excitations to the higher MOs are neglected. The total number of configuration state functions (CSFs) in the active space amounts to 479.

5.2.1.2. Static Properties of Dimer Anion $(H_2O)_2^-$. We here study $(H_2O)_n$ with monomer number $n = 2$ (dimer) and $n = 3$ (trimer). These clusters are known to have a couple of locally stable structures.[184] In this study, we will focus on two distinct equilibrium structures of water anion dimers as shown in Figure 3. The structures shown here are stable within the accuracy of our calculation, whereas previous calculations with a larger basis set indicate different structures. The planar structure is close to "C2h" in ref 184. According to the calculations using a larger basis set, this was not in fact an equilibrium structure. Nevertheless, this planar structure is still of interest because the binding mechanism of the excess electron is clearly different from that of the nonplanar structure. In addition, other water molecules surrounding the excess electron with their electronic dipole momenta pointing inward may stabilize the planar structure in larger systems. Indeed, it is also argued that related types of binding structures may exist in larger clusters and/or in the presence of other ions.[183] Therefore, the small cluster under investigation may be regarded as a model subsystem being sampled out of a larger cluster.

5.2.1.3. Electronic Propagation. The initial conditions for SET dynamics were chosen as follows. Let us consider a system with three water monomers with an excess electron: one dimer anion plus one neutral molecule at the beginning. The first two monomers (m1 and m2) are placed in the configuration of the planar anion dimer. The other monomer (m3) is set to approach the dimer from a distance in such a manner that m3−m2 eventually forms the nonplanar anion configuration (see Figure 4). This

dx.doi.org/10.1021/cr200096s |*Chem. Rev.* 2012, 112, 499–542

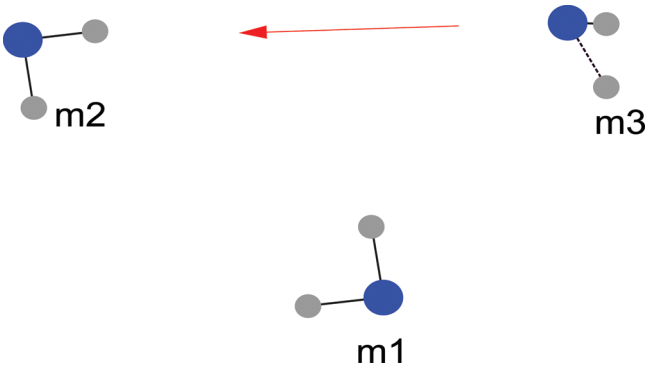

Figure 4. Configuration of collision between the planar dimer anion consisting of m1 and m2 and a water monomer m3.

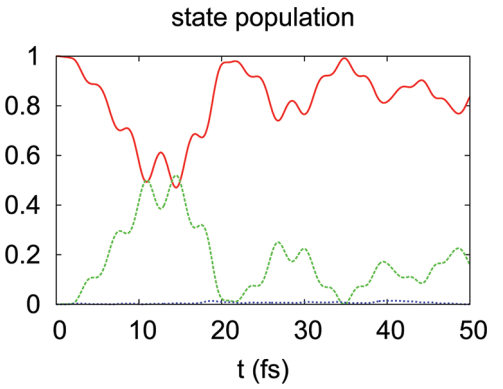

Figure 5. Time-dependent behavior of the adiabatic state populations during the collision of a water dimer anion and a water monomer as shown in Figure 4. The red solid line, green dashed line, and blue dotted line represent the ground, first excited, and second excited states, respectively. Changes in the populations of these states indicate nonadiabatic transitions.

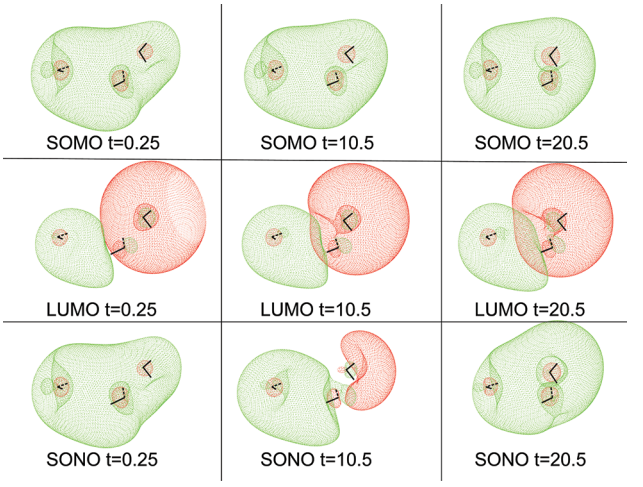

Figure 6. Selected snapshots of the spatial distribution of the SOMO (upper row), the LUMO (middle row), and the real part of the SONO (bottom row) during the collision of a water dimer anion and a water monomer. Green and red surfaces indicate the isocontour surfaces of the electronic orbitals at the amplitudes +0.01 Bohr$^{-3/2}$ and −0.01 Bohr$^{-3/2}$, respectively. Water molecules are indicated as a pair of black thin lines, each representing an OH bond. From left to right, times are t = 0.25, t = 10.50, and t = 20.50 (in units of fs). Although either the SOMO or the LUMO do not change their characters during the reaction, the SONO changes significantly.

arrangement was chosen with the expectation that electron migration is possibly more favorable than other random orientations. We also examined other collision geometries that are not explicitly shown here. The relative translational velocity given to the colliding monomer (m3 in Figure 4) is set to 0.17 Bohr/fs. Although this translational velocity is large, in the sense that the corresponding energy is much larger than the VDE predicted by a more accurate calculation such as in ref 184, it does not directly affect the binding structure, since it is a translational energy. Rather, a velocity of this magnitude is required to finish the calculations within a realistic time. The vibrational modes are then determined using the standard mode analysis on the equilibrium structures of the dimer and monomer. Each vibrational mode is treated approximately as an independent classical harmonic oscillator. Each oscillator is given an energy equal to the zero-point energy with a randomly chosen phase. We prepared a set of initial conditions scanning only the phases, which gives rise to about 30 collision paths in total, in order to confirm that the qualitative conclusions drawn are not pathological. No statistical sampling is taken with a view to calculating the average rate. Finally, the time steps for integrating the coupled equations for SET are set to 0.125 and 0.005 fs for nuclear and electronic dynamics, respectively. It was confirmed that finer time steps did not change the results qualitatively.

5.2.2. Nonadiabatic Migration of the Hydrated Electron. As a result of our SET simulation, basically two types of migration mechanisms for the excess electron were identified. One is what can be called the adiabatic migration, which is driven simply by the adiabatic change of the total electronic state. It has a rather long migration time scale reflecting the time scale of cluster deformation. Adiabatic electron migration has already been thoroughly studied by Tachikawa[188] and Head-Gordon.[189] Hence, here we will consider the nonadiabatic mechanism in depth from the analysis of the collision shown in Figure 4.

To demonstrate that this collision really induces nonadiabatic electron transfer, we expand the electronic wavepacket of SET in the adiabatic electronic states at each nuclear configuration and, thereby, attain the state population for the relevant adiabatic states. Figure 5 shows such population dynamics for the ground, the first excited, and the second excited state configurations. It is clearly observed that the interchange between the ground and the first excited states took place two times in between 10 and 15 fs. A large fluctuation in the state populations follows after that. In this graph, two characteristic time scales are observed: one with a period as short as about 8 fs, whereas the large amplitude component of the period can be as long as about 20 fs. The shorter time period is almost the same as that of the antisymmetric stretching mode of a water monomer. The longer time scale will be addressed below.

To see how the electronic states change nonadiabatically, a comparison of the SOMO, the LUMO, and the singly occupied natural orbital (SONO) is useful, as shown in Figure 6. Here, the SONO is defined as the natural orbital whose occupation number is closest to unity. As we mentioned above, natural orbitals are in general complex-valued (see eqs 128 and 129). In these figures we observe a characteristic change in the phase of SONO. Let us track the shape of the SOMO, the LUMO, and the real part of SONO as shown in Figure 6 and see the deformation in the

dx.doi.org/10.1021/cr200096s |*Chem. Rev.* 2012, 112, 499–542

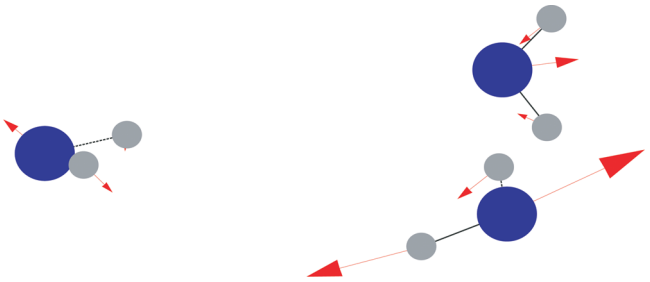

Figure 7. Approximate nonadiabatic coupling vector $\tilde{\mathbf{X}}_{g1}$ (see the text for the definition) at t = 18.625 fs, at which the nonadiabatic coupling term reaches its maximum value in the collision of a water dimer anion and a water monomer. Although the vectors are time-dependent, their spatial orientations change only minimally during the periods of the vibration motions.

electron migration. It is clear that the topology of either the SOMO or the LUMO does not appreciably change during the course of the collision, whereas that of the SONO changes significantly. This is obviously due to a mixing of the SOMO and LUMO. It should also be noted that the occupation number of the SONO remains very close to unity. Thus, it is in the smooth change in the shape of the SONO that the electron-dynamical effect of the nonadiabatic transition manifests itself most clearly.

5.2.3. Nuclear Motion Inducing Nonadiabatic Transitions. We next study the geometrical aspects of the observed nonadiabatic transition. The observed nonadiabatic transitions originate from the matrix element of the nonadiabatic coupling operator $\hbar\dot{\mathbf{R}}\cdot\mathbf{X}$ between the two adiabatic states: $|\Psi_g(\mathbf{R}(t))\rangle$ and $|\Psi_1(\mathbf{R}(t))\rangle$ (see eq 46). It is therefore pertinent, in the first instance, to study a spatial vector of $\hbar X_{g1} \equiv \hbar\langle\Psi_g(\mathbf{R}(t))|\hat{\mathbf{X}}|\Psi_1(\mathbf{R}(t))\rangle$. Since the nonadiabatic coupling element $\hbar\dot{\mathbf{R}}\cdot\mathbf{X}$ is an inner product between the nuclear velocity vector $\dot{\mathbf{R}}$ and the coupling element vector $\hbar\mathbf{X}_{g1}$, nuclear modes that are parallel to the latter vector should strongly enhance the nonadiabatic transition.

For the adiabatic functions expanded in the CSF basis set as $|\Psi_\alpha\rangle = \Sigma_I C_{\alpha,I}|\Phi_I\rangle$, the nonadiabatic coupling is decomposed into

$$\langle\Psi_\alpha(\mathbf{R})\left|\frac{\partial}{\partial R^\mu}\right|\Psi_\beta(\mathbf{R})\rangle = \sum_{I,J} C^*_{\alpha,J} X^\mu_{JI} C_{\beta,I} + \sum_I C^*_{\alpha,J}\frac{\partial}{\partial R^\mu} C_{\beta,I} \tag{130}$$

Therefore, even if the transition through the above elements of X^μ_{IJ} is set to zero, the left-hand side is not necessarily reduced to zero, because of the presence of the last term. In Figure 7, we plot the first term on the right-hand side of eq 130 times $\hbar$, redefined below more explicitly

$$\hbar\tilde{\mathbf{X}}_{g1} \equiv \hbar\sum_{I,J} C^*_{gJ}\mathbf{X}_{JI}C_{1I} \tag{131}$$

where $C_{gJ} \equiv \langle\Psi_g(\mathbf{R})|\Phi_J(\mathbf{R})\rangle$ and $C_{1I} \equiv \langle\Psi_1(\mathbf{R})|\Phi_I(\mathbf{R})\rangle$. It is immediately clear from this figure that $\hbar\tilde{\mathbf{X}}_{g1}$ strongly couples to the OH antisymmetric stretching mode of the water dimer.

The nonadiabatic coupling term $\hbar\dot{\mathbf{R}}\cdot\mathbf{X}_{g1}$ undergoes a rapid oscillation mainly due to the fast oscillatory motion of the nuclei. Its angular frequency has a value around 0.0017 in atomic units, which clearly reflects the frequency of the OH antisymmetric stretching (as) mode, ω_{as} in dimer anions: $\omega_{as}/2\pi \sim 3700\ \mathrm{cm}^{-1}$. As a result, both the spatial distribution of $\hbar\tilde{\mathbf{X}}_{g1}$ and the time series of $\hbar\dot{\mathbf{R}}\cdot\langle\Psi_g(\mathbf{R})|\hat{\mathbf{X}}|\Psi_1(\mathbf{R})\rangle$ strongly suggest that the OH

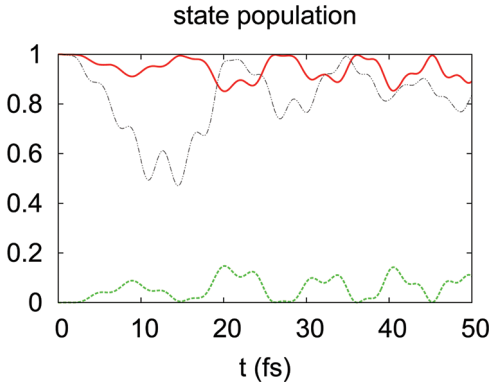

Figure 8. Time-dependent behavior of the adiabatic state populations during the collision of fully deuterized molecules (water dimer anion and water monomer). The electronic state populations in the adiabatic basis are shown. The red solid line, green dashed line, and blue dotted line represent that of the ground, first excited, and second excited states, respectively. The time evolution of the ground state population obtained from the corresponding calculation with undeuterized molecules is also plotted with thin black dotted lines for comparison (see Figure 5).

antisymmetric stretching motion should trigger the nonadiabatic migration of the hydrated electron.

5.2.4. Isotope Effects. The present electron migration is heavily dependent on the nonadiabatic coupling elements, which is in turn a function of the nuclear (reduced) masses. Therefore, it is readily anticipated that the migration should be significantly affected by exchanging the protons by deuterons. Indeed it is the case, as we will exemplify below. We track the dynamics of such isotope effects by choosing the same initial configuration, orientation, and kinetic energies as those in Figures 4 and 5. The results in Figure 8 clearly show a significant suppression in nonadiabatic transitions. To see it more clearly, in Figure 9 we show the snapshots of the SOMO, LUMO, and SONO for this collision at selected instances. It is obvious that neither the SOMO or LUMO is affected by deuterium substitution, whereas the SONO most definitely is (compare with Figure 6). This highlights one of the crucial differences between the SET calculations and *ab initio* MD type (or CI type) static calculations, in which virtually no change in electronic properties is expected to be induced by deuterium substitution. As seen in the figure, the SONO in the current case is quite similar to the SOMO. This clearly illustrates that the SOMO and LUMO do not mix much into the SONO (compare again with the SONO in Figure 6).

5.2.5. Origin of the Longer Time Scale. Finally we survey the origin of the longer time scale, around 20 fs, as found in Figure 5. This is directly responsible for the time scale of the gross electronic transition. In other words, it is a characteristic time scale for a vibration-electron coupled mode. To see this more clearly, we must first reduce the original system into a simplified model. We need only two electronic states, since the state population transfer occurs predominantly between the ground $|\Psi_g(\mathbf{R}_t)\rangle$ and the first excited electronic states, $|\Psi_1(\mathbf{R}_t)\rangle$. If we expand the electronic wavepacket only in two states as $|\Psi(t)\rangle = C_g(t)|\Psi_g(\mathbf{R}_t)\rangle + C_1(t)|\Psi_1(\mathbf{R}_t)\rangle$, we obtain the nonadiabatic time evolution equation as

$$i\hbar\frac{\partial}{\partial t}\begin{pmatrix} C_g \\ C_1 \end{pmatrix} = \begin{pmatrix} E_g & -i\hbar\dot{\mathbf{R}}\cdot\mathbf{X}_{g1} \\ -i\hbar\dot{\mathbf{R}}\cdot\mathbf{X}_{1g} & E_1 \end{pmatrix}\begin{pmatrix} C_g \\ C_1 \end{pmatrix} \tag{132}$$

dx.doi.org/10.1021/cr200096s |*Chem. Rev.* 2012, 112, 499–542

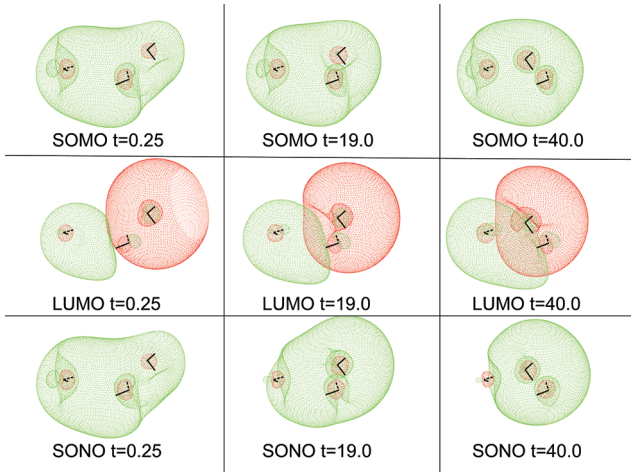

Figure 9. Selected snapshots of the spatial distribution of the SOMO (upper row), the LUMO (middle row), and the real part of the SONO (bottom row) for the collision of fully deuterized molecules (water dimer anion and water monomer). Green and red surfaces indicate the isocontour surfaces of the electronic orbitals at the amplitudes +0.01 $\text{Bohr}^{-(3)/(2)}$ and −0.01 $\text{Bohr}^{-(3)/(2)}$, respectively. Water molecules are indicated as a pair of black thin lines, each representing an OH bond. From left to right, times are $t = 0.25$, $t = 19.00$, and $t = 40.00$ (in units of fs). This figure should be compared to the undeuterized counterpart (Figure 6).

where E_g and E_1 are the energies of the ground and the first excited state, respectively. We next approximate the contribution of nuclear motion to a single oscillation mode (actually the OH antisymmetric stretching mode as indicated above) as

$$\begin{aligned}\hbar\dot{\mathbf{R}}\cdot\mathbf{X}_{g1} &= \hbar A_{as}\cos(\omega_{as}t)\boldsymbol{\varepsilon}_{as}\cdot\mathbf{X}_{g1}\\ &= V_{g1}^{0}(e^{i\omega_{as}t} + e^{-i\omega_{as}t})\end{aligned} \tag{133}$$

where ω_{as}, $\boldsymbol{\varepsilon}_{as}$, and A_{as} are the angular frequency, the direction, and the velocity amplitude of the asymmetric stretching mode, respectively. Here $V_{g1}^{0} \equiv 1/2\hbar A_{as}\boldsymbol{\varepsilon}_{as}\mathbf{X}_{g1}$ is half of the oscillation amplitude of the matrix element $\hbar\dot{\mathbf{R}}\mathbf{X}_{g1}$. The time evolution equation eq 132 is then essentially equivalent to the Rabi oscillation model. An approximate solution is then obtained using the rotating wave approximation. The upper state population oscillates as

$$|C_1|^2 = \frac{4|V_{1g}^{0}|^2}{(E_1 - E_g - \hbar\omega_{as})^2 + 4|V_{1g}^{0}|^2}\sin^2(\lambda t)$$

where λ is defined as

$$\lambda \equiv \sqrt{|V_{g1}^{0}|^2 + \left(\frac{E_1 - \hbar\omega_{as} - E_g}{2}\right)^2}$$

Thus, the characteristic time scale of the electronic state oscillation is $2\pi/\lambda$, which is different from either the electronic time scale $2\pi\hbar/(E_1 - E_g)$ or the nuclear oscillation time scale $2\pi/\omega_{as}$. Our model prediction of $2\pi/\lambda$ using the quantities obtained in the current calculations roughly agrees with the observed time scale 20 fs. Again, it should be noted, however, that the quantitative accuracy is limited due to the rather small basis set. Nonetheless, we expect that the underlying mechanism of nonadiabatic dynamics may apply to larger calculations.

5.2.6. Summary. As illustrated above, nonadiabatic dynamics exhibits vividly how electrons move in and between molecules. Complex natural orbitals, in particular the SONO in the present case, clearly illustrate how the electronic wave function evolves in time. In addition to the time scale, the driving mechanism for the electron migration has also been illustrated. By clarifying such complex electron behavior, not available using stationary-state quantum chemistry, our understanding of realistic chemical reactions is greatly enhanced. As a result, it has clearly been shown that nonadiabatic electron wavepacket theory is invaluable in the analysis of nonrigid and mobile electronic states of molecular systems.

5.3. Role of Nonadiabaticity in Chemical Dynamics under Intense Laser Fields

We next show a couple of numerical examples of how electronic nonadiabaticity in chemical reaction dynamics can be modulated by laser fields. Even in a case with medium intense laser field, the interaction of the field and nuclear derivative coupling (NDC) of the electronic state affects the dynamics in a qualitative level.[82,151] More precisely, we observe that the presence of nonadiabatic coupling can alter the channels of reaction more than the relevant case without a nuclear derivative coupling element. Toward a goal of control of chemical reactions through modulation or creation of electronic states in terms of laser fields, we here briefly survey some general responses of selected molecules to pulse lasers through *ab initio* calculations of electronic wavepackets. The computational level here is only qualitative without pursuit of numerical accuracy, and we use the semiclassical Ehrenfest theory with laser fields throughout this subsection.

Path branching due to nonadiabatic interaction, electromagnetic fields by lasers, and their coexistence are presented with the PSANB scheme in ref 157.

5.3.1. Methyl Alcohol as an Example. Our first system to be examined is CH_3OH. Figure 10 highlights the role of NDC in chemical dynamics under the influence of different types of laser field. *Ab initio* calculations were carried out using the configuration interaction with a single excitation (CIS)/restricted Hartree−Fock (RHF)/6-31G(d) level. The frozen core orbitals were the two 1s orbitals of C and O. The starting molecular structure is set to the optimized geometry for the electronic ground state. The schematic view along with the coordinate system used are depicted in panel a of Figure 10. In all these computations represented in Figure 10, the initial electronic states are set to the first adiabatic excited state in the singlet manifold. The initial momenta of the nuclei are set at zero. In panels b and c, the time progressions of the CO and OH bond lengths under two different laser fields are depicted. In each system, two cases are compared, one with the proper NDC and the other where NDC is intensionally neglected. Due to the single occupation of the antibonding orbital for this initial condition, OH bond tends to cleavage in the case without a laser field. This is well illustrated by the blue dotted lines on the right side panels of parts b and c.

Panel b in Figure 8 shows the dynamical responses to a static linear electronic field (cw laser), whose field strength E_s is as weak as 0.005 au; this corresponds to an intensity 8.75×10^{11} W/cm^2. The direction of the electric field is along the y axis, which is approximately equivalent to the initial direction of the CO bond line. On the other hand, panel c in Figure 10 shows the

dx.doi.org/10.1021/cr200096s |*Chem. Rev.* 2012, 112, 499–542

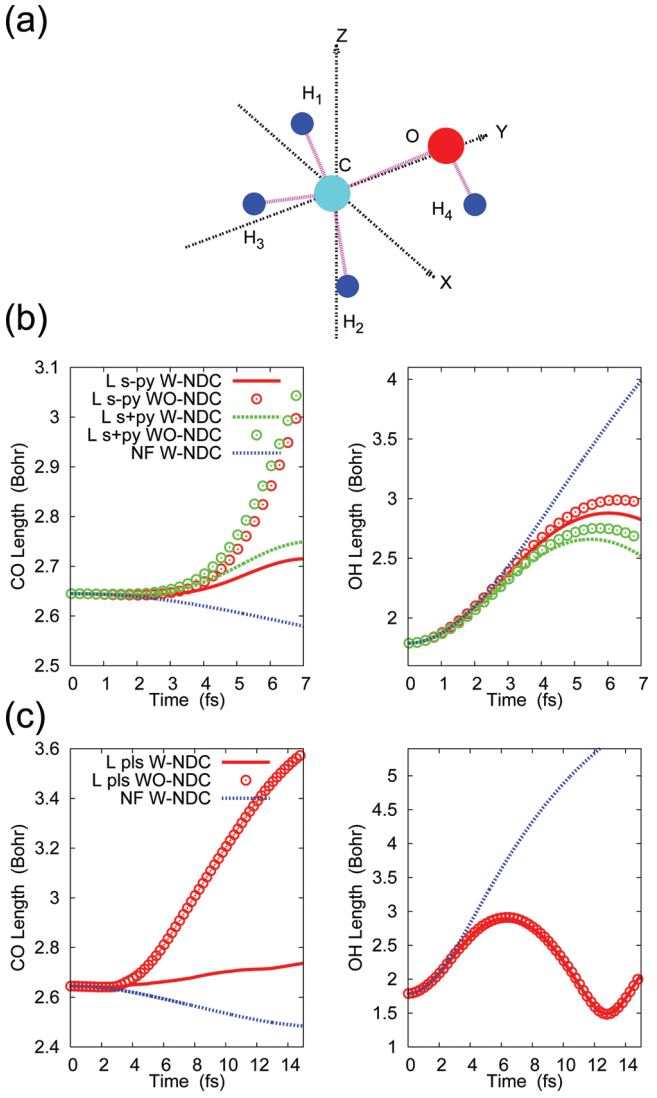

Figure 10. Role of nuclear derivative coupling (NDC) in dynamics under static (cw) and pulse lasers (in panels b and c, respectively). The system examined is CH_3OH, starting from the first electronic excited state with the initial geometry (panel a) set at the optimized structure in the electronic ground state. In both panels b and c, the progression of the CO and OH bond lengths is plotted under different conditions. The letter "L" in the panels indicates the cases with a laser field, while NF denotes the case in the absence of a laser field. "W" and "WO NDC", respectively, represent the cases with and without the NDC term in the electron wavepacket dynamics. In the case of application of a laser, the results are shown in red solid lines and open circles, respectively.

case for the strong laser pulse field. The radiation vector field $\mathbf{A}(t)$, as a function of time, is constructed in the form of

$$\mathbf{A}(t) = A_s \exp\left(-\left(\frac{t-t_c}{t_w}\right)^2\right) \sin(\omega(t-t_c))\cdot\hat{u} \qquad (134)$$

where $A_s = cE_s/\omega$, with E_s being the electronic field strength and c the velocity of light. A unit vector $\hat{u}$ denotes a polarization direction of the radiation field. The corresponding electric field is given by $\mathbf{E}(t) = -(1/c)(d\mathbf{A}(t)/dt)$. The field direction is the same as that in Figure 10 panel b, but the field strength is set to $E_s = 0.1$, with the corresponding intensity 3.5×10^{14} W/cm^2. The pulse parameters applied are as follows: central field frequency $\omega = 0.057$, duration time width $t_w = 2.42$ fs, and central peak time $t_c = 4.84$ fs. Note that the period corresponding to ω is 2.66 fs and that this is sufficiently long compared to the electronic motion but short enough with respect to the typical period of molecular vibrational motion.

In Figure 10 panels b and c, we immediately notice that the applied laser fields along the y axis significantly suppress the cleavage of the OH bond for both static and pulse lasers, respectively. Instead, the pulse laser in Figure 10 left (c) prolongs the CO bond dissociation, while the static field does not enhance the CO dissociation as in panel b left. The result is that the lasers have totally altered the channel of chemical reaction.

It is also well recognized that NDC can bring about a qualitative effect on the CO bond length in the dynamics of a static laser field. If we neglect the NDC in the semiclassical Ehrenfest theory, the result is CO bond dissociation. On the other hand, this is not the case in the presence of NDC (see left panel of Figure 10c). In the case of the pulse laser, the effect of NDC on the CO bond length only occurs at a quantitative level.

5.3.2. Example of Hydroxylamine. In Figure 11 we illustrate the role of NDC in the case of the electronic excited dynamics of NH_2OH under the influence of external laser fields. The same notations are used as described above for methyl alcohol. *Ab initio* calculations were performed within the CIS/RHF/6-31G(d) level. The frozen core orbitals were the two 1s orbitals of N and O. The initial electronic state was set as the second excited state in the singlet manifold. This state has a strong interaction with the first excited state in the early stage of dynamical relaxation starting from the optimized geometry at ground electronic states. We, therefore, chose the optimized geometry at electronic ground state as the initial molecular geometry. The structure is drawn in Figure 10 panel a. We set the initial momenta to zero. The dynamical relaxation in the absence of a laser field under this initial condition is characterized by the NO cleavage within tens of femtoseconds. This is well illustrated by the red circles in the far left box of panel b in Figure 10.

Panel b in Figure 10 presents the time dependence of NO (left panel), terminal OH lengths (central panel), and the HNH angle (right panel) under the static laser fields of the field strength $E_s = 0.005$ au. The polarization vectors of the resultant electric field lie on the x, y, and z axes. Only in the case of the x-directed field, is a stronger laser of $E_s = 0.01$ au applied. In addition, the dynamics in the absence of laser fields is also shown. As seen in the figure, the laser field polarized along the y axis gives rise to the most drastic reduction in the NO cleavage accompanied by the enlargement of the HNH angle. The increase in the bond length of NO is almost one-half within 7 fs as a result of the presence of the electric field in the y-direction. On the other hand, the laser in the z-direction leads to a moderate elongation of the OH bond. More importantly, this is accompanied by a slight suppression of the NO bond cleavage. This indicates the rearrangement of bond breaking from NO to OH.

To closely examine the role of NDC on the rearrangement of the reaction pathway under these particular laser conditions, it is necessary to compare the dynamics between the two cases, namely with and without NDC in the z-polarized field in panel c. The significant OH enlargement is observed only in the case without NDC. We also find that a suppression of NO cleavage is weakened by NDC. This suggests that NDC within the CSF representation plays a key role in the suppression of dynamical energy transfer by lasers from electrons to nuclei subsystems.

dx.doi.org/10.1021/cr200096s |*Chem. Rev.* 2012, 112, 499–542

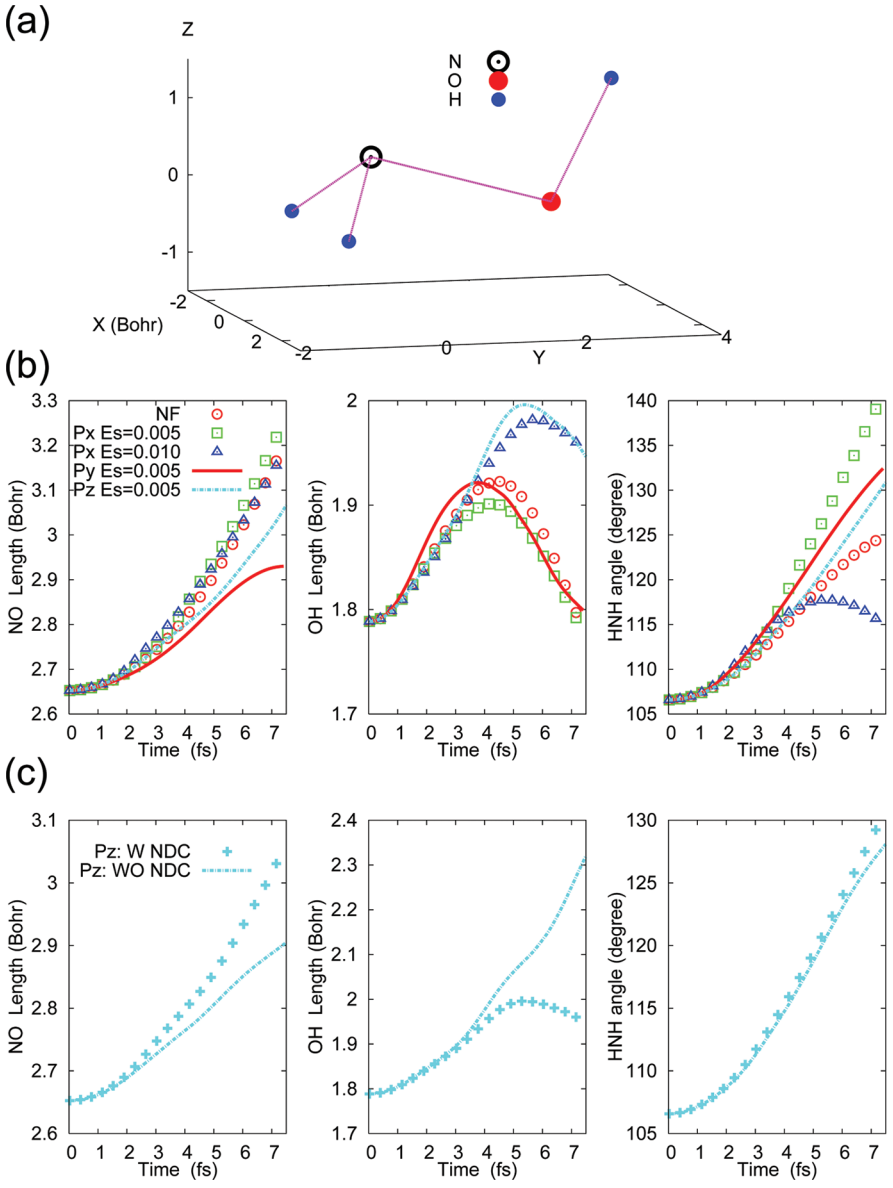

Figure 11. Dynamics of NH_2OH under static laser fields of three different polarizations in the *x*, *y*, and *z* directions, denoted respectively as P_x, P_y, and P_z. The field strength E_s is 0.005 au, cooresponding to the intensity 8.75×10^{11} (W/cm^2). Panel a shows the initial structure of the molecule. Panel b presents the dynamics of the bond lengths of NO and OH and the HNH angle in cases of no laser field (NF) and under the presence of static laser fields. Nuclear derivative couplings are fully taken into account. Panel c compares the structure dynamics with and without NDC, which are represented by points and lines, respectively. Only the results for P_z are shown.

Hopefully, these numerical studies have served as an illustrative presentation of the basic methodology of electron wavepacket dynamics for the study of the laser modulation of chemical reactions. This is just a preliminary step toward the ultimate design of laser fields that will in fact be capable of controlling chemical reactions with a view to yielding our target molecules.

5.4. Electron Wavepacket Dynamics across Conical Intersections

A conical intersection is a continuous manifold of molecular geometry, for which the two or more adiabatic potential energy surfaces degenerate in energy and the nonadiabatic coupling elements within them are divergent.[15,202] In the diabatic representation of a two-state system, a conical intersection satisfies the following equation

$$H_{11}^{\mathrm{el}}(\mathbf{R}) = H_{22}^{\mathrm{el}}(\mathbf{R}) \quad \text{and} \quad H_{12}^{\mathrm{el}}(\mathbf{R}) = 0 \tag{135}$$

thereby forming a $3N - 8$ dimensional manifold in the **R** space. This particular nonadiabatic region is characterized in terms of a very rapid electronic relaxation in photochemical reactions.[203] As mentioned in section 1.3, the passage of a wavepacket across a conical intersection can be experimentally observed[49,50,52] and optically controlled.[51]

The importance of a conical intersection in chemical reactions has been revealed by great progress in the field of quantum chemistry for electronic excited states.[15,202] In particular, the elaboration in *ab initio* methods for correlated electronic wave functions has made a significant contribution. Of note among

dx.doi.org/10.1021/cr200096s |*Chem. Rev.* 2012, 112, 499–542

these methods are the following: multireference configuration interaction (MRCI),[204] multistate multiconfigurational second-order perturbation (MS-CASPT2),[205] and symmetric-adapted-cluster configuration interaction (SAC-CI).[206]

In addition, it should be mentioned that progress in the theory of excited states and in time dependent density functional theory played an important role.[207] For the state coupling matrix elements, see refs 208−211, and for the study of larger systems, readers are referred to refs 212 and 213. However, because the study of the conical intersection with electron wavepacket dynamics is quite rare, we therefore explore it below with PSANB. Electron dynamics involved in conical intersection constitutes a key factor for the further elucidation of electronic relaxation phenomena accompanied by structural change triggered by photoexcitation and electron attachment to and detachment from molecules.

An adiabatic representation generally fails in describing nonadiabatic dynamics at a conical intersection because of the divergent nature of the relevant nonadiabatic coupling elements, and therefore good and effective diabatic representations have been devised.[16,214,215] The CSF basis turns out to provide a rather good approximation to the diabatic representation, which has been successfully employed in studies on electron dynamics within the semiclassical Ehrenfest theory.[82,99,100,124,129,151,156] On the other hand, there are studies on construction of effective adiabatic surfaces that include the effect of a geometrical phase around the singular point and on their application to realistic chemical reactions as a part of quantum scattering phenomena.[104,216,217]

One of the most interesting features of conical intersection is a curious phase, first discovered by Herzberg and Longuet-Higgins.[102] By examining the Teller first order model in the vicinity of a conical intersection point, they showed that an adiabatic electronic wave function, guided by adiabatic parameters such as a smooth nuclear path, accumulates a quantum phase as much as π while it makes a single circuit around this point.[102] In this article, therefore, we collectively name the phases arising from the relevant phenomena "the Longuet-Higgins phase". This phase was rediscovered in the general study of level repulsion in chaotic dynamics by Berry; it is now called the Berry phase.[103] However, it was Mead who first studied and pointed out the theoretical similarity of the Longuet-Higgins phase to the Aharonov-Bohm effect.[104,105] Later, Mukunda and Simons established its common mathematical foundation for a geometric phase in terms of anholonomy in fiber bundle theory.[218] The effects of the Longuet-Higgins phase on chemical dynamics have been discussed extensively in conjunction with quantum scattering phenomena[15,104,216,217,219−223] and vibronic spectroscopy in a Na_3 system, which was examined theoretically by Kendrick.[224−227] In a control theory of chemical reactions, Domcke et al. examined the effect of phase on a photodissociation branching ratio of phenol.[167] The geometric phase is critically important, not only in molecular science, but also in solid state physics; for instance, it is claimed that the quantum hole effect in quantum transport is related to the geometric phase.[228,229]

In this subsection, we will present a multidimensional extension of the PSANB method. Using it we analyze a generally complicated quantum interference phenomenon associated with the electron−nuclear simultaneous dynamics around a conical intersection in a rather qualitative manner. We examine how appropriately the path branching can describe not only the geometric phase but also the resultant quantum interference.

5.4.1. Longuet-Higgins Phase. Let us now briefly review the original work by Herzberg and Longuet-Higgins, since it is not only instructive but also pertinent to our argument. They considered a two-state model Hamiltonian in a diabatic representation with two variables x and y,

$$H = \begin{pmatrix} H_{11} & H_{12} \\ H_{21} & H_{22} \end{pmatrix} = \begin{pmatrix} W + (m + k)x & ly \\ ly & W + (m - k)x \end{pmatrix}, \quad k \neq 0 \tag{136}$$

where l, m, and k are the parameters used to control the system and its interactions. The two eigenvalues are readily found as

$$E_{\pm} = W + mx \pm \sqrt{k^2x^2 + l^2y^2} \tag{137}$$

Since a conical intersection point is defined so as to satisfy $E_+ = E_-$, it is located at $(x_0,y_0) = (0,0)$. It should be noted that the coupling element $H_{12} = H_{21}$ changes its sign by $y \rightarrow -y$. To examine the $x-y$ dependency of the adiabatic wave functions around this singular point, they introduced a polar representation as $R = (k^2x^2 + l^2y^2)^{1/2}$ and $\theta = \arctan(y/x)$. Then, since the lower state wave function, $|\phi\rangle = C_1^L|1\rangle + C_2^L|2\rangle$, satisfies

$$\begin{pmatrix} C_1^L(\theta) \\ C_2^L(\theta) \end{pmatrix} = \exp(i\alpha) \begin{pmatrix} +\sin\dfrac{\theta}{2} \\ -\cos\dfrac{\theta}{2} \end{pmatrix} \tag{138}$$

with an arbitrary real value α, this immediately leads to

$$\begin{pmatrix} C_1^L(\theta + 2\pi) \\ C_2^L(\theta + 2\pi) \end{pmatrix} = -\begin{pmatrix} C_1^L(\theta) \\ C_2^L(\theta) \end{pmatrix} \quad \text{and} \quad \begin{pmatrix} C_1^L(\theta + 4\pi) \\ C_2^L(\theta + 4\pi) \end{pmatrix} = +\begin{pmatrix} C_1^L(\theta) \\ C_2^L(\theta) \end{pmatrix} \tag{139}$$

Thus, an electron wavepacket obtains a phase π during a single circuit.

Then, let us consider two paths in configuration space, one of which makes a circuit in a clockwise manner and the other of which is counterclockwise. We also suppose that they are both symmetric with respect to the inversion $y \leftrightarrow -y$, and one moves from $\theta = 0 \rightarrow \pi/2 \rightarrow \pi$ and the other from $\theta = 0 \rightarrow -\pi/2 \rightarrow -\pi$. Then, if we track the two paths starting from the same point (R,θ) with the same phase, they meet again at a confluence point $(R,\theta + \pi) = (R,\theta - \pi)$, where the following equation is satisfied such that

$$\begin{pmatrix} C_1^{L:p1}(\theta + \pi) \\ C_2^{L:p1}(\theta + \pi) \end{pmatrix} = \exp(i\alpha) \begin{pmatrix} +\cos\dfrac{\theta}{2} \\ -\sin\dfrac{\theta}{2} \end{pmatrix} \quad \text{and} \quad \begin{pmatrix} C_1^{L:p2}(\theta - \pi) \\ C_2^{L:p2}(\theta - \pi) \end{pmatrix} = \exp(i\alpha) \begin{pmatrix} -\cos\dfrac{\theta}{2} \\ +\sin\dfrac{\theta}{2} \end{pmatrix} \tag{140}$$

This completes the proof.

dx.doi.org/10.1021/cr200096s |Chem. Rev. 2012, 112, 499–542

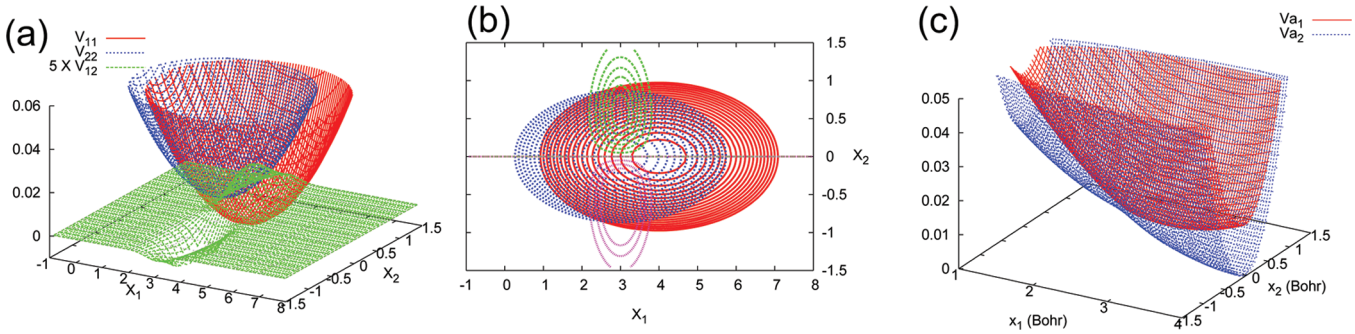

Figure 12. Panel a for the diabatic potentials (V_{11} and V_{22} with V_{12} the coupling function) and panel c for the adiabatic one in the present model system with a conical intersection. Panel b presents a contour plot of the diabatic potential functions.

5.4.2. Present System To Be Studied. We then study how the non-Born−Oppenheimer paths in the PSANB theory can materialize the effect of the geometrical phase by employing the same model functions as recently used in the work of the optimal Gaussian spawning scheme by Martinez's group.[118] Their model is related to the one proposed in the paper by Ferretti et al.[230] A model similar to this has also been used by Kapral et al. in a study of the environmental effect on the electron dynamics around a conical intersection.[231] The diabatic potential energies V_{11}, V_{22} and coupling matrix elements V_{12} are depicted in Figure 12. The potential functions of diabatic states #1 and #2 are defined as

$$V_{11} = \frac{1}{2}k_x(x_1 - X_{c1})^2 + \frac{1}{2}k_y x_2^2 \tag{141}$$

$$V_{22} = \frac{1}{2}k_x(x_1 - X_{c2})^2 + \frac{1}{2}k_y x_2^2 + \Delta \tag{142}$$

respectively. The state coupling matrix element is given by

$$V_{12} = \gamma x_2 \exp(-\alpha(x_1 - X_{c3})^2 - \beta x_2^2) \tag{143}$$

Here, the parameters are set to $X_{c1} = 4$, $X_{c2} = 3$, $X_{c3} = 3$, $k_x = 0.01$, $k_y = 0.1$, $\Delta = 0.01$, $\alpha = 3$, $\beta = 1.5$, and $\gamma = 0.01$. The masses associated with the x_1 and x_2 coordinates are set to 20000 and 6667 in atomic units, respectively. Note that the point $(x_1,x_2) = (2.5,0)$ provides the degenerate adiabatic energies. The key feature of this system is that the diabatic coupling matrix has two maxima in their absolute values, each having the opposite signs in a symmetric position with respect to the x_2 axis, thereby leading to a node along this axis. The profiles of the system functions are presented in Figure 12, in which the existence of the conical intersection point is clearly recognized.

We here note the symmetry of this system. Let us consider a situation in which the initial wavepacket on a single electronic state has a symmetric shape in position and momentum space with respect to the x_2 axis and the corresponding momentum axis as well. We also suppose that this initial wave function is placed at a region where no state coupling is present. Then, by looking at Figure 12 we immediately notice that the fate of this wave function cannot be represented in terms of a single nuclear path, because the coupling magnitude along this path retaining symmetry is zero all the way. Thus, we have to think about a symmetric pair of paths, both of which start from a distribution function that represents the initial wave function. Such a method has previously been established,[157] in which the Monte Carlo importance sampling was employed.

In the following discussion we consistently adopt the diabatic representation because the nuclear derivative coupling elements diverge in the adiabatic representation.

5.4.3. Electronic Phase on non-Born−Oppenheimer Paths. Let us now consider in more precise detail the electronic phase arising from the path branching around the conical intersection. For simplicity, let us assume that the initial electronic state is state #1. According to PSANB theory, the electron wavepacket at t, slightly after a single branch at t^* (but before the next branch), is expressed as a specific form of eq 83

$$\begin{pmatrix} |\Psi_1(t)\rangle \\ |\Psi_2(t)\rangle \end{pmatrix} = \begin{pmatrix} C_1^1(t-t^*)\, C_1(t^*)|\Phi_1(\mathbf{R}_1(t))\rangle + C_1^2(t-t^*)\, C_2(t^*)|\Phi_1(\mathbf{R}_2(t))\rangle \\ C_2^1(t-t^*)\, C_1(t^*)|\Phi_2(\mathbf{R}_1(t))\rangle + C_2^2(t-t^*)\, C_2(t^*)|\Phi_2(\mathbf{R}_2(t))\rangle \end{pmatrix} \tag{144}$$

where $C_K(t^*)$ is the K-th state electronic amplitude at the branch time t^* and $C_K(0) = \delta_{1K}$. Additionally, at time t later than t^*, $C_K^1(t-t^*)$ and $C_K^2(t-t^*)$ are the K-th state electronic amplitudes on a branching path running dominantly on states #1 and #2, respectively. Ψ_K and Φ_K correspondingly denote the K-th time-dependent component and K-th electronic states while $\mathbf{R}_I$ denotes a PSANB path running predominantly on the I-th state. It should be noted that the state vector on the left-hand side provides a formal description of the total electronic wave function from the electron dynamics point of view. The branching paths restart from the branching point as initial conditions with $C_K^1(0) = \delta_{1K}$ and $C_K^2(0) = \delta_{2K}$, respectively. The product form appearing in these amplitudes ensures that electronic coherence along the paths is retained.

5.4.4. Parity Conservation of the Electronic Phase along Paired Symmetric Paths. The potential function in the two-state electronic Hamiltonian can be split into the diagonal and off-diagonal parts, respectively, as

$$\underline{V}_0 = \begin{pmatrix} V_{11} & 0 \\ 0 & V_{22} \end{pmatrix} \quad \text{and} \quad \underline{V}_I = \begin{pmatrix} 0 & v_I \\ v_I & 0 \end{pmatrix} \tag{145}$$

with $v_I \equiv V_{12} = V_{21}$. Also the time dependent electronic-state coefficients can be written in a vector form as follows

$$\underline{C}(t) = \begin{pmatrix} C_1(t) \\ C_2(t) \end{pmatrix} \tag{146}$$

dx.doi.org/10.1021/cr200096s |Chem. Rev. 2012, 112, 499–542

Furthermore, a symmetric pair of PSANB paths $\mathbf{R}^{\pm}(t)$ defined by

$$\mathbf{R}^{\pm}(t) = (x_1(t), \pm x_2(t)) \tag{147}$$

can be introduced and the corresponding electron wavepackets evolving on these paths are referred to $\underline{C}^{\pm}(t)$. It should be recalled that the state coupling matrix elements $v_I \equiv V_{12} = V_{21}$ are odd functions with respect to x_2. That is,

$$v_I(\mathbf{R}^{+}(t)) = -v_I(\mathbf{R}^{-}(t)) \tag{148}$$

while the diagonal potential functions are even functions of x_2,

$$V_{II}(\mathbf{R}^{+}(t)) = V_{II}(\mathbf{R}^{-}(t)) \tag{149}$$

where $I = 1, 2$.

In a PSANB scheme, a single wavepacket component accumulates phases from both electronic and nuclear dynamics in such a manner as that described in eq 111. First the phases along the pair of nuclear paths are studied. These phases evolve in time according to the effective electronic potential $V_{\mathrm{eff}}^{\pm}(t)$ and effective nuclear kinetic energies $T_{\mathrm{nuc}}^{\pm}(t)$ along paths

$$S(\mathbf{R}^{\pm}(t)) = \int_0^t \mathrm{d}\tau\, (T_{\mathrm{nuc}}^{\pm}(\tau) - V_{\mathrm{eff}}^{\pm}(\tau))$$

where

$$T_{\mathrm{nuc}}^{\pm}(\tau) \equiv \sum_k^{1,2} \frac{(\dot{R}_k^{\pm}(\tau))^2}{2M_k} \quad \text{and}$$
$$V_{\mathrm{eff}}^{\pm}(\tau) \equiv \{\underline{C}^{\pm}(\tau)\}^{\dagger} \underline{\underline{H}}(\mathbf{R}^{\pm}(\tau)) \underline{C}^{\pm}(\tau)$$

with masses M_k associated with the coordinate x_k. The contributions of the kinetic energies to the phases from these two symmetric paths $\mathbf{R}^{\pm}(t)$ should be exactly identical.

The phase associated with the electronic state is much more involved. To survey the symmetric property of the electronic phases, we must first examine an infinitesimal evolution from t_0 to $t_0 + \mathrm{d}t$ for electron wavepackets $\underline{C}^{\pm}$ on a path starting from their own symmetric conditions. Let us suppose that the electron wavepackets are running on the first diabatic surface (V_{11}) with the following initial condition $C_k^{\pm}(t_0) = \delta_{k1}$. Within the first order expansion with respect to a short time-step $\mathrm{d}t$, the Schrödinger equation of the electron wavepacket gives

$$\begin{aligned} C_1^{\pm}(t_0 + \mathrm{d}t) &= 1 - \frac{i}{\hbar} V_{11}(\mathbf{R}^{\pm}(t_0))\, \mathrm{d}t, \\ C_2^{\pm}(t_0 + \mathrm{d}t) &= -\frac{i}{\hbar} v_I(\mathbf{R}^{\pm}(t_0))\, \mathrm{d}t \end{aligned} \tag{150}$$

By taking into consideration the relations in eqs 148 and 149, we know

$$\begin{aligned} C_1^{\pm}(t_0 + \mathrm{d}t) &= 1 - \frac{i}{\hbar} V_{11}(\mathbf{R}^{+}(t_0))\, \mathrm{d}t, \\ C_2^{\pm}(t_0 + \mathrm{d}t) &= \mp \frac{i}{\hbar} v_I(\mathbf{R}^{+}(t_0))\, \mathrm{d}t \end{aligned} \tag{151}$$

which immediately shows

$$C_1^{+}(t_0 + \mathrm{d}t) = +C_1^{-}(t_0 + \mathrm{d}t) \tag{152}$$

$$\begin{aligned} \mathrm{Re}\{C_1^{+}(t_0 + \mathrm{d}t)\} &= \mathrm{Re}\{C_2^{+}(t_0 + \mathrm{d}t)\} = 0, \\ \mathrm{Im}\{C_1^{+}(t_0 + \mathrm{d}t)\} &= -\mathrm{Im}\{C_2^{+}(t_0 + \mathrm{d}t)\} \end{aligned} \tag{153}$$

It should be noted that these relations satisfy

$$\begin{aligned} C_1^{+}(t_0 + \mathrm{d}t) &= +C_1^{-}(t_0 + \mathrm{d}t), \\ C_2^{+}(t_0 + \mathrm{d}t) &= -C_2^{-}(t_0 + \mathrm{d}t) \\ &= \exp(-i\pi) C_2^{-}(t_0 + \mathrm{d}t) \end{aligned} \tag{154}$$

Moreover, the initial condition, $C_k^{\pm}(t_0) = \delta_{k1}$ also satisfies

$$\begin{aligned} C_1^{+}(t_0) &= +C_1^{-}(t_0), \\ C_2^{+}(t_0) &= -C_2^{-}(t_0) = \exp(-i\pi) C_2^{-}(t_0) \end{aligned} \tag{155}$$

Therefore, using these relations as expressed in eq 155, one can prove a parity conservation

$$\begin{aligned} C_1^{+}(t) &= +C_1^{-}(t), \\ C_2^{+}(t) &= -C_2^{-}(t) = \exp(-i\pi) C_2^{-}(t) \end{aligned} \tag{156}$$

Further, if the relations in eq 156 hold at a time $t = \tau\ (\geq t_0)$, the electronic wave functions at the time $t = \tau + \mathrm{d}\tau$ on the paired symmetric paths $\mathbf{R}^{\pm}(\tau + \mathrm{d}\tau)$ are rearranged into the following forms

$$\begin{aligned} C_1^{+}(\tau + \mathrm{d}\tau) &= \left(1 - \frac{i}{\hbar} V_{11}(\mathbf{R}^{+}(\tau))\, \mathrm{d}\tau\right) C_1^{+}(\tau) \\ &- \frac{i}{\hbar} v_I(\mathbf{R}^{+}(\tau))\, \mathrm{d}\tau\, C_2^{+}(\tau) = \left(1 - \frac{i}{\hbar} V_{11}(\mathbf{R}^{-}(\tau))\, \mathrm{d}\tau\right) C_1^{-}(\tau) \\ &- \frac{i}{\hbar} (-v_I(\mathbf{R}^{-}(\tau)))\, \mathrm{d}\tau (\mathrm{e}^{-i\pi} C_2^{-}(\tau)) = C_1^{-}(\tau + \mathrm{d}\tau) \end{aligned} \tag{157}$$

and

$$\begin{aligned} C_2^{+}(\tau + \mathrm{d}\tau) &= \left(1 - \frac{i}{\hbar} V_{22}(\mathbf{R}^{+}(\tau))\, \mathrm{d}\tau\right) C_2^{+}(\tau) \\ &- \frac{i}{\hbar} v_I(\mathbf{R}^{+}(\tau))\, \mathrm{d}\tau\, C_1^{+}(\tau) = \left(1 - \frac{i}{\hbar} V_{22}(\mathbf{R}^{-}(\tau))\, \mathrm{d}\tau\right) (\mathrm{e}^{-i\pi} C_2^{-}(\tau)) \\ &- \frac{i}{\hbar} (-v_I(\mathbf{R}^{-}(\tau)))\, \mathrm{d}\tau C_1^{-}(\tau) = \mathrm{e}^{-i\pi} C_2^{-}(\tau + \mathrm{d}\tau) \end{aligned} \tag{158}$$

where the system symmetry also plays a critical role. Thus, the phase relation expressed by eq 156 also holds at $t = \tau + \mathrm{d}\tau$. This result assures the preservation of both in-phase and out-of-phase relations along *given* paired symmetric paths for all time $t \geq t_0$.

5.4.5. Parity Conservation of the Mean Forces. Due to the system symmetry, the force matrix in a diabatic representation given by $F_{IJ}^{k} = -\partial H_{IJ}^{\mathrm{el}}/\partial R_k$ satisfies the following symmetry relations

$$\begin{aligned} F_{II}^{1}(R^{+}) &= +F_{II}^{1}(R^{-}) \quad F_{II}^{2}(R^{+}) = -F_{II}^{2}(R^{-}) \\ F_{IJ}^{1}(R^{+}) &= -F_{IJ}^{1}(R^{-}) \quad F_{IJ}^{2}(R^{+}) = +F_{IJ}^{2}(R^{-}) \end{aligned} \tag{159}$$

where $I \neq J$. Consequently, the mean force vectors defined at $\mathbf{R}^{\pm}$ by $f_k^{MF\pm} \equiv (\underline{C}^{\pm})^{\dagger}\, \underline{\underline{F}}^{k} \underline{C}^{\pm}$ retain the symmetry properties in them as

$$f_1^{MF+} = +f_1^{MF-}, f_2^{MF+} = -f_2^{MF-} \tag{160}$$

Thus, the parity is conserved in the mean force. Therefore, the paths driven by the mean force in the process of phase-space averaging in the PSANB scheme also preserve the relevant symmetry.

5.4.6. Parity of Phase in Quantum Dynamics and Semiclassics. We will now demonstrate a realization of parity conservation of the electron wavepackets. Here, for clarity, we

dx.doi.org/10.1021/cr200096s |*Chem. Rev.* 2012, 112, 499–542

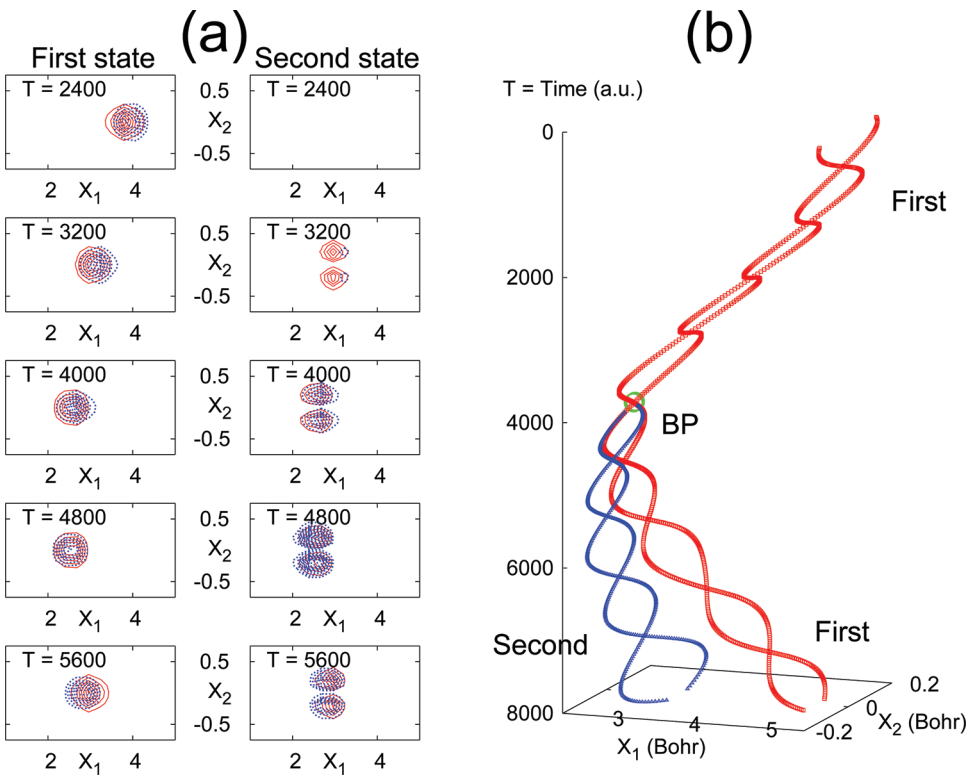

Figure 13. Semiclassical and quantum dynamics of a wavepacket passing across a conical intersection. (a) Nodal features appearing in the linear combinations of Gaussian wavepackets guided by two symmetric PSANB paths. The increment of the contour plot for the probability density plot of the first state is 40 times that of the second one. Red solid and blue dotted lines represent the quantum and PSANB wavepackets, respectively. (b) Trajectory of symmetric PSANB paths in (x_1,x_2,t)-space and their one-time branching. "First" and "Second" in the panel indicate paths are running on the first state and the second states, respectively. "BP" is a branching point set at the exit of the nonadiabatic region.

track the dynamics of symmetric initial conditions. This is possible because other dynamics lacking symmetry can be fragmented into the symmetric pieces. So, we confirm that we are thinking of an initial wavepacket lying on a single electronic state (on V_{11}) which has a symmetric shape in position and momentum space with respect to the x_2 axis. It is also necessary to assume that this initial wave function is placed at a region where no state coupling is present. All the quantum dynamics calculations were carried out with use of the second order split operator method.[232]

Again it should be noted that the portion of the wavepacket amplitude transferred from the first diabatic state to the second one has odd symmetry due to the antisymmetry of v_I, namely, $v_I(x_1,x_2) = -v_I(x_1, -x_2)$, if starting from an even parity with respect to the x_2 inversion operation. The other portion left in the first state is even. These symmetry properties play the key role in the transition dynamics around the conical intersection. In particular, as already clarified above, the total wavepackets located at an asymmetric position with respect to the x_2 have mutually different signs. That is

$$c\Phi_2(\mathbf{r};\mathbf{R}^+(t))\,\chi_2(\mathbf{R}^+(t),t) = -c\Phi_2(\mathbf{r};\mathbf{R}^-(t))\,\chi_2(\mathbf{R}^-(t),t) \quad (161)$$

for t after the passage of the region of the conical intersection, where $\chi_2(\mathbf{R}^+(t),t)$ $[\chi_2(\mathbf{R}^-(t),t)]$ is the nuclear wavepacket running on the place of $x_2 > 0$ $[x_2 < 0]$ and c is a constant. Thus, the total wave function on the second diabatic state V_{22} should have a definite nodal line at $x_2 = 0$ starting from the conical intersection. This is explicitly observed in the quantum nuclear wavepacket propagating on the second state in panel a of Figure 12 (red contour lines). On the other hand, the packet remaining on the first state does not experience such cancellation and concomitantly does not form such a node. (See also the similar nodal structure in the *ab initio dynamics* of NO_2 around a conical intersection.[50])

We next examine the wavepacket propagation guided by a symmetric pair of the PSANB non-Born−Oppenheimer path. These are designed to mimic the condition of the above full quantum wavepacket dynamics. Here we focus on a Gaussian wave packet with a center position $(x_1,x_2) = (5.5,0.0)$ on the first diabatic state (V_{11}). The initial two phase-space points are sampled symmetrically with respect to the x_2 axis, by using the Wigner phase-space distribution function for this wavepacket as a weighting function. Below, we track these paths and their branching along with the semiclassical wave packets on them. Panel b of Figure 13 shows the history of this pair of paths in (x_1,x_2)-space that undergoes bifurcation (at the bifurcation point as indicated as "BP" in the figure) only once. Not only the geometrical symmetry observed in this panel but also the invisible phases studied above are associated individually with the pieces of paths. A frozen Gaussian function is placed on each piece of path (either before or after branching), which is guided to propagate on the path. A propagation of the nuclear wavepackets is described by the blue contour lines in panel a of Figure 13. It is confirmed that the wavepacket on the second state has successfully reproduced the nodal structure. (Incidentally, a large deviation of the red (full quantum) and blue (PSANB) contours is due to the so-called

dx.doi.org/10.1021/cr200096s |*Chem. Rev.* 2012, 112, 499–542

late-kick-off property of the path-based based method.[118,157] The front edge of the quantum wavepacket begins to bifurcate earlier than the part at the central position that is mimicked by path dynamics.) Thus, it turns out that the branching paths of PSANB carry the correct phase information; indispensable for the study of electron dynamics coupled with nuclear motion.

5.4.7. Summary. As far as we can ascertain, this is the first study on how the non-Born−Oppenheimer branching paths can correctly accumulate the phases from both nuclear and electronic dynamics around a conical intersection. It has been shown that the Longuet−Higgins phase is well reproduced and preserved using such a nonadiabatic dynamics. The present study is convincing enough that the nonadiabatic electron wavepacket dynamics provides a useful tool for the analyses of photochemical processes in complicated yet realistic systems.

6. CONCLUDING REMARKS

In this review our aim has been to cover the most relevant recent progress in the study of nonadiabaticity. A special emphasis is placed on the nonadiabatic electron wavepacket dynamics in light of some recent technical advances in quantum chemistry. We hope that the molecular electronic structure theory will be developed within the realm of electron dynamics as driven mainly by laser technology, which further demands the simultaneous development of theoretical analysis, interpretation, and prediction.

Starting from the very basic Landau−Zener model, we first reviewed the classic semiclassical theories and proceeded up to the state-of-art one, such as the Zhu−Nakamura theory. Theories of this kind commonly assume the presence of a priori (mostly one-dimensional) potential energy surfaces and do not really consider the dynamics of electrons. All these methods have been thoroughly examined numerically, and it is well-known that they give accurate nonadiabatic transition amplitudes (or probabilities) within their validity ranges. It is stressed, on the other hand, that those validity ranges are not necessarily wide or even far from reality, depending on the molecular systems under study. In addition, it is not easy to incorporate the true multidimensional effects of nonadiabaticity into them. The most critical difficulty encountered, for which, it must be admitted, these classic theories are not totally responsible, is that they were developed before the progress of ultrafast laser chemistry. Where such chemistry is involved, novel nonadiabatic coupling mediated by the vector potentials, in addition to the native nonadiabatic transition, must be explicitly taken into account.

The theories of nonadiabatic electron wavepackets can overcome most of the above difficulties within the level of *ab initio* calculations (without assuming specific model potentials), and thus, section 3 constitutes the heart of this review. However, there is a price to the fact that the electronic wavepackets are propagated rather faithfully, namely the treatment of the resultant nuclear paths presents theoretical difficulties: (i) First, it was not even known whether a non-Born−Oppenheimer global path did indeed exist: one connecting two end points on two different adiabatic potential energy surfaces. (ii) Next, how can the coherence of electronic-state mixing naturally diminish after the passage across a nonadiabatic region? (iii) Finally, how can such natural decoherence be compatible with the electron−nuclear strong entanglement, which is represented by wavepacket branching in a full quantum mechanics? We reviewed the representative theories from this point of view, beginning with the Pechukas theory to the semiclassical Ehrenfest theory, the theory of natural decay of mixing, and the theory of path branching. The present authors are of the opinion that the path branching representation resolves the above problems both in principle and in practice. Numerical examples have shown what the geometry of branching paths looks like and how accurately the theory performs in estimating the transition amplitude.

It has been stressed that, even without laser fields, the dynamical electron theory can offer a useful tool to analyze and conceptualize chemical reactions from the viewpoint of electron flow in and between molecule(s). The theory is hence expected to contribute to a wide range of chemical dynamics ranging from attosecond electron wavepacket dynamics to modern analysis of the dynamcial foundation of the classic notions in chemistry, such as the Pauling resonance theory. We also discuss the interaction of the laser field and the nonadiabatic coupling. The last numerical example presented illustrated the fact that the quantum mechanical phase interference due to the Longuet−Higgins phase around the conical intersection is correctly reproduced by such branching paths.

Finally, it is hoped that this review will serve as that for a general theory of dynamics in which quantum and classical subsystems kinematically contact each other while allowing the quantum mechanical entanglement to survive within the classical subsystem.

APPENDIX A: QUANTUM CHEMICAL CALCULATIONS OF THE MATRIX ELEMENTS OF NONADIABATIC INTERACTIONS

We will now briefly review some of the methods used to calculate the nonadiabatic coupling elements. As can be easily surmised, the computational scheme of nonadiabatic coupling elements depends heavily on the methods of electronic state calculation, such as configuration interaction, multiconfigurational self-consistent field (MCSCF) method, and so on. Computational efficiency and/or limitations are often determined by the choice of methods, and hence, the relevant methodological study is important from a practical point of view and requires much developmental effort. Since the relevant calculations are somewhat technical, we describe them here in an Appendix. Nevertheless, we do want to emphasize that it is possible to catch a glimpse of the deep aspects of quantum mechanical nonadiabatic dynamics in such technical details.

A. Diabatic Representation. The nuclear derivative couplings emerge from a connection matrix for the orthogonal electronic basis states $|\Phi_I\rangle$, which are generated along a trajectory that is characterized in terms of an adiabatic parameter vector $\mathbf{R}$. Suppose that $\mathbf{R}$ depends smoothly on time t and the electron basis set is determined at each point in $\mathbf{R}$-space, namely, $\mathbf{R}(t)$. The wavefunction $|\Phi(t;\mathbf{R}(t))\rangle$ can be expanded in terms of this basis set in the form of

$$|\Phi(t;\mathbf{R}(t))\rangle = \sum_I C_I(t)|\Phi_I(\mathbf{R}(t))\rangle \tag{162}$$

It should obey the Schrödinger equation with a system Hamiltonian operator, $\hat{H}(\mathbf{R}(t))$, which also depends on $\mathbf{R}(t)$, as shown below

$$i\hbar\partial_t|\Phi(t;\mathbf{R}(t))\rangle = (\hat{H} - i\hbar\dot{\mathbf{R}}(t)\nabla_R)|\Phi(t;\mathbf{R}(t))\rangle \tag{163}$$

dx.doi.org/10.1021/cr200096s |*Chem. Rev.* 2012, 112, 499–542

Multiplication of $\langle\Phi_I(\mathbf{R}(t))|$ in this equation of motion from the left side yields

$$i\hbar\dot{C}_I(t) = \sum_J (H_{IJ} - i\hbar\dot{\mathbf{R}}(t)\,\mathbf{X}_{IJ}(\mathbf{R}(t)))\,C_J(t) \quad (164)$$

where

$$X_{IJ}(\mathbf{R}(t)) \equiv \langle\Phi_I(\mathbf{R})|\nabla_R|\Phi_J(\mathbf{R})\rangle \quad (165)$$

is the adiabatic parameter derivative coupling. A dot denotes a time derivative. This term originated from

$$\langle\Phi_I(\mathbf{R}(t))|\partial_t|\Phi_J(\mathbf{R}(t))\rangle \quad (166)$$

Furthermore, the time derivative appears as an element in

$$\langle\Phi_I(\mathbf{R}(t))|\Phi_J(\mathbf{R}(t+\Delta t))\rangle = \langle\Phi_I(\mathbf{R}(t))|\Phi_J(\mathbf{R}(t))\rangle + \langle\Phi_I(\mathbf{R}(t))|\partial_t|\Phi_J(\mathbf{R}(t))\rangle\Delta t \quad (167)$$

Indeed the overlap integral on the left-hand-side of this equation appears as an origin of the nonadiabatic coupling in the path integral formalism as shown in eq 44. Therefore, a comparison of these expressions from eq 165 to 167 gives a clear geometrical meaning in the form of a connection matrix between neighboring electron basis sets in the adiabatic parameter space. Concomitantly, there are two basic ways to evaluate the nonadiabatic coupling elements, through either eq 165 or 166, and both of them are outlined below. If we set $\mathbf{R}(t)$ to a referential nuclear classical trajectory point at t, $\mathbf{R}(t)$ and $\mathbf{X}_{IJ}$ are referred to as the nuclear derivative coupling matrix elements. In what follows, we discuss two representations of the electronic states, namely, the diabatic and adiabatic.

We first consider a formal equation for such a transformation. (See refs 16 and 234 for an extensive review of the transformation by Baer.) We start with an adiabatic basis set $\{\Phi_I(\mathbf{r};\mathbf{R})\}$, each term of which is associated with the eigen-energy E_I. If we expand the total wavefunction in the form $\Psi(\mathbf{r},\mathbf{R},t) = \Sigma_I\Phi_I(\mathbf{r};\mathbf{R})\,\chi_I(\mathbf{R},t)$, then the Schrödinger equation becomes

$$i\hbar\frac{\partial}{\partial t}\chi_I = \left[\sum_j \frac{-\hbar^2}{2M_j}(\nabla^{(j)} + \mathbf{X}^{(j)})^2 + H^{\mathrm{el}}(\mathbf{R})\right]_{IJ}\chi_J \quad (168)$$

The diabatic basis $\{F_a(\mathbf{r};\mathbf{R})\}$ is such a basis set that eliminates the derivative coupling (only locally). If we write the transformation matrix U, such that $\Sigma_J\Phi_J U_{Ja} = F_a$, then the associated nuclear wavefunctions ξ_a are related by $\chi_J = \Sigma_a U_{Ja}\xi_a$. For an $\mathbf{X}$ in the adiabatic representation, a transformation matrix that satisfies the equation

$$\nabla U + \mathbf{X}U = 0 \quad (169)$$

makes the nuclear derivative coupling vanish, which is to be integrated with appropriate boundary conditions. If the dimension of the nuclear derivative ∇ is greater than one, then there is an integrability condition[215]

$$\frac{\partial X^\mu}{\partial R^\nu} - \frac{\partial X^\nu}{\partial R^\mu} + [X^\mu, X^\nu] = 0 \quad \text{for all} \quad \mu < \nu \quad (170)$$

The condition eq 170 actually poses a certain limitation on the existence of the diabatic representation. One of its outcomes is the inexistence of a perfect diabatic basis in the finite dimensional expansion. To see this, we denote the projection on the finite basis set explicitly by $\equiv \Sigma_{J\in\Omega}|\Phi_J\rangle\langle\Phi_J|$, where Ω represents the label set of the basis. The requirement for diabatization becomes

$$\mathscr{P}\{\nabla U + \mathbf{X}U\}\mathscr{P} = 0 \quad (171)$$

and the integrability condition then becomes

$$\mathscr{P}\left\{\frac{\partial X^\mu}{\partial R^\nu} - \frac{\partial X^\nu}{\partial R^\mu} + [X^\mu, X^\nu]\right\}\mathscr{P} = 0 \quad \text{for all} \quad \mu < \nu \quad (172)$$

Here, the last term on the right hand side of this equation inevitably involves such terms that cannot be calculated within the projected space, that is,

$$\mathscr{P}X^\mu(1-\mathscr{P})X^\nu\mathscr{P} - \mathscr{P}X^\nu(1-\mathscr{P})X^\mu\mathscr{P} \quad (173)$$

Thus, the perfect diabatic representation does not in fact generally exist unless the basis set is complete.[14] Practical theories of diabatic representation, including those for multidimensional systems, have been studied extensively by Smith[233] and Baer.[16,234] Another scheme was proposed using a different perspective.[235,236] In this approximate but practical treatment, a diabatization is pursued by requiring the basis states to retain their individual characters smoothly, rather than minimizing the magnitude of derivative coupling.

B. General Framework of Evaluation of the Nuclear Derivative Coupling Matrix Elements with Canonical Molecular Orbitals.

There exist both similarities and difference between the computational schemes for the energy gradient with respect to the nuclear coordinates[237] and the nuclear derivative coupling elements (NDCs).[15,238] The common difficulty lies in the treatment of the implicit geometry-dependence of the variational coefficients, such as those of MOs, CSFs, and so on. These coefficients depend only indirectly on the nuclear positions through the dynamical equations used to determine them. Therefore, in order to make such dependence explicit, the following methods are usually taken: (i) The first order expansion of the one- or multielectron basis set with respect to the slight displacement of the nuclear positions (giving rise to NDCs) is represented within the same basis functions of the original position. (ii) Or, the similar first order expansion is determined by solving dynamical equations. These in turn are obtained by the derivative of orthogonal relations, which must be satisfied by the properties of the basis functions. These equations are generally known as coupled-perturbed equations.

First, we consider the case of the configuration state function (CSF) to be used in configuration interactions as the basis functions. These are an antisymmetrized product of one-electron orbitals or a symmetry-adapted linear combination of them. The linear equations, with respect to the infinitesimal nuclear displacement, are derived from the nuclear differentiation of orthogonality relation between the occupied and virtual molecular orbitals of the Fock operator. This suffices to obtain the nuclear derivative coupling matrix element in the CSF representation. The computation of the nonadiabatic coupling elements for general state-averaging multiconfigurational self-consistent wavefunctions is more involved. In this scheme, the total energy is defined by the weighted sum of state energies and it is optimized simultaneously with respect to molecular orbitals and the CSF coefficients. The nuclear derivatives of the stationary conditions of this averaged energy with respect to these two sets of coefficients

yield equations to determine the perturbation coefficients. Although complicated, these methodologies are indeed necessary for the compact and accurate representation of nonadiabatic chemical dynamics.[239,240]

In the evaluation of the nuclear derivative coupling elements around a crossing seam, the electronic phase should be appropriately taken into account. In addition, it should be noted that NDCs are singular at crossing seams. If we treat the dynamics of passing across a crossing seam, then the state coupled dynamics within an adiabatic representation does not work. Hence, some appropriate diabatic representation is required. Our experience[124,129] suggests that the CSF representation is a good and practical alternative to a diabatic representation, if the molecular orbitals to be utilized are smoothly connected along a nuclear path (see below). Nonetheless, the nuclear-derivative coupling elements are not exactly zero and the electronic Hamiltonian matrix has large off-diagonal elements. It is recommended, therefore, that the nuclear derivative coupling elements $\mathbf{X}_{IJ}$ are always taken into account explicitly. A CSF representation has already been employed in the study of electron dynamics within the semiclassical Ehrenfest theory.[82,99,100,124,129,151,156]

As mentioned above briefly, there is a method that does not resort to the direct application of the nuclear derivative of electronic wavefunctions. Instead, an overlap integral between two electronics states at slightly different times (or nuclear positions) as in eq 167, which is free of some of difficulties, such as the singularity at a crossing seam, can be used. The physical meaning of theses transfer-like integrals between the states is clear. In addition, this overlap integral does not strongly depend on how the state function is constructed, either simple CI or MCSCF. In order to perform such an overlap integral for two electronic state functions, it is rigorous conditions that all the basis functions be tied to each other in a one-to-one manner along a nuclear path. However, in the context of practical calculations, it is not always easy in practical calculations to make such a unique correspondence among them.

C. Nuclear Derivative Coupling Elements in the CSF Representation.

We here concentrate on the CSF representation in somewhat greater detail. The first order nuclear derivative CSF coupling elements are expressed in terms of the following equation

$$X_{IJ}^{k} \equiv \langle \Phi_I | \partial_k | \Phi_J \rangle = \sum_{i,j} a_{ij}^{IJ} \langle \phi_i | \partial_k | \phi_j \rangle \tag{174}$$

where $a_{ij}^{IJ} = \langle \Phi_I | \hat{E}_i^{\dagger} \hat{E}_j | \Phi_J \rangle$ denotes a one-electron coupling constant with $\hat{E}_i^{\dagger}$ and $\hat{E}_i$ being the creation and annihilation operators for the ith molecular orbital ϕ_i. Orthonormality is imposed on them as $\langle \phi_i | \phi_j \rangle = \delta_{ij}$. The electronic spin is omitted for the sake of simplicity. ∂_k denotes a nuclear derivative with respect to the kth nuclear degree of freedom. It is sufficient to formulate the first order nuclear derivative coupling matrix element of the molecular orbital functions as

$$d_{ij}^{k} \equiv \langle \phi_i | \partial_k | \phi_j \rangle \tag{175}$$

Since MO's $\{\phi_i\}$ are usually prepared as a linear combination of the atomic orbitals (AO) $\{\chi_\mu\}$ with the coefficients c_μ^i as

$$\phi_i = \sum_{\mu} c_\mu^i \chi_\mu \tag{176}$$

the nuclear derivative couplings are written in terms of the AOs and their associated coefficients as

$$d_{ij}^{k} = \sum_{\mu} \sum_{\nu} c_\mu^i c_\nu^j S_{\mu\nu}^{k} + \sum_{\mu} \sum_{\nu} c_\mu^i \frac{\partial c_\nu^j}{\partial R_k} S_{\mu\nu} \tag{177}$$

where

$$S_{\mu\nu} = \langle \chi_\mu | \chi_\nu \rangle \quad \text{and} \quad S_{\mu\nu}^{k} = \langle \chi_\mu | \partial_k | \chi_\nu \rangle \tag{178}$$

It is convenient for later purposes to antisymmetrize d_{ij}^{k} as

$$d_{ij}^{k} = \frac{1}{2} (\langle \phi_i | \partial_k | \phi_j \rangle - \langle \phi_j | \partial_k | \phi_i \rangle) \tag{179}$$

which naturally arises from the derivative of orthonormalized molecular orbitals.

a. First Order Derivative of the MO Coefficients

Since the case for the AOs is rather straightforward, here we are concerned only with the first order derivative over MO coefficients with respect to the nuclear coordinates. There are four points to be considered: (i) Implicitly the term $\{c_\mu^i\}$ depends only on $\{R_k\}$. (ii) We should formulate their response to a slight nuclear displacement $\mathbf{R}$ using a perturbation theory. (iii) Consequently, the spaces thus spanned by the perturbed MO's are determined by the unperturbed (original) Fock matrix as the linear combination of the original AO's. (iv) It follows then that the derivative of the MO coefficients $\{c_\mu^i\}$ should be determined by the quantities related to a "derivative" of the Fock matrix. These are the basic ideas behind the application of the coupled perturbed Hartree−Fock method to this matter. Their generalization is included in the literature.[241−243]

If we represent the nuclear derivative of MO coefficients in the form of the following equation

$$\partial_k c_\mu^i = \sum_{m}^{MO} c_\mu^m U_{mi}^{k} \tag{180}$$

where U_{mi}^{k} are the coefficients to be determined, in particular, we need to determine U_{mi}^{k} between $c_\mu{}^i$ for occupied MO's and c_μ^m for unoccupied MO's. The orthonormality condition gives the conditions

$$U_{ij}^{k} + U_{ji}^{k} + S_{ij}^{k} = 0 \tag{181}$$

where

$$S_{ij}^{k} \equiv \sum_{\mu\nu}^{AO} c_\mu^i c_\nu^j \frac{\partial S_{\mu\nu}}{\partial k} = \sum_{\mu\nu}^{AO} c_\mu^i c_\nu^j (S_{\mu\nu}^{kR} + S_{\mu\nu}^{kL}) \tag{182}$$

with $S_{\mu\nu}^{kR} \equiv \langle \chi_\mu | \partial_k \chi_\nu \rangle$ and $S_{\mu\nu}^{kL} \equiv \langle \partial_k \chi_\mu | \chi_\nu \rangle$. By using them, the derivative couplings are reduced to the form

$$d_{ij}^{k} = \sum_{\mu} \sum_{\nu} c_\mu^i c_\nu^j S_{\mu\nu}^{k} + U_{ij}^{k} \tag{183}$$

b. Using the CPHF Equation To Determine U_{ij}^{k}

Next the terms U_{ij}^{k} between the MO's in both occupied and unoccupied space are obtained using the coupled perturbed Hartree−Fock method (CPHF). First, we recall that the Fock

dx.doi.org/10.1021/cr200096s |Chem. Rev. 2012, 112, 499–542

matrix for the closed-shell system is written as

$$F_{ij} = h_{ij} + \sum_{k}^{d.o.} \{2(ij|kk) - (ik|jk)\} \quad (184)$$

where

$$h_{ij} = \langle \phi_i | \left(-\frac{1}{2}\Delta_r + \sum_A \frac{Z_A}{r_A} \right) | \phi_j \rangle \quad (185)$$

with Z_A being the nuclear charge of atom A and

$$(ij|kl) = \int \mathrm{d}r_1\, \mathrm{d}r_2\, \phi_i^*(r_1)\, \phi_j(r_1) r_{12}^{-1} \phi_k^*(r_2)\, \phi_l(r_2) \quad (186)$$

For the sake of simplicity, we introduce the following notation

$$h_{ij}^a \equiv \sum_{\mu\nu} c_\mu^i c_\nu^j (\partial_a h_{\mu\nu}) \quad (187)$$

$$(ij|kl)^a \equiv \sum_{\mu\nu\delta\sigma}^{AO} c_\mu^i c_\nu^j c_\delta^k c_\sigma^l \partial_a \int \mathrm{d}r_1 \mathrm{d}r_2 x_\mu^*(r_1) x_\nu(r_1) r_{12}^{-1} x_\delta^*(r_2) x_\sigma(r_2) \quad (188)$$

and

$$F_{ij}^a \equiv h_{ij}^a + \sum_{k}^{d.o.} \{2(ij|kk)^a - (ik|jk)^a\} \quad (189)$$

$$A_{ij,kl} \equiv 4(ij|kl) - (ik|jl) - (il|jk) = A_{kl,ij} = A_{ij,lk} \quad (190)$$

where d.o. in eq 189 means a summation over the doubly occupied MO space. Finally, with the help of the stationary condition F_{ij} with respect to the displacement of a, namely, $\partial F_{ij}/\partial a = 0$ ($\neq F_{ij}^a$), we arrive at the following compact form of the equation for the virtual (virt) and doubly occupied (d.o.) orbital pairs

$$\sum_{k}^{\mathrm{virt}} \sum_{l}^{d.o.} \tilde{A}_{ij,kl} U_{kl}^a = B_{0,ij}^a \quad (191)$$

where ($i \in$ virt, $j \in$ d.o.) and

$$\tilde{A}_{ij,kl} \equiv (\epsilon_j - \epsilon_i)\delta_{ik}\delta_{jl} - A_{ij,kl} \quad (192)$$

$$B_{0,ij}^a \equiv F_{ij}^a - S_{ij}^a \epsilon_j - \frac{1}{2} \sum_{k}^{d.o} \sum_{l}^{d.o.} S_{kl}^a A_{ij,kl} \quad (193)$$

Equation 191 gives $\{U_{kl}^a\}$ by inversion, unless $\epsilon_j - \epsilon_i = 0$.

D. Construction of X_{IJ}^k. Using the properties introduced above, the nuclear derivative coupling elements for MO space now become

$$d_{ij}^k = S_{ij}^{kR} + U_{ij}^k \quad (194)$$

with

$$S_{ij}^{kR} \equiv \sum_{\mu\nu}^{AO} c_\mu^i c_\nu^j S_{\mu\nu}^{kR} \quad (195)$$

which directly yields the CSF derivative coupling elements

$$X_{IJ}^k = \sum_{ij}^{MO} a_{ij}^{IJ} (U_{ij}^k + S_{ij}^{kR}) \quad (196)$$

However, one problem now arises. The U_{ij}^k terms for the same occupied or unoccupied MO space are not determined uniquely from the CPHF equation based on the orthogonality of occupied and virtual space. However, this problem can be avoided by using the following approximation. Namely that the symmetric part of $\{U_{ij}^k\}$ is a physically meaningful part of a CSF derivative coupling matrix element, $\langle \phi_i | \partial_k | \phi \rangle$, for the $i - j$ pairs that belong to the same MO space. This approximation allows the replacement of $-1/2 S_{ij}^k$ with U_{ij}^k, and for any inner space rotation pair, $(i,j) \in$ occ. or virt. We thus obtain a derivative coupling matrix element for these MO pairs in such an approximate manner as

$$\langle \phi_i | \partial_k \phi_j \rangle = U_{ij}^k + S_{ij}^{kR} \approx \frac{1}{2}(U_{ij}^k + U_{ji}^k) + S_{ij}^{kR} = -\frac{1}{2} S_{ij}^k + S_{ij}^{kR}$$
$$= -\frac{1}{2}(S_{ij}^{kR} + S_{ij}^{kL}) + S_{ij}^{kR} = \frac{1}{2}(S_{ij}^{kR} - S_{ij}^{kL}) \quad (197)$$

in the antisymmetric form. Finally, the nuclear derivative coupling matrix elements for CSF can be written down as

$$\langle \Phi_I | \partial_k | \Phi_J \rangle = \Big(\sum_{ij}^{\mathrm{occ}} + \sum_{ij}^{\mathrm{virt}}\Big) a_{ij}^{IJ} d_{ij}^k + \sum_{i}^{\mathrm{occ}} \sum_{j}^{\mathrm{virt}} a_{ij}^{IJ} d_{ij}^k$$
$$+ \sum_{i}^{\mathrm{virt}} \sum_{j}^{\mathrm{occ}} a_{ij}^{IJ} d_{ij}^k \quad (198)$$

$$= \Big(\sum_{ij}^{\mathrm{occ}} + \sum_{ij}^{\mathrm{virt}}\Big) a_{ij}^{IJ} \frac{1}{2}(S_{ij}^{kR} - S_{ij}^{kL}) + \sum_{i}^{\mathrm{occ}} \sum_{j}^{\mathrm{virt}} (a_{ij}^{IJ} - a_{ij}^{JI})(U_{ij}^k + S_{ij}^{kR}) \quad (199)$$

E. Nonadiabatic Coupling without the Use of a Nuclear Derivative. With increasing system size, the implementation of *ab initio* electron wavepacket dynamics, such as the semiclassical Ehrenfest theory, using nuclear derivative coupling tends to be computationally more demanding because of the necessity of solving coupled perturbed equations. We therefore propose a useful treatment of nonadiabatic coupling, in which one can avoid the tedious coupled perturbed equations for the nuclear derivative of MO's and CSF's.

Let us presume the Schrödinger equation for an electronic wavefunction with nonadiabatic state coupling is written as follows

$$i\hbar \frac{\mathrm{d}}{\mathrm{d}t}|\Phi\rangle = \hat{H}|\Phi\rangle \Leftrightarrow i\hbar \dot{C}_I = \sum_J (H_{IJ} - i\hbar D_{IJ}) C_J \quad (200)$$

The electronic wavepacket is expanded in terms of CSFs as $|\Phi\rangle = \Sigma_I C_I |\Phi_I\rangle$. A dot denotes the time derivative. The time-derivative overlap matrix, which causes state mixing, has the form

$$D_{IJ} \equiv \langle \Phi_I | \dot{\Phi}_J \rangle = \sum_{ij}^{MO} a_{ij}^{IJ} \langle \phi_i | \dot{\phi}_j \rangle \equiv \sum_{ij}^{MO} a_{ij}^{IJ} d_{ij} \quad (201)$$

where the MO nuclear derivative coupling matrix element is defined by

$$d_{ij} \equiv \langle \phi_i | \frac{\mathrm{d}}{\mathrm{d}t} | \phi_j \rangle = \frac{A_{ij} - A_{ji}}{2} \quad (202)$$

dx.doi.org/10.1021/cr200096s |Chem. Rev. 2012, 112, 499–542

with

$$A_{ij}(t) \equiv \langle \phi_i(t)|\dot{\phi}_j(t)\rangle = \sum_{\mu\nu}^{AO} [c_\mu^i(t)\, \dot{c}_\nu^j(t)\, S_{\mu\nu}(t) + c_\mu^i(t)\, c_\nu^j(t)\, \dot{R}S_{\mu\nu}^R(t)] \quad (203)$$

Here the orthogonality of real MO functions is exploited. $S_{\mu\nu}(t) \equiv \langle \chi_\mu(t)|\chi_\nu(t)\rangle$ and $S_{\mu\nu}^R(t) \equiv \langle \chi_\mu(t)|\nabla_R|\chi_\nu(t)\rangle$ are the atomic orbital (AO) overlap matrix elements and the nuclear derivative overlap matrix elements, respectively. Thus, we can avoid the coupled perturbed Hartree−Fock equations or their analogues to obtain the nuclear derivative over MO coefficients. Also, the computation of the time derivative is much less time consuming. However, the price for gaining these advantages is an efficient and accurate computation of $\{\dot{c}_\mu^i\}$. They are numerically available with the aid of orbital continuity along the time coordinate in the propagation of the electronic wavepackets. In this scheme, the derivative coupling matrix for CSF state vectors does not appear. In a further simplified implementation of it, one can neglect the force component originating from the nuclear derivative coupling, that is assuming that they are generally small.

APPENDIX B: TRACKING THE CONTINUITY OF MOLECULAR ORBITALS ALONG A NUCLEAR PATH

In propagating an electronic wavepacket along a path, molecular orbitals are generally used for its expansion as a one-electron basis. MO's are, however, generated at each nuclear configuration (geometry) as an eigenfunction of the static one-electron Hamiltonian, with the Fock operator as an example. Therefore, no information about time is included at this level. Hence, any phase factor can be attached on, yet still keeping the constituent total density matrices invariant. This is because the individual molecular orbitals are determined independently irrespective of the neighboring counterparts. Nevertheless, one needs to identify how the molecular orbitals are actually connected with each other in terms of their orbital character. Without such a correct correspondence of the successive molecular orbitals, that is $\phi_i(\mathbf{R}(t)) \leftrightarrow \phi_i(\mathbf{R}(t+\Delta t))$, one may lose the correct identification of the CSF $\Phi_I(\mathbf{R}(t))$ or the total electronic states, which could result in a wrong time propagation of eq 162. A most serious situation arises when two or more molecular orbitals are energetically degenerate. This is exactly the situation where a nonadiabatic transition is expected to be the most significant. It is therefore extremely vital to track the unique continuity of the molecular orbitals in order that the time propagation of the electronic wavepacket is successful.

One typical example that may appeal to readers and that emphasizes the seriousness of the matter is as follows: Let us consider two degenerated π molecular orbitals in a diatomic molecule, whose bond direction is in the z-coordinate. At each internuclear distance, a computer program can generate a pair of π orbitals with an arbitrary orientation in the x,y-plane. That is of course unless one enforces them to align along, say, the x and y directions, respectively. Without this special care, the resultant CSF's which include them will become useless as expansion bases in the practical propagation of an electronic wavepacket as in eq 162.

A method for obtaining a set of MOs that is proposed as being appropriate for dynamical simulation was proposed by Truhlar's group.[236,244] It uses a variational functional to obtain a set of diabatic MOs as a function of the nuclear geometry. An advantage of this method is that such diabatization is possible without prior knowledge of the nuclear paths.

A. Concept of Molecular Orbital Unique-Continuity. Let us now concentrate on this problem with respect to the more technical aspects. It should be noted that this kind of issue arises in any quantum dynamics problem, in which a time-dependent nonorthogonal basis set is used to track the wavepacket dynamics. Suppose that we have two sets of molecular orbitals (MO), $\{\phi_i(t-\delta t)\}$ and $\{\phi_i(t)\}$, at slightly different times. Here, the suffix i runs from 1 to M, which is equal to the number of atomic orbitals (AOs) employed. t and $t+\delta t$ are a particular time and its next neighbor, respectively. It is a usual practice to sort the ordering of the MOs with respect to the magnitude of their energies. However, here we need to track their identity smoothly in terms of their physical character (usually referred to as the orbital character) but not the energy. The smooth connection can be achieved by setting the new MOs in such a way as to maximize an overlap between $\{\phi_i(t-\delta t)\}$ and $\{\phi_i(t)\}$. Let the set of the resulting new MOs be $\{\tilde{\phi}_j\}$, which are represented by appropriate linear combinations of $\{\phi_i(t)\}$. If the time step δt is sufficiently small, we can thus obtain a natural connection between the two orbital sets. By repeating this method precisely, a sign-matching between the corresponding molecular orbitals as well as labeling of molecular ordering can be achieved.

The new MOs as trial functions, $\{\tilde{\phi}_j(t)\}$, are given by the linear combination of $\{\phi_i(t)\}$ so that the overlap error estimation function should be minimized. The cost function for the overlapping matrix is defined as the square of the difference from the unit matrix

$$f(\underline{\underline{\mathbf{c}}}) = ||\underline{\underline{\mathbf{I}}} - \underline{\underline{\tilde{s}}}||^2 \equiv \sum_{i,j=1}^{M} (\delta_{ij} - \tilde{s}_{ij})^2 \quad (204)$$

where δ_{ij} is the Kronecker delta function and the overlap concerned is defined by

$$\tilde{s}_{ij} \equiv \langle \phi_i(t-\delta t)|\tilde{\phi}_j(t)\rangle \quad (205)$$

with

$$|\tilde{\phi}_j(t)\rangle = \sum_{k=1}^{N} |\phi_k(t)\rangle c_{kj} \quad (206)$$

$[\underline{\underline{\mathbf{c}}}]$ is the MO mixing matrix to be optimized and $[\underline{\underline{\mathbf{c}}}]_{ij} = c_{ij}$ has a mathematical meaning of the contribution of the ith primitive MO to the jth trial orbital at time t. A bold character with a double underbar denotes an $M \times M$ square matrix. One can further elaborate the overlap matrix. Nonetheless, we here employ the present form to focus on the concept of orbital uniformity (unique-continuity) along a nuclear path.

Next, we introduce the primitive MO overlapping matrix as

$$o_{ik} \equiv \langle \phi_i(t-\delta t)|\phi_k(t)\rangle \quad (207)$$

Substituting this into the cost function above yields

$$f(\underline{\underline{\mathbf{c}}}) \equiv \sum_{i,j=1}^{N} (\delta_{ij} - \sum_{k=1}^{N} o_{ik} c_{kj})^2 \quad (208)$$

dx.doi.org/10.1021/cr200096s |Chem. Rev. 2012, 112, 499–542

The requirement of closest overlap to the unit matrix is written as

$$\frac{\partial f}{\partial c_{ij}} = 0 \tag{209}$$

for all i and j. It's formal solution is given by

$$\underline{\underline{\mathbf{c}}} = \underline{\underline{\mathbf{o}}}^{-1} \tag{210}$$

Conceptually, this provides the unique continuity of the neighboring molecular orbitals.

B. Practice of Molecular Orbital Unique-Continuity. Suppose we use the linear combinations of atomic orbitals (LCAO) in constructing molecular orbitals. We also make the rather optimistic assumption that the time interval δt is so small for AO overlaps between $t - \delta t$ and t that it can be approximated safely by $\langle \chi_\mu(t - \delta t)|\chi_\nu(t)\rangle \approx \langle \chi_\mu(t)|\chi_\nu(t)\rangle$. Here, $\{\chi_\mu\}$ is a set of AOs. This can be employed in evaluating an approximation of the overlap $\underline{\underline{\mathbf{o}}}$ among the MOs at different times. Since the constructed overlap matrix is not exactly unitary, it is preferable to introduce a natural modification of the MO overlap $\underline{\underline{\mathbf{o}}}$ to achieve the orthonormality of the resultant transformed orbitals. In fact, this orthonormality plays a key role, not only in the relevant mathematical properties but also as working equations for constructing the gradient properties of electrons. One way to achieve this orthogonality is to apply the Gramm−Schmidt technique for the columns of vectors of $\underline{\underline{\mathbf{o}}}$. This is equivalent to the unitarization of $\underline{\underline{\mathbf{o}}}$. We refer this unitary matrix obtained here to $\underline{\underline{\tilde{\mathbf{o}}}}$. Because of the unitarity of $\underline{\underline{\tilde{\mathbf{o}}}}$, the mixing matrix $\underline{\underline{\mathbf{c}}}$ is effectively set to

$$\underline{\underline{\mathbf{c}}} \approx \underline{\underline{\mathbf{o}}}^{T} \tag{211}$$

where T on the shoulder of the matrix means taking its transpose.

The proposed scheme is reduced into a form taking linear combinations within the restricted MO subspace, in which the molecular orbitals strongly correlate with each other during an adiabatic change. This is aimed at removing any negligible mixing to attain numerical stability. In doing so, we merely need to construct the matrix $\underline{\underline{\tilde{\mathbf{o}}}}$ for such MOs. Practically, we can select them by checking the diagonal part of $\tilde{s}_{ij}$. Our practical procedure is summarized below:

(1) For extracting MO subspace with a view to strong mixing among them, we pick up the set of orbital indices $\Omega = \{k\}$, which satisfy

$$1 - |\langle \phi_k(t - \delta t)|\phi_k(t)\rangle| > p \tag{212}$$

where p is a preset threshold value. Note that the mixing space can be readily divided into sub-blocks, among which they do not correlate by examining the off-diagonal elements, $|\langle \phi_k(t - \delta t)|\phi_l(t)\rangle|$.

(2) Next calculate the matrix

$$o_{ij} = \langle \phi_i(t - \delta t)|\phi_j(t)\rangle \tag{213}$$

with i and j being elements of Ω.

(3) Then prepare $\tilde{\mathbf{o}}$ by making o unitary as explained above.

(4) Next obtain a reconstructed canonical MO set at t, which is uniformly connected to the set at $t - \delta t$,

$$|\tilde{\phi}_j(t)\rangle = \sum_{k=1}^{N} |\phi_k(t)\rangle[\tilde{o}^T]_{kj} = \sum_{k=1}^{N} |\phi_k(t)\rangle\tilde{o}_{jk} \tag{214}$$

The orbital energy, $\tilde{\varepsilon}_i$, corresponding to the uniformed orbital, $\tilde{\phi}_i(t)$, is set by

$$\tilde{\varepsilon}_i = \langle \tilde{\phi}_i(t)|\hat{F}|\tilde{\phi}_i(t)\rangle = \sum_k \varepsilon_k |\tilde{o}_{ik}|^2 \tag{215}$$

with ε_k being the canonical orbital energy of ϕ_k. Here we have used the unitary property of $\underline{\underline{\tilde{\mathbf{o}}}}$.

AUTHOR INFORMATION

Corresponding Author

*E-mail: kaztak@mns2.c.u-tokyo.ac.jp.

BIOGRAPHIES

Takehiro Yonehara was born in Osaka, Japan, in 1975. After he graduated a Faculty of Science, the Kyoto University, in 1999, he received a Ph.D in theoretical chemistry in 2006 at Kyoto University under the direction of Professor Shigeki Kato, the title of his dissertation being "Theoretical study on the multichannel dissociation and isomerization reactions of formaldehyde". Since 2006, he has been a postdoctoral research fellow at the University of Tokyo with Professor Kazuo Takatsuka. His current research interest is quantum entangled non-Born−Oppenheimer dynamics of nuclei and electrons in molecular systems under an external electromagnetic field (yota@mns1.c.u-tokyo.ac.jp).

Kota Hanasaki was born in Tokyo, Japan, in 1979. He graduated from the Faculty of Science at the University of Tokyo in 2002 and received his Masters Degree in theoretical physics in 2004. After he had worked as a systems engineer in a company, he

has become a student at the University of Tokyo under the direction of Professor Kazuo Takatsuka since 2009. His current research interest is nonadiabatic dynamics in electron−nucleus coupled systems (hanasaki@mns2.c.u-tokyo.ac.jp).

Kazuo Takatsuka received his Dr. of Engineering Science from Osaka University (Prof. Takayuki Fueno), Japan, in 1978. After postdoctoral work at North Dakota State University (Prof. Mark Gordon) and Caltech (Prof. Vincent McKoy), he joined Institute of Molecular Science, Japan. In 1992 he started to serve as a professor for Nagoya University, and he then moved to the University of Tokyo in 1997. His current interests are in the theory of electronic and nuclear dynamics beyond the Born−Oppenheimer framework, nuclear wavepacket dynamics with pump−probe photoelectron spectroscopy, nonadiabatic electron wavepacket dynamics in chemical reactions, many-body semiclassics, chaos and nonlinear dynamics in atomic clusters, semiclassical quantization of chaos, dynamics of morphology, and so on.

ACKNOWLEDGMENT

The authors thank Drs. Y. Arasaki and S. Takahashi for valuable discussions. This work has been supported by a Grant-in-Aid for Scientific Research (S) from the Japan Society for the Promotion of Science.

ACRONYMS USED IN THIS REVIEW

ABMD	ab initio molecular dynamics
BO	Born−Oppenheimer
CI	configuration interaction
CIS	configuration interaction with single excitations
CPHF	coupled perturbed Hartree Fock
CSF	configuration state function
LUMO	lowest unoccupied molecular orbital
NDC	nuclear derivative coupling
PES	potential energy surface
PSANB	phase space averaging and natural branching
RHF	restricted Hartree−Fock
ROHF	restricted open-shell Hartree−Fock
SET	semiclassical Ehrenfest theory
SOMO	singly occupied molecular orbital
SONO	singly occupied natural orbital
TDDFT	time-dependent density-functional theory
TZV	triple ζ valence
VDE	vertical detachment energy
WKB	Wentzel−Kramers−Brillouin

REFERENCES

(1) Landau, L. D. *Phys. Z. Sowjetunion* **1932**, *2*, 46.
(2) Zener, C. *Proc. R. Soc. London, A* **1932**, *137*, 696.
(3) Stueckelberg, E. C. G. *Helv. Phys. Acta* **1932**, *5*, 369.
(4) London, F. *Z. Phys. A* **1932**, *74*, 143.
(5) Zhu, C.; Nakamura, H. *J. Chem. Phys.* **1995**, *102*, 7448. *J. Chem. Phys.* **1997**, *106*, 2599.
(6) Tully, J. C. *J. Chem. Phys.* **1990**, *93*, 1061.
(7) Jasper, A. W.; Hack, M. D.; Chakradorty, A.; Truhlar, D. G.; Piecuch, P. *J. Chem. Phys.* **2001**, *115*, 7945.
(8) Zhu, C.; Nangia, S.; Jasper, A. W.; Truhlar, D. G. *J. Chem. Phys.* **2004**, *121*, 7658.
(9) Zhu, C.; Jasper, A. W.; Truhlar, D. G. *J. Chem. Phys.* **2004**, *120*, 5543.
(10) Valero, R.; Truhlar, D. G.; Jasper, A. W. *J. Phys. Chem. A* **2008**, *112*, 5756.
(11) Hellmann, V. H. *Einführung in die Quantenchemie*; F. Deuticke: Leipzig und Wien, 1937; Chapter VIII.
(12) Child, M. S. *Molecular Collision Theory*; Academic Press: 1974; *Semiclassical Mechanics with Molecular Approximations*; Claredon Press: Oxford, 1991.
(13) Nakamura, H. *Nonadiabatic Transition*; World Scinetific: Hackensack, NJ, 2002.
(14) Jasper, A.; Kendrick, B. K.; Mead, C. A.; Truhlar, D. G. In *Modern Trends in Chemical Reaction Dynamics Part I Chapter 8*; Yang, X., Liu, K., Eds.; World Scientific: Singapore, 2004.
(15) Domcke, W.; Yarkony, D. R.; Köppel, H. *Conical Intersections: Electronic Structure, Dynamics Spectroscopy*; World Scientific: Hackensack, NJ, 2004.
(16) Baer, M. *Beyond Born-Oppenheimer*; Wiley: Hoboken, NJ, 2006.
(17) Nanbu, S.; Ishida, T.; Nakamura, H. *Chem. Sci.* **2010**, *1*, 663.
(18) Born, M.; Oppenheimer, R. *Ann. Phys.* **1927**, *84*, 457.
(19) Heitler, W.; London, F. *Z. Phys.* **1927**, *44*, 455.
(20) Eyring, H. *J. Chem. Phys.* **1935**, *3*, 107.
(21) Evans, M. G.; Polyani, M. *Trans. Faraday Soc.* **1935**, *31*, 875.
(22) Born, M.; Huang, K. *Dynamical Theory of Crystal Lattices*; Oxford University Press: Oxford, 1954.
(23) Daniel, C.; Heitz, M.-C.; Manz, J.; Ribbing, C. *J. Chem. Phys.* **1995**, *102*, 95.
(24) Chu, T.-S.; Zhang, Y.; Han, K.-L. *Int. Rev. Phys. Chem.* **2006**, *25*, 201.
(25) Garrett, B. C.; Redmon, M. J.; Truhlar, D. G.; Helius, C. F. *J. Chem. Phys.* **1981**, *74*, 412.
(26) Schwenke, D. W.; Mielke, S. L.; Tawa, G. J.; Friedman, R. S.; Halvick, P.; Truhlar, D. G. *Chem. Phys. Lett.* **1993**, *203*, 565.
(27) Mielke, S. L.; Tawa, G. J.; Truhlar, D. G.; Schwenke, D. W. *Int. J. Quantum Chem. Symp.* **1993**, *27*, 621.
(28) Tawa, G. J.; Mielke, S. L.; Truhlar, D. G.; Schwenke, D. W. *J. Chem. Phys.* **1994**, *100*, 5751.
(29) Mielke, S. L.; Tawa, G. J.; Truhlar, D. G.; Schwenke, D. W. *Chem. Phys. Lett.* **1995**, *234*, 57.
(30) Mielke, S. L.; Truhlar, D. G.; Schwenke, D. W. *J. Phys. Chem.* **1995**, *99*, 16210.
(31) Topaler, M. S.; Hack, M. D.; Allison, T. C.; Liu, Y. -P.; Mielke, S. L.; Schwenke, D. W.; Truhlar, D. G. *J. Chem. Phys.* **1997**, *106*, 8699.
(32) Worth, G. A.; Meyer, H.-D.; Köppel, H.; Cederbaum, L. S.; Burghard, I. *Int. Rev. Phys. Chem.* **2008**, *27*, 569.
(33) Lucchese, R. R.; Takatsuka, K.; McKoy, K. *Phys. Rep.* **1986**, *131*, 147.
(34) Arasaki, Y.; Takatsuka, K.; Wang, K.; McKoy, V. *J. Chem. Phys.* **2010**, *132*, 124307. Zimmermann, B.; Rolles, D.; Langer, B.; Hentges, R.; Braune, M.; Cvejanovic, S.; Gener, O.; Heiser, F.; Korica, S.; Lischke, T.; Reinkoster, A.; Viefhaus, J.; Döner, R.; McKoy, V.; Becker, U. *Nature Phys.* **2008**, *4*, 649. Rolles, D.; Braune, M.; Cvejanovi, S.; Getzner, O.;

Hentges, R.; Korica, S.; Langer, B.; Lischke, T.; Prüper, G.; Reinköter, A.; Viefhaus, J.; Zimmermann, B.; McKoy, V.; Becker, U. *Nature* **2005**, *437*, 711.
(35) Takatsuka, K.; McKoy, K. *Phys. Rev. A* **1981**, *24*, 2473. **1984**, *30*, 1734.
(36) Khakoo, M. A.; Hong, L.; Kim, B.; Winstead, C.; McKoy, V. *Phys. Rev. A* **2010**, *81*, 022720. Winstead, C.; d'Almeida Sanchez, S.; McKoy, V. *J. Chem. Phys.* **2007**, *127*, 085105. Flaherty, D. W.; Kasper, M. A.; Baio, J. E.; Graves, D. B.; Winters, H. F.; Winstead, C.; McKoy, V. *J. Phys. D: Appl. Phys.* **2006**, *39*, 4393.
(37) Takada, Y.; Cui, T. *J. Phys. Soc. Jpn.* **2003**, *72*, 2671.
(38) Sutcliffe, B. T. *J. Math. Chem.* **2008**, *44*, 988.
(39) Herman, M. S. *Ann. Henri Poincaré* **2010**, *11*, 23.
(40) Takahashi, S.; Takatsuka, K. *J. Chem. Phys.* **2006**, *124*, 144101.
(41) Nakai, H.; Sodeyama, K. *J. Chem. Phys.* **2003**, *118*, 1119.
(42) Nakai, H.; Hoshino, M.; Miyamoto, K.; Hyodo, S. *J. Chem. Phys.* **2005**, *122*, 164101.
(43) Hammes-Schiffer, S.; Soudackov, A. V. *J. Phys. Chem. B* **2008**, *112*, 14108.
(44) Hammes-Schiffer, S.; Hatcher, E.; Ishikita, H.; Skone, J. H.; Soudackov, A. V. *Coord. Chem. Rev.* **2008**, *252*, 384.
(45) Chakraborty, A.; Hammes-Schiffer, S. *J. Chem. Phys.* **2008**, *129*, 204101.
(46) Chakraborty, A.; Pak, M. V.; Hammes-Schiffer, S. *Phys. Rev. Lett.* **2008**, *101*, 153001.
(47) Grosser, J.; Hoffmann, O.; Rakete, C.; Rebentrost, F. *J. Phys. Chem. A* **1997**, *101*, 7627.
(48) Arasaki, Y.; Takatsuka, K.; Wang, K.; McKoy, V. *Phys. Rev. Lett.* **2003**, *90*, 248303. *J. Chem. Phys.* **2003**, *119*, 7913.
(49) Horio, T.; Fuji, T; Suzuki, Y.-I; Suzuki, T. *J. Am. Chem. Soc.* **2009**, *131*, 10392.
(50) Arasaki, Y.; Takatsuka, K.; Wang, K.; McKoy, V. *J. Chem. Phys.* **2010**, *132*, 124307.Arasaki, Y.; Wang, K.; McKoy, V.; Takatsuka, K. *Phys. Chem. Chem. Phys.*, in press (DOI: 10.1039/C0CP02302G).
(51) Arasaki, Y.; Takatsuka, K. *Phys. Chem. Chem. Phys.* **2010**, *12*, 1239.
(52) Arasaki, Y.; Wang, K.; McKoy, V.; Takatsuka, K. *Phys. Chem. Chem. Phys.* **2011**, *13*, 8681.
(53) Hentschel, M.; Kienberger, R.; Spielmann, C.; Reider, G. A.; Milosevi, N.; Brabec, T.; Corkum, C.; Heinzmann, U.; Drescher, M.; Krausz, F. *Nature* **2001**, *414*, 509.
(54) Niikura, H.; Légaré, F.; Hasbani, R.; Bandrauk, A. D.; Ivanov, M. Y.; Villeneuve, D. M.; Corkum, P. B. *Nature* **2002**, *417*, 917.
(55) Baltuška, A.; Udem, T.; Uiberacker, M.; Hentschel, M.; Goulielmakis, E.; Gohle, C.; Holzwarth, R.; Yakovlev, V. S.; Scrinzi, A.; Hänsch, A.; Krausz, F. *Nature* **2003**, *421*, 611.
(56) Posthumus, J. H. *Rep. Prog. Phys.* **2004**, *67*, 623.
(57) Mairesse, Y.; de Bohan, A.; Frasinski, L. J.; Merdji, H.; Dinu, L. C.; Monchicourt, P.; Breger, P.; Kovacev, M.; Auguste, T.; Carrè, B.; Muller, H. G.; Agostini, P.; Salierès, P. *Phys. Rev. Lett.* **2004**, *93*, 163901.
(58) Nabekawa, Y.; Shimizu, T.; Okino, T.; Furusawa, K.; Hasegawa, K.; Yamanouchi, K.; Midorikawa, K. *Phys. Rev. Lett.* **2006**, *96*, 083901.
(59) Carrera, J. J.; Tong, X. M.; Chu, S.-I. *Phys. Rev. A* **2006**, *74*, 023404.
(60) Hatsagortsyan, Z.; Keitel, C. H. *Phys. Rep.* **2006**, *427*, 41.
(61) Corkum, P. B.; Krausz, F. *Nature Phys.* **2007**, *3*, 381.
(62) Krausz, F.; Ivanov, M. *Rev. Mod. Phys.* **2009**, *81*, 163.
(63) Kling, M. F.; Vrakking, M. J. *Annu. Rev. Phys. Chem.* **2008**, *59*, 263.
(64) Chu, S.-I. *Chem. Phys. Lett.* **1978**, *54*, 367.
(65) Chu, S.-I. *Chem. Phys. Lett.* **1978**, *58*, 3.
(66) Maquet, A.; Chu, S.-I.; Reinhardt, W. P. *Phys. Rev. A* **1983**, *27*, 2946.
(67) Ivanov, M.; Corkum, P. B.; Zuo, T.; Bandrauk, A. *Phys. Rev. Lett.* **1995**, *74*, 2933.
(68) Chelkowski, S.; Zuo, T.; Atabek, O.; Bandrauk, A. D. *Phys. Rev. A* **1995**, *52*, 2977. Chelkowski, S.; Conjusteau, A.; Zuo, T.; Bandrauk, A. D. *Phys. Rev. A* **1996**, *54*, 3235.
(69) Tong, X.-M.; Chu, S.-I. *Phys. Rev. A* **1998**, *57*, 452.
(70) Harumiya, K.; Kawata, I.; Kono, H.; Fujimura, Y. *J. Chem. Phys.* **2000**, *113*, 8953.
(71) Harumiya, K.; Kono, H.; Fujimura, Y.; Kawata, I.; Bandrauk, A. D. *Phys. Rev. A* **2002**, *66*, 043403.
(72) Saenz, A. *Phys. Rev. A* **2002**, *66*, 063407.
(73) Kono, H.; Sato, Y.; Tanaka, N.; Kato, T.; Nakai, K.; Koseki, S.; Fujimura, Y. *Chem. Phys.* **2004**, *304*, 203.
(74) Paramonov, G. K. *Chem. Phys. Lett.* **2005**, *411*, 350.
(75) Martin, F.; Fernández, J.; Havermeier, T.; Foucar, L.; Weber, Th.; Kreidi, K.; Schöffler, M.; Schmidt, L.; Jahnke, T.; Jagutzki, O.; Czasch, A.; Benis, E. P.; Osipov, T.; Landers, A. L.; Belkacem, A.; Prior, M. H.; Schmidt-Bocking, H.; Cocke, C. L.; Dorner, R. *Science* **2007**, *315*, 629.
(76) Staudte, A.; Pavičić, D.; Chelkowski, S.; Zeidler, D.; Meckel, M.; Niikura, H.; Schöffler, M.; Schössler, S.; Ulrich, B.; Rajeev, P. P.; Weber, T.; Jahnke, T.; Villeneuve, D. M.; Bandrauk, A. D.; Cocke, C. L.; Corkum, P. B.; Dörner, R. *Phys. Rev. Lett.* **2007**, *98*, 073003.
(77) Paramonov, G. K. *Chem. Phys.* **2007**, *338*, 329.
(78) Kato, T.; Kono, H. *J. Chem. Phys.* **2008**, *128*, 184102.
(79) Bandrauk, A. D.; Chelkowski, S.; Kawai, S.; Lu, H. *Phys. Rev. Lett.* **2008**, *101*, 153901.
(80) Kato, T.; Kono, H.; Kanno, M.; Fujimura, Y.; Yamanouchi, K. *Laser Phys.* **2009**, *19*, 2009.
(81) Chelkowski, S.; Bandrauk, A. D. *Phys. Rev. A* **2010**, *81*, 062101.
(82) Takatsuka, K.; Yonehara, T. *Adv. Chem. Phys.* **2010**, *144*, 93.
(83) Lewenstein, M.; Balcou, P.; Ivanov, M. Y.; L'Huillier, A.; Corkum, P. B. *Phys. Rev. A* **1994**, *49*, 2117.
(84) Paul, P. M.; Toma, E. S.; Breger, P.; Mullot, G.; Augé, F.; Balcou, P.; Muller, H. G.; Agostini, P. *Phys. Rev. A* **2001**, *292*, 1689.
(85) Itatani, J.; Levesque, J.; Zeidler, D.; Niikura, H.; Pépin, H.; Kieffer, J. C.; Corkum, P. B.; Villeneuve, D. M. *Nature* **2004**, *432*, 867.
(86) Smirnova, O.; Mairesse, Y.; Patchkovskii, S.; Dudovich, N.; Villeneuve, D.; Corkum, P.; Ivanov, M. Y. *Nature* **2009**, *460*, 972.
(87) Corkum., P. B. *Phys. Rev. Lett.* **1993**, *71*, 1994.
(88) Diestler, D. J. *Phys. Rev. A* **2008**, *78*, 033814.
(89) Nobusada, K.; Yabana, K. *Phys. Rev. A* **2004**, *70*, 043411.
(90) Barth, I.; Manz, J.; Shigeta, Y.; Yagi, K. *J. Am. Chem. Soc.* **2006**, *128*, 7043.
(91) *Progress in Ultrafast Intense Laser Science VI*; Yamanouchi, K., Bandrauk, A. D., Gerber, G., Eds.; Springer: Berlin, 2010.
(92) Nest, M. *Chem. Phys. Lett.* **2009**, *472*, 171.
(93) Nest, M.; Remacle, F.; Levine, R. D. *New J. Phys.* **2008**, *10*, 025019.
(94) Remacle, F.; Levine, R. D. *Proc. Natl. Acad. Sci. U.S.A.* **2006**, *103*, 6793.
(95) Klinkusch, S.; Klamroth, T.; Saalfrank, P. *Phys. Chem. Chem. Phys.* **2009**, *11*, 3875.
(96) Lorin, E.; Chelkowski, S.; Bandrauk, A. D. *New J. Phys.* **2008**, *10*, 025033. Lorin, E.; Chelkowski, S.; Bandrauk, A. D. *Comput. Chem. Commun.* **2007**, *177*, 908.
(97) Wodtke, A. M.; Tully, J. C.; Auerbach, D. J. *Int. Rev. Phys. Chem.* **2007**, *23*, 513.
(98) Mitrič, R.; Petersen, J.; Bonačič-Koutecký, V. *Phys. Rev. A* **2009**, *79*, 053416.
(99) Nagashima, K.; Takatsuka, K. *J. Phys. Chem. A* **2009**, *113*, 15240.
(100) Okuyama, M.; Takatsuka, K. *Chem. Phys. Lett.* **2009**, *476*, 109.
(101) Andrae, D.; Barth, I.; Bredtmann, T.; Hege, H.-C.; Manz, J.; Marquardt, F.; Paulus, B. *J. Phys. Chem. B* **2011**, *115*, 5476.
(102) Longuet-Higgins, H. C.; Öpik, U.; Pryce, M. H. L.; Sack, R. A. *Proc. R. Soc. London, Ser. A* **1958**, *244*, 1. Herzberg, G.; Longuet-Higgins, H. C. *Discuss. Faraday Soc.* **1963**, *35*, 77. Longuet-Higgins, H. C. *Adv. Spectrosc.* **1961**, *2*, 429.
(103) Berry, M. V. *Proc. R. Soc. London, A* **1984**, *392*, 45.
(104) Mead, C. A.; Truhlar, D. G. *J. Chem. Phys.* **1979**, *70*, 2284.
(105) Mead, C. A. *Chem. Phys.* **1980**, *49*, 23.
(106) Yamada, A.; Okazaki, S. *J. Chem. Phys.* **2006**, *124*, 094110.
(107) Yamada, A.; Okazaki, S. *J. Chem. Phys.* **2008**, *128*, 044507.

(108) Agarwal, P. K.; Billeter, S. R.; Rajagopalan, P. T. R.; Benkovic, S. J.; Hammes-Schiffer, S. *Proc. Natl. Acad. Sci. U.S.A.* **2002**, *99*, 2794.
(109) Rose, T. S.; Rosker, M. J.; Zewail, A. H. *J. Chem. Phys.* **1988**, *88*, 6672.
(110) Takatsuka, K.; Nakamura, H. *J. Chem. Phys.* **1986**, *85*, 5779.
(111) Bykhovskii, V.; Niktin, E.; Ovchinikova, M. *Eksp. Teor. Phys.* **1964**, *47*, 750. *Sov. Phys. JETP* **1965**, *20*, 500.
(112) Delos, J. B.; Thorson, W. R. *Phys. Rev. A* **1972**, *6*, 720.
(113) Miller, W. H.; George, T. F. *J. Chem. Phys.* **1972**, *56*, 5637.
(114) Pechukas, P. *Phys. Rev.* **1969**, *181*, 174.
(115) Morse, P.; Feshbach, H. *Methods of Theoretical Physics, Part I*; McGraw-Hill: New York, 1953; pp 609.
(116) Tully, J. C.; Preston, R. K. *J. Chem. Phys.* **1971**, *55*, 562.
(117) Shenvi, N. *J. Chem. Phys.* **2009**, *130*, 124117.
(118) Yang, S.; Coe, J. D.; Kaduk, B.; Martínez, T. J. *J. Chem. Phys.* **2009**, *130*, 134113.
(119) Miller, W. H. *J. Phys. Chem. A* **2009**, *113*, 1405.
(120) Blais, N. C.; Truhlar, D. G. *J. Chem. Phys.* **1983**, *79*, 1334.
(121) Chapman, S. *J. Chem. Phys.* **1985**, *82*, 4033.
(122) Parlant, G.; Gislason, E. A. *J. Chem. Phys.* **1989**, *91*, 4416.
(123) Ushiyama, H.; Takatsuka, K. *Angew. Chem., Int. Ed.* **2005**, *4*, 1237.
(124) Ushiyama, H.; Takatsuka, K. *Angew. Chem., Int. Ed.* **2007**, *46*, 587.
(125) Feynman, R. P.; Hibbs, A. R. *Quantum Mechanics and Path Integrals*; McGraw-Hill: New York, 1965.
(126) Schulman, L. S. *Techniques and Application of Path Integration*; Wiley: New York, 1981.
(127) Krishna, V. *J. Chem. Phys.* **2007**, *126*, 134107.
(128) Hanasaki, K.; Takatsuka, K. *Phys. Rev. A* **2010**, *81*, 052514.
(129) Amano, M.; Takatsuka, K. *J. Chem. Phys.* **2005**, *122*, 084113.
(130) Miller, W. H. *J. Chem. Phys.* **1970**, *53*, 1949.
(131) Miller, W. H. *J. Chem. Phys.* **1970**, *53*, 3578.
(132) Stine, J. R.; Marcus, R. A. *Chem. Phys. Lett.* **1984**, *29*, 575.
(133) Meyer, H.-D.; Miller, W. H. *J. Chem. Phys.* **1979**, *70*, 3214.
(134) Sun, X.; Miller, W. H. *J. Chem. Phys.* **1997**, *106*, 6346.
(135) Sun, X.; Wang, H.; Miller, W. H. *J. Chem. Phys.* **1997**, *109*, 7064.
(136) Stock, G.; Thoss, M. *Adv. Chem. Phys.* **2005**, *131*, 243.
(137) Stock, G.; Thoss, M. *Phys. Rev. Lett.* **1997**, *78*, 578.
(138) Jasper, A. W.; Stechmann, S. N.; Truhlar, D. G. *J. Chem. Phys.* **2002**, *116*, 5424.
(139) Hack, M. D.; Wensman, A. M.; Truhlar, D. G.; Ben-Nun, M.; Martínez, T. J. *J. Chem. Phys.* **2001**, *115*, 1172.
(140) Heller, H. J.; Bilha, S.; Sergeev, A. V. *J. Phys. Chem. B* **2002**, *106*, 8471.
(141) Giulini, D.; Joos, E.; Kiefer, C.; Kupsch, J.; Stamatescu, I.-O.; Zeh, H. D. *Decoherence and the appearance of a classical world in quantum theory*; Springer: Berlin, Germany, 1994.
(142) Fujisaki, H.; Takatsuka, K. *Phys. Rev. E* **2001**, *63*, 066221.
(143) Fujisaki, H.; Takatsuka, K. *J. Chem. Phys.* **2001**, *114*, 3497.
(144) Higuchi, H.; Takatsuka, K. *Phys. Rev. E* **2002**, *66*, 035203.
(145) Vaníček, J. *Phys. Rev. E* **2004**, *70*, 055201.
(146) Vaníček, J. *Phys. Rev. E* **2006**, *73*, 046204.
(147) Bittner, E. R.; Rossky, P. J. *J. Chem. Phys.* **1995**, *103*, 8130. **1997**, *107*, 8611.
(148) Neria, E.; Nitzan, A. *J. Chem. Phys.* **1993**, *99*, 1109.
(149) Subotnik, J. E. *J. Chem. Phys.* **2010**, *132*, 134112.
(150) Subotnik, J. E.; Shenvi, N. *J. Chem. Phys.* **2011**, *134*, 024105.
(151) Yonehara, T.; Takatsuka, K. *J. Chem. Phys.* **2008**, *128*, 154104.
(152) Aharonov, Y.; Bohm, D. *Phys. Rev. (Ser. 2)* **1959**, *115*, 485.
(153) Takatsuka, K. *J. Phys. Chem. A* **2007**, *111*, 10196.
(154) Yonehara, T.; Takatsuka, K. *J. Chem. Phys.* **2008**, *129*, 134109.
(155) Yonehara, T.; Takahashi, S.; Takatsuka, K. *J. Chem. Phys.* **2009**, *130*, 214113.
(156) Yonehara, T.; Takatsuka, K. *Chem. Phys.* **2009**, *366*, 115.
(157) Yonehara, T.; Takatsuka, K. *J. Chem. Phys.* **2010**, *132*, 244102.
(158) Martínez, T. J.; Ben-Nun, M.; Levine, R. D. *J. Phys. Chem.* **1996**, *100*, 7884.
(159) Martínez, T. J.; Ben-Nun, M.; Levine, R. D. *J. Phys. Chem. A* **1997**, *101*, 6389.
(160) Martnez, T. J. *Acc. Chem. Res.* **2006**, *39*, 119.
(161) Virshup, A. M.; Punwong, C.; Pogorelov, T. V.; Lindquist, B. A.; Ko, C.; Martínez, T. J. *J. Phys. Chem. B* **2009**, *113*, 3280and references cited therein.
(162) Heller, E. J. *J. Chem. Phys.* **1981**, *75*, 2923.
(163) Inoue-Ushiyama, A.; Takatsuka, K. *Phys. Rev. Lett.* **1997**, *78*, 1404. *Phys. Rev. A* **1999**, *59*, 3256.
(164) Takahashi, S.; Takatsuka, K. unpublished.
(165) Krishna, V. *Phys. Rev. Lett.* **2009**, *102*, 053002.
(166) Geppert, D.; von den Hoff, P.; de Vivie-Riedle, R. *J. Phys. B: At. Mol. Opt. Phys.* **2008**, *41*, 074006.
(167) Abe, M.; Ohtsuki, Y.; Fujimura, Y.; Lan, Z.; Domcke, W. *J. Chem. Phys.* **2006**, *124*, 224316.
(168) Ben-Nun, M.; Martínez, T. J. *J. Chem. Phys.* **1998**, *108*, 7244.
(169) Levine, B. G.; Coe, J. D.; Virshup, A. M.; Martínez, T. J. *Chem. Phys.* **2008**, *347*, 3.
(170) Schiff, L. I. *Quantum Mechanics*; McGraw-Hill: New York, 1968.
(171) Barth, I.; Hege, H.-C.; Ikeda, H.; Kenfack, A.; Koppitz, M.; Manz, J.; Marquardt, F.; Paramonov, G. K. *Chem. Phys. Lett.* **2009**, *481*, 118.
(172) Kenfack, A.; Marquardt, F.; Paramonov, G. K.; Barth, I.; Lasser, C.; Paulus, B. *Phys. Rev. A* **2010**, *81*, 052502.
(173) Hart, E. J.; Boag, J. W. *J. Am. Chem. Soc.* **1962**, *84*, 4090.
(174) Hart, E. J. *Science* **1964**, *146*, 19.
(175) Kevan, L. *Acc. Chem. Res.* **1981**, *14*, 138.
(176) Combariza, J.; Kestner, R.; Jortner, J. *J. Chem. Phys.* **1994**, *100*, 2851.
(177) Haberland, H.; Ludewigt, C.; Schindler, H. G.; Worsnop, D. R. *J. Chem. Phys.* **1984**, *81*, 3742.
(178) Rossky, P. J.; Schnitker, J. *J. Phys. Chem.* **1988**, *92*, 4277.
(179) Jordan, K. D. *Science* **2004**, *306*, 618.
(180) Sobolewski, A. L.; Domcke, W. *Phys. Chem. Chem. Phys.* **2007**, *9*, 3818.
(181) Simons, J. *J. Phys. Chem. A* **2008**, *112*, 6401.
(182) Ehrler, O. T.; Neumark, D. M. *Acc. Chem. Res.* **2009**, *42*, 769.
(183) Iwata, S.; Tsurusawa, T. *Adv. Met. Semicond. Clusters* **2001**, *5*, 39.
(184) Kim, J.; Suh, S. B.; Kim, K. S. *J. Chem. Phys.* **1999**, *111*, 10077. Lee, H. M.; Lee, S.; Kim, K. S. *J. Chem. Phys.* **2003**, *119*, 187.
(185) Hammer, N. I.; Shin, J.-W.; Headrick, J. M.; Diken, E. G.; Roscioli, J. R.; Weddle, G. H.; Johnson, M. A. *Science* **2004**, *306*, 675.
(186) Roscioli, J. R.; Hammer, N. I.; Johnson, M. A.; Diri, K.; Jordan, K. D. *J. Chem. Phys.* **2008**, *128*, 104314.
(187) Choi, T.; Jordan, K. *Chem. Phys. Lett.* **2009**, *475*, 293. Also see: Jordan, K.; Johnson, M. *Science* **2010**, *329*, 42.
(188) Tachikawa, H. *J. Chem. Phys.* **2006**, *125*, 144307.
(189) Herbert, J. M.; Head-Gordon, M. *Proc. Natl. Acad. Sci. U.S.A.* **2006**, *103*, 14282.
(190) Shkrob, I. A.; Glover, W. J.; Larsen, R. E.; Schwartz, B. J. *J. Phys. Chem. A* **2007**, *111*, 5232.
(191) Frigato, T.; VandeVondele, J.; Schmidt, B.; Schütte, C.; Jungwirth, P. *J. Phys. Chem. A* **2008**, *112*, 6125.
(192) Turi, L.; Hantal, G.; Rossky, P.; Borgis, D. *J. Chem. Phys.* **2009**, *131*, 024119.
(193) Bragg, A. E.; Verlet, J. R. R.; Kammrath, A.; Cheshnovsky, O.; Neumark, D. M. *Science* **2004**, *306*, 669.
(194) Pshenichnikov, M. S.; Baltuska, A.; Wiersma, D. A. *Chem. Phys. Lett.* **2004**, *389*, 171.
(195) Nakanishi, R.; Nagata, T. *J. Phys. Chem.* **2009**, *130*, 224309.
(196) Webster, F. J.; Schnitker, J.; Friedrichs, M. S.; Friesner, R. A.; Rossky, P. J. *Phys. Rev. Lett.* **1991**, *66*, 3172. Webster, F. J.; Rossky, P. J.; Friesner, R. A. *Comput. Phys. Commun.* **1991**, *63*, 494.
(197) Prezhdo, O. V.; Rossky, P. J. *J. Phys. Chem.* **1996**, *100*, 17094.
(198) Verlet, J. R. R.; Bragg, A. E.; Kammrath, A.; Cheshnovsky, O.; Neumark, D. M. *Science* **2005**, *307*, 93.

(199) Schmidt, M. W.; Baldridge, K. K.; Boatz, J. A.; Elbert, S. T.; Gordon, M. S.; Jensen, J. H.; Koseki, S.; Matsunaga, N.; Nguyen, K. A.; Su, S. J.; Windus, T. L.; Dupuis, M.; Montgomery, J. A. *J. Comput. Chem.* **1993**, *14*, 1347. Since the original GAMESS code (version 11) does not have an analytic gradient calculation code for ROHF-CI, we additionally implemented a numerical gradient calculation code.
(200) Dunning, T. H. *J. Chem. Phys.* **1971**, *55*, 716.
(201) Roothaan, C. C. J. *Rev. Mod. Phys.* **1960**, *32*, 179.
(202) Yarkony, D. R. *Rev. Mod. Phys.* **1996**, *68*, 985.
(203) Crespo-Hernández, C. E.; Cohen, B.; Hare, P. M.; Kohle, B. *Chem. Rev.* **2004**, *104*, 1977.
(204) Werner, H. J.; Knowles, P. J. *J. Chem. Phys.* **1988**, *89*, 5803.
(205) Finley, J.; Malmqvist, P.; Roos, B. O.; Serrano-Andres, L. *Chem. Phys.* **1998**, *288*, 299.
(206) Nakatsuji, H. *Chem. Phys. Lett.* **1979**, *67*, 329.
(207) Casida, M. E.; Jamorski, C.; Casida, K. C.; Salahub, D. R. *J. Chem. Phys.* **1998**, *108*, 4439.
(208) Baer, R. *Chem. Phys. Lett.* **2002**, *364*, 75.
(209) Hu, C.; Sugino, O.; Tateyama, Y. *J. Chem. Phys.* **2009**, *131*, 114101.
(210) Tvernelli, I.; Tapavisza, E.; Rothlisberger, U. *J. Chem. Phys.* **2009**, *130*, 124107.
(211) Send, R.; Furche, F. *J. Chem. Phys.* **2010**, *132*, 044107.
(212) Duncan, W. R.; Stier, W. M.; Prezhdo, O. V. *J. Am. Chem. Soc.* **2005**, *127*, 98195.
(213) Ulrich, C. A.; Tokatly, I. V. *Phys. Rev. B* **2006**, *73*, 235102.
(214) Mead, C. A.; Truhlar, D. G. *J. Chem. Phys.* **1982**, *77*, 6090.
(215) Baer, M. *Chem. Phys. Lett.* **1975**, *35*, 112.
(216) Baer, R.; Charutz, D. M.; Kosloff, R.; Baer, M. *J. Chem. Phys.* **1996**, *105*, 9141.
(217) Adhikari, S.; Billing, G. D. *J. Chem. Phys.* **1999**, *111*, 40.
(218) Mukunda, N.; Simons, R. *Ann. Phys.* **1993**, *228*, 205.
(219) Mead, C. A. *Rev. Mod. Phys.* **1992**, *64*, 51.
(220) Althorpe, S. C.; Stecher, T.; Bouakline, F. *J. Chem. Phys.* **2008**, *129*, 214117.
(221) Kuppermann, A. *J. Phys. Chem. A* **2006**, *110*, 809.
(222) Thompson, T. C.; Izmirlian, G., Jr.; Lemon, S. J.; Truhlar, D. G. *J. Chem. Phys.* **1985**, *82*, 5697.
(223) Abrol, R.; Shaw, A.; Kuppermann, A.; Yarkony, D. R. *J. Chem. Phys.* **2001**, *115*, 4640.
(224) Kendrick, B. *Phys. Rev. Lett.* **1997**, *79*, 2431.
(225) Kendrick, B.; Pack, R. T. *J. Chem. Phys.* **1996**, *104*, 7475.
(226) Kendrick, B.; Pack, R. T. *J. Chem. Phys.* **1996**, *104*, 7502.
(227) Kendrick, B.; Pack, R. T. *J. Chem. Phys.* **1997**, *106*, 3519.
(228) Zhang, Y.; Tan, Y.-W.; Stormer, H. L.; Kim, P. *Nature* **2005**, *438*, 201.
(229) Resta, R. *Rev. Mod. Phys.* **1994**, *66*, 899.
(230) Ferretti, A.; Granucci, G.; Lami, A.; Persico, M.; Villani, G. *J. Chem. Phys.* **1996**, *104*, 5517.
(231) Kelly, A.; Kapral, R. *J. Chem. Phys.* **2010**, *133*, 084502.
(232) Yoshida, H. *Phys. Lett. A* **1990**, *150*, 262. Takahashi, K.; Ikeda, K. *J. Chem. Phys.* **1993**, *99*, 8680. Kosloff, R. *J. Phys. Chem.* **1988**, *92*, 2087. Suzuki, M. *Phys. Lett. A* **1992**, *165*, 387. Feit, M. D.; Fleck, J. A., Jr.; Steiger, A. *J. Comput. Phys.* **1982**, *47*, 412.
(233) Smith, F. T. *Phys. Rev.* **1969**, *179*, 111.
(234) Baer, M. *Phys. Rep.* **2002**, *358*, 75.
(235) Atchity, G. J.; Ruedenberg, K. *Theor. Chem. Acc.* **1997**, *97*, 47.
(236) Nakamura., H.; Truhlar, D. G. *J. Chem. Phys.* **2001**, *115*, 10353.
(237) Yamaguchi, Y.; Osamura, Y.; Goddard, J. D.; Schaefer, H. F., III *A New Dimension to Quantum Chemistry: Analytic Derivative Methods in ab initio Molecular Electronic Structure Theory*; Oxford University Press: New York, Oxford, 1994.
(238) Bonačìc-Koutecký, V.; Mitrìc, R. *Chem. Rev.* **2005**, *105*, 11.
(239) Hoffman, M. R.; Fox, D. J.; Gaw, J. F.; Osamura, Y.; Yamauchi, Y.; Grev, R. S.; Fitzgerald, G.; Schaefer, H. F.; Knowles, P. J.; Handy, N. C. *J. Chem. Phys.* **1984**, *80*, 2660.
(240) Dudley, T. J.; Olson, R. M.; Schmidt, M. W.; Gordon, M. S. *J. Comput. Chem.* **2006**, *27*, 353.
(241) Lengsfield, B. H.; Saxe, P.; Yarkony, D. R. *J. Chem. Phys.* **1984**, *81*, 4549.
(242) Lischka, H.; Dallos, M.; Szalay, P. G.; Yarkony, D. R.; Shepard, R. *J. Chem. Phys.* **2004**, *120*, 7322.
(243) Lengsfield, B. H.; Yarkony, D. R. *Nonadiabatic Interactions Between Potential Energy Surfaces: Theory and Applications In State-Selected and State to State Ion−Molecule Reaction Dynamics: Part 2 Theory*; Baer, M., Ng, C.-Y., Eds.; John Wiley and Sons: New York, 1992; Vol. 82; pp 1−71.
(244) Nakamura, H.; Truhlar, D. G. *J. Chem. Phys.* **2002**, *117*, 5576.